Studies on Design of Automatic Driving Systems and Analysis of Driving Behavior based on Driver's Visual Perception

Okafuji, Yuki

(Degree)
博士（工学）

(Date of Degree)
2018-09-25

(Date of Publication)
2019-09-01

(Resource Type)
doctoral thesis

(Report Number)
甲第7303号

(URL)
https://hdl.handle.net/20.500.14094/D1007303

Doctoral Thesis

Studies on Design of Automatic Driving Systems and Analysis of Driving Behavior based on Driver's Visual Perception

Yuki Okafuji

July 2018

Graduate School of Engineering
Kobe University

Abstract

Due to the advances in technology in recent years, various automated driving systems have been developed for improving safety. In particular, driving assistance systems need to be designed to include three factors: "Vehicle, Environment, and Human". However, introducing human factors into automated systems is very difficult, and the research field on understanding human drivers is not sufficient for developing such systems. Automated systems without human factors could give human drivers a feeling of discomfort and distrust. Thus, there are still problems that hamper the spread of automatic systems, although automated driving systems have the potential to solve various social problems. This is because it is difficult to develop a system that includes the aspects of both Engineering and Psychology based on human understanding, although the autonomous vehicle should be a Human-in-the-Loop system. In this thesis, we construct automated driving systems and understand driver behavior based on the approaches of both Engineering and Psychology.

Firstly, we design an automated steering system including human factors. In particular, we focus on visual cues that drivers perceive and use while driving, and construct automated systems based on optical flow, which is one of the visual cues. We model the optical flow information and directly apply it to the nonlinear control method. This method applies knowledge from the field of psychology, making it possible to design human-like automated steering systems. Next, we put forward a hypothesis in terms of the relationship of driver visual-steering based on the simulation/experiment results generated by the proposed method. We conduct a psychological experiment referring to the hypothesis in order to figure out new driver behaviors. Consequently, we can design automated driving systems that can simulate driver steering behavior, and simultaneously understand driver behavior. In this way, we construct Human-in-the-Loop research systems, in which Psychology can contribute to Engineering and Engineering can contribute to Psychology, and the aim of this thesis is to facilitate both research fields based on the approach of each other.

博　士　論　文

ドライバの視覚特性に基づいた自動走行システムの構築と運転特性の解析に関する研究

岡藤　勇希

2018年7月

神戸大学大学院工学研究科

摘要

近年の技術の進歩により，様々な自動走行システムが開発され，世の中に普及しつつある．この中でも特に運転支援システムでは，“自動車· 環境· 人間” の三つを考慮した設計が必要であるにも関わらず，ヒューマン· ファクタをシステムに組み込むことは困難であり，人間系の研究が最も困難な領域となっている．ヒューマン· ファクタを考慮出来ていないシステムは，ドライバに違和感や不信感を与えてしまう可能性がある．これにより，自動走行システムは社会の様々な問題が解決する見込みがあるにも関わらず，普及が遅れるなどの問題点が挙げられる．自動走行システムは人間を含んだ，いわゆる Human-in-the-loop なシステムであるにも関わらず，工学と心理学分野が独立して考えられることが多く，学際的な研究促進が出来ていないためと考えられる．そこで本研究では，制御工学と心理学の両側面からのアプローチに基づいて，自動走行システムの構築とドライバ特性の理解を行っていく．

本研究ではまず，ヒューマン· ファクタを考慮した車両制御系の設計を行う．特に，ドライバの視覚特性に着目し，オプティカルフローに基づいた自動操舵システムを構築する．ドライバが知覚する情報自体を数理モデルとして指標化し，直接的に非線形制御の枠組みに適用する手法を用いる．心理学分野における知見に基づいた手法を直接的に導入することで，ヒューマンライクな挙動を示すことの可能な制御手法を構築することを目的とする．次に，視覚特性に基づいた自動走行システムの実験結果から得られた知見により，ドライバの知覚-操舵系の仮説を立て，心理学実験を行うことで，ドライバ特性の解明を行っていく．その結果として，人間の理解に基づいた自動走行システムが構築可能となると同時に，ドライバの理解も進むこととなる．このように，工学から心理学へ，心理学から工学へといった，Human-in-the-loop な学術体系を構築することを目的とし，両研究分野への効率的な促進を図る．

Acknowledgments

I have been involved in several collaborators throughout this thesis. I express my gratitude to all collaborators here.

I would like to thank Professor Yasuyoshi Yokokohji. I have been able to train the foundation as a researcher through rigorous discussions. I appreciate for giving me permission to belong to other universities in Japan and UK during most of the Ph.D. period in order to broaden my perspective. I would like to thank my thesis readers. I am grateful to Professor Keiichi Shirase, Professor Hisashi Tamaki, and Dr. Yuichi Tazaki for lots of their advise and comments for this thesis.

I would like to appreciate Professor Takanori Fukao at Ritsumeikan University for giving me an opportunity to be Ph. D. student. For over 5 years, I have learned a lot of important things as not only a researcher but also a human being. He is always thinking of how to change the society better, and this positive attitude has influenced me. This work could not be completed anywhere besides him.

I would like to thank Dr. Hiroshi Inou at DENSO International America Inc.. This work has been influenced by his previous awesome research, and he always gives me insightful advice. I would like to thank Professor Natasha Merat and Dr. Richard M. Wilkie, and Dr. Callum D. Mole at University of Leeds in the UK for kindly hosting me who is unfamiliar with overseas experiences. They had given me a passionate guidance on the research of psychology, and I got various experiences to expand the view of research.

During long periods of work, I would like to thank Dr. Tatsuya Yoshimoto, Takuma Ario, Mami Yoneda, Takanari Hanabusa, Kenta Mukouya, Mizuki Ota, Asano Kitahara, and members at MA-1 Lab. and IVeS Lab. for giving me the fulfilling and happy days.

Finally, I am sincerely thankful to my parents who always watched me warmly during my doctoral program. To be able to pursue academic for longer than a person was really happy, and that was an irreplaceable and wonderful thing to me.

謝 辞

本研究を進めるにあたり，多くの方々から多大なるご支援，ご協力を賜りました．ここに感謝の意を表します．

最初に，指導教員である横小路泰義教授に感謝申し上げます．日々の研究会等での厳しい議論を通じて，研究者としての素地を鍛えることができました．博士課程のほとんどの期間，自身の視野を広げるために，国内外の他大学に所属する許可を与えていただき，誠にありがとうございました．また，本博士論文の審査委員をお引き受けいただきました白瀬敬一教授，玉置久教授，田崎勇一准教授には論文審査を通じて大変有意義なご意見を承りました．ここに感謝申し上げます．

立命館大学の深尾隆則教授には，博士課程に進学する機会を与えて頂きました．5年半に渡る長いご指導の間，研究だけではなく，人としてのあり方を学ぶことが出来ました．深尾教授の，社会を良くするといった常に前向きな姿勢に感化され，研究者として大切なものを受け取ることが出来ました．本博士論文は深尾教授のご指導なくしては成し得ませんでした．心から感謝申し上げます．

次に，本研究に対する先駆的な研究を行い，様々な知識と経験から研究を支えていただいた，DENSO International America, Inc. の伊能寛博士にも感謝申し上げます．また，英国 Leeds 大学の Natasha Merat 教授，Richard M. Wilkie 准教授，Dr. Callum D. Mole に感謝申し上げます．心理学の研究を根気強くご指導していただき，研究の視野を広げる様々な経験をさせていただきました．誠にありがとうございます．

長期の研究を共に励んだ，立命館大学の吉本達也助教，有尾拓誠様，米田真美様，英峻成様，向家研太様，太田瑞己様，北原麻乃様を始め，複雑系機械工学研究室，知的ビークルシステム研究室の皆様に感謝申し上げます．皆様と寝食を共に研究をした日々は常に充実し，楽しく研究を行うことができました．

最後に，博士課程の間，常に暖かく見守ってくれた両親に心から感謝いたします．人よりも長く学問を追求出来たことは何にも代えがたい幸せでした．今まで本当にありがとうございました．

Contents

List of Figures

List of Tables

Chapter 1

General Introduction

1.1 Background

Automobiles have played an important role in human society as a mean of transportation to move from one place to another. However, due to the advances in technology in recent years, the roles of automobiles have become more diverse compared to the previous meaning, as represented by the acronym of CASE (Connected, Autonomous, Shared, Electric) [1]. "Connected" is realized by high-speed communication technologies such as the 5th generation wireless systems (5G), and it can comprehensively manage information among human, vehicle, and infrastructure in real time. It is expected that "Autonomous" can reduce car accidents, provide new transportation methods for vulnerable road users, and alleviate driving stress. "Shared" helps in mitigating environmental problems such as air pollution by alleviating congestion by reducing the number of vehicles on the road. Finally, "Electric" is considered as a solution for the exhaust gas problem, and has good compatibility with "Autonomous" due to the simplification of the vehicle design. These technologies are expected to not only solve various social problems caused by a large number of vehicles but also improve productivity in the world. Simultaneously, the original meaning of automobile itself as a personal possession is about to change [2–8].

In these issues, we focus on the relationship between "Autonomous" and car accidents. For instance, the number of traffic accidents in Japan had increased along with the number of vehicles owned, as shown in Figure 1.1 [9, 10]. However, since around 1990, passive safety technologies for mitigating the damage caused by accidents, such as airbags, have become widely used, resulting in a constant decrease in the number of casualties compared to the number of accidents. In addition, during this decade, active safety

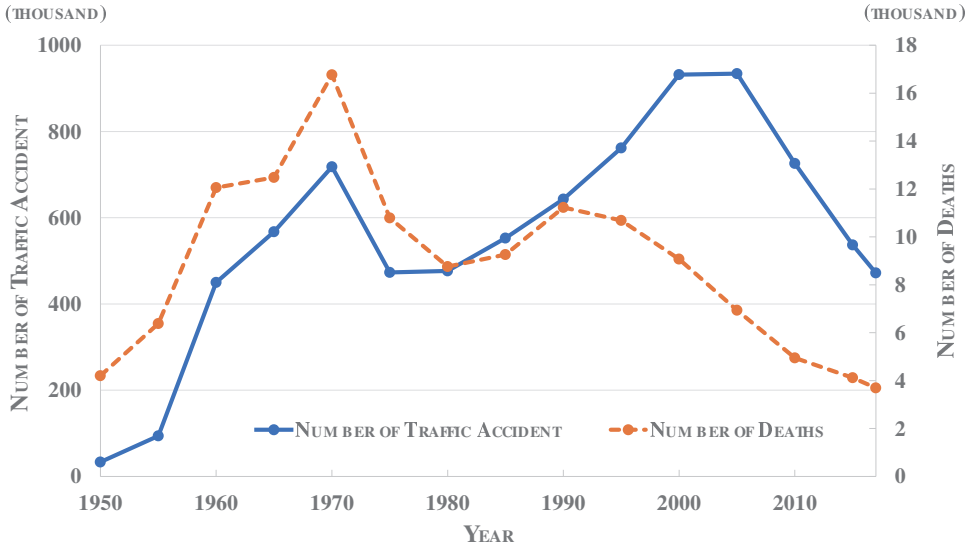

Figure 1.1: Transition of the number of traffic accidents and casualties in Japan

technologies for directly preventing accidents itself have been spread among people, and therefore the number of accidents has also decreased. It is often said that human error, especially related to recognition and judgement, contributes to 90% of all traffic accidents. Therefore, autonomous systems will gain in popularity in the near future, and they seem capable of achieving a society without any traffic accident by reducing the opportunities for humans to drive [4, 8, 11]. In general, these automation systems are classified into 6 levels by SAE International as shown in Figure 1.2 [12]. The automation under level 3 mainly implies the use of assistance systems since human drivers are always involved in some operation such as resuming control except under the allowed environments, whereas they do not need to fallback the driving tasks over level 4 automation. Various companies and research institutes have been developing these technologies; however, the aims of development are different for these institutes. Existing car manufacturers follow the steps of automation in order, and the automation systems in level 2 and 3 are becoming common under limited conditions such as the highway. Meanwhile, tech/emerging companies are trying to directly develop level 4 automation. As described, in recent years, autonomous vehicles have been developed by a large number of companies and research institutes around the world.

In order to develop these autonomous systems, we need to introduce three factors into systems: “Vehicle, Environment, and Human” [13]. In particular, automated systems under level 3 always involve humans during autonomous driving since human drivers need

Level	Name	Narative Definition	Execution of steering and acceleration/ deceleration	Monitoring of driving environment	Fallback performance of dynamics driving task	System capability (driving modes)
Human driver monitors the driving environment						
0	**No Automation**	the full-time performance by the human driver of all aspects of the dynamic driving task, even when enhanced by warming or intervention systems	Human driver	Human driver	Human driver	n/a
1	**Driver Assistance**	the driving mode-specific execution by a driver assistance system of either steering or acceleration/deceleration using information about the driving environment and with the expectation that the human driver perform all remaining aspects of the dynamic driving	Human driver and system	Human driver	Human driver	Some driving modes
2	**Partial Automation**	the driving mode-specific execution by one or more driver assistance systems of both steering and acceleration/deceleration using information about the driving environment and with the expectation that the human driver perform all remaining aspects of the dynamic driving task	**system**	Human driver	Human driver	Some driving modes
Automated driving system ("system") monitors the driving environment						
3	**Conditional Automation**	the driving mode-specific performance by an automated driving system of all aspects of the dynamic driving task with the expectation that the human driver will respond appropriately to a request to intervene	system	**system**	Human driver	Some driving modes
4	**High Automation**	the driving mode-specific performance by an automated driving system of all aspects of the dynamic driving task, even if a human driver does not respond appropriately to a request to intervene	system	system	**system**	Some driving modes
5	**Full Automation**	the full-time performance by an automated driving system of all aspects of the dynamic driving task under all roadway and environmental conditions that can be managed by a human driver	system	system	system	**All driving modes**

Figure 1.2: SAE International: Summary of levels of driving automation for on-road vehicles

to resume vehicle operations from the automation system or intervene during emergency situations. These systems that involve humans are often called “Human-in-the-Loop” systems. Besides, we need to design a system that can be trusted by humans and used widely. The Engineering aspects such as vehicle control and environment recognition can be dealt with by using the mathematical theory, and there have been good progress in its development due to the improvements in computational power. However, understanding humans with complex and sophisticated systems is the most difficult research area, and it is hard to directly introduce human factors into automated systems. In the research field of security, this situation, where we cannot design systems with human factors although human behavior always intervenes in the systems, is called “Weakest Link”, and a design based on understanding user behavior is recommended [14]. The autonomous vehicle should be a system with Human-in-the-Loop; however, it is difficult to develop a system that includes the aspects of both Engineering and Psychology based on human understanding. Hence, in recent years, each research area for automated vehicles is independent of each other.

For instance, due to the remarkable development of machine learning techniques in recent years, methods based on big data such as Deep Learning are often used in automated systems [15]. Deep Learning itself is a model that mimics the brain structure of humans. It can simulate human behavior with high accuracy. However, it is not easy to understand how they work and ensure the stability of the model compared to the mathematical model. In methods such as Deep Learning, it is difficult to incorporate both systems and human factors without understanding the models. As a result, the system strongly depends on the Engineering aspect. On the other hand, some studies have been conducted based on the Psychology aspect in order to estimate the necessary time for human drivers to resume control from automation systems [16]. This estimated time is often applied to alarming systems. It is effective to construct these systems based on the results of the measurement experiments; however, such a system will not have advanced intelligence equivalent to that of drivers because this is not considered to directly introduce human factor indicators.

Therefore, even though it is necessary to construct automated systems with the deep interaction between Engineering and Psychology, the current autonomous systems cannot sufficiently include both the elements. The automated systems that do not have high affinity with human drivers could give drivers a feeling of discomfort and distrust. This could disturb the spread of automated driving vehicles although it has the potential to solve various social problems. Therefore, a new technology based on a fusion of Engineering and Psychology is necessary for the future.

1.2 Aims of This Study

As described in Section 1.1, in order to solve various social problems, we need to design Human-in-the-Loop automated driving systems that involve the aspects of both Engineering and Psychology. For this, we use a method to model the visual information drivers perceive while their driving as a mathematical model, and apply the modeling results to a nonlinear control approach. Thereby, a system that incorporates human factors can be constructed. This method implements the general knowledge of human behavior from the field of Psychology into the automated system, so that there is a possibility that this system can simulate human-like behavior. In addition, the simulation/experiment results generated by the proposed human-like driving system give us some insight into the

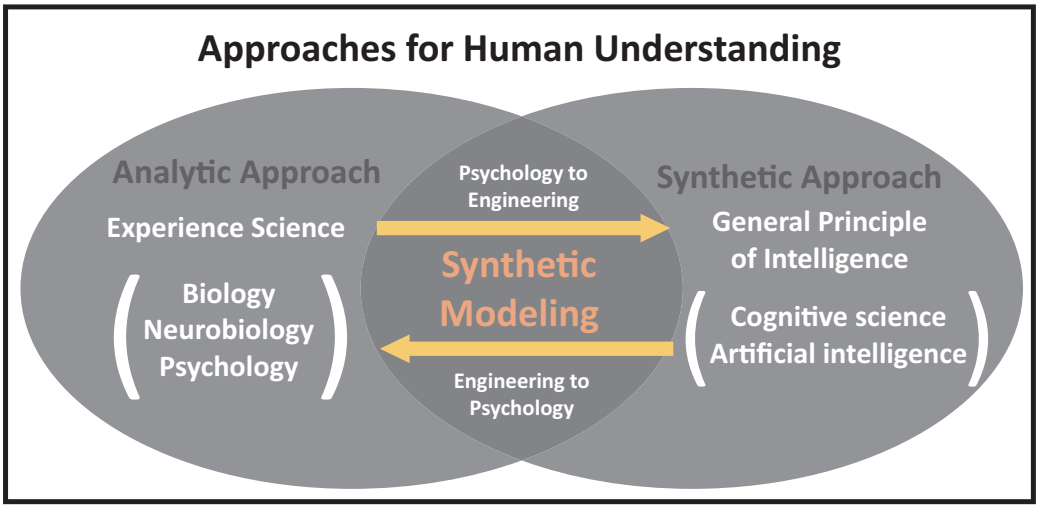

Figure 1.3: Overview of Synthetic Modeling

driver's perception-steering behavior. The psychological experiment based on the knowledge from Engineering aspects is tested in order to figure out new driver behaviors. In general, hypotheses are made by researcher insight. In contrast, the hypothesis in this study is made on the basis of the results of the proposed human-like systems. Therefore, we can design an effective experimental system. This Human-in-the-Loop research system is called 'Synthetic Modeling', in which Psychology can contribute to Engineering and Engineering can contribute to Psychology. There are mainly two approaches for human understanding: Analytic Approach (experience science) and Synthetic Approach (understanding by building). Synthetic Modeling includes two aspects of them (Figure 1.3) [17]. Thus, the aim of this study is to advance both research fields based on the approach of each other in accordance with Synthetic Modeling. It can contribute to the development of automated driving systems that have high intelligence and can understand driver behavior.

1.3 Related Studies

Locomotion is defined as the ability of organisms to move and propel itself from place to place. This is very important for animals including human beings to live in this world. Under complex environments, successful locomotion is achieved by estimating a safe tracking path to the target point, obtaining feedback from physical errors and disturbances, and propelling the body. We humans routinely carry out locomotion based on such

Figure 1.4: Optic flow field generated by observer movement

perception-judgment-motion behavior, regardless of the type of motion such as walking, running, cycling, or driving. If we can understand the locomotion behavior of humans as the mathematical model and implement it into automated driving systems, we can construct driving systems with high intelligence that can reflect the driver's intention. Such systems would contribute to the aims of this study.

The foundation for the use of perception information and control strategy in locomotion behavior was presented by Gibson [18, 19]. Gibson noted that locomotion behavior towards the target point mainly involves visual input. In particular, the visual cue that we need to focus in order to understand locomotion is the "Optic Flow". Optic flow is defined as the velocity vector generated by an animal's motion through a static environment, as shown in Figure 1.4. This optic flow can reflect the translation and rotation movements of observers. Various studies have shown that humans use not only indicators such as distance and angle but also optic flow information for their locomotion strategy towards the target point. One of the features of optic flow is the Focus of Expansion (FoE), which is the point group where the optic flow is 0. FoE is assumed to be capable of reflecting the direction of self-motion of human's movement. Gibson suggested that humans achieve successful locomotion by using optic flow information because humans can move towards the target point if they coincide FoE with the target point.

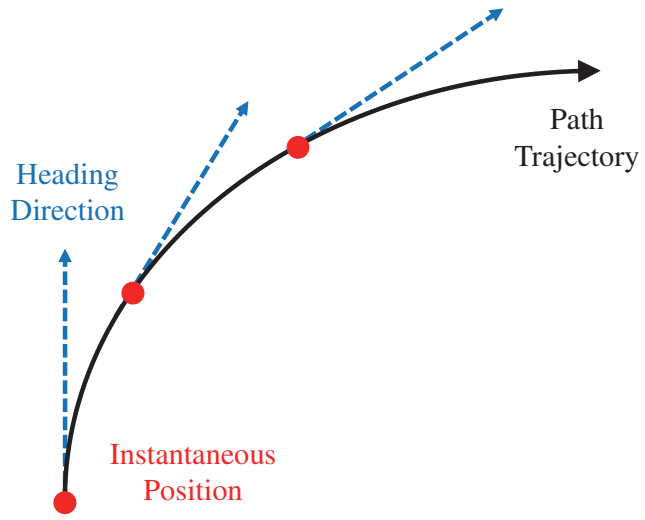

Figure 1.5: Difference between heading direction and path trajectory

Pure optic flow is generated by their body motion; however, the flow pattern on the retina is changed by additional signals of the eye and neck motion, which are often called extra-retinal signals. This changed flow pattern is called "Retinal Flow", and humans perceive the retinal flow pattern rather than optic flow. In situations where humans move along a straight path, FoE is located on an infinity point and its direction is the same as the direction of self-motion. Thus, humans can perceive the heading direction information from FoE if they can acquire extra-retinal signals [20–23]. However, in the case of curved paths, the instantaneous heading direction is located in the tangential direction of the path, as shown in Figure 1.5. Humans cannot move along the target path with high accuracy if they use a strategy in which the heading direction is matched to the target point. Therefore, future path control (or anticipatory control) is more effective for human's movement during curved path than heading control [24–27]. Various studies have verified this issue through psychological experiments, and they have shown that humans can perceive their future path information generated by their current motion from the retinal flow information [21, 28–33]. A straight path is considered as a singular point where the curvature of the curved path is 0; therefore retinal flow information is effective for locomotion in any path. However, humans can also perform locomotion in situations where there is no flow information within human's vision; therefore, in general, optic flow is interpretable as an additional information for locomotion behavior. Other necessary information for locomotion is "Visual Direction", which is the angle between the egocentric direction and the direction toward to the target point, as shown in Figure 1.6 [34–38].

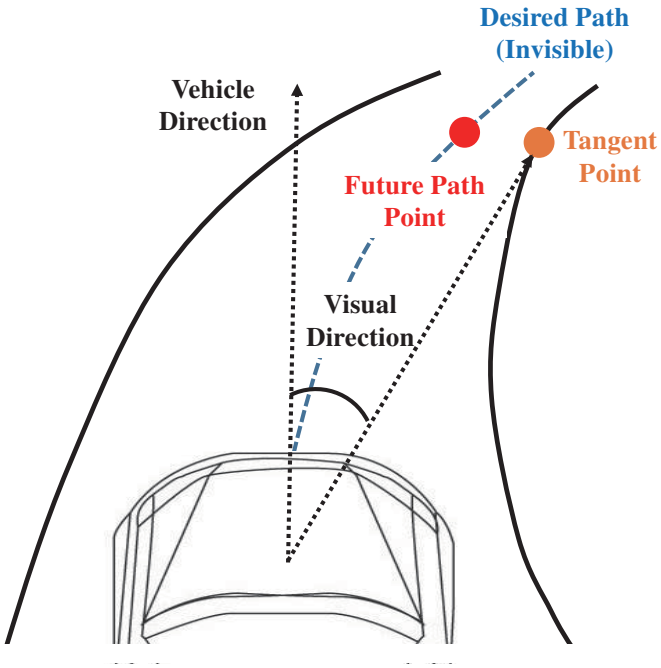

Figure 1.6: Difference between Tangent Point and Future Path Point

The importance of retinal flow for locomotion was shown by some studies; however, we additionally need to consider a point on the tracking path where humans are looking at. As mentioned above, the retinal flow pattern that humans perceive is changed by the eye and neck motion, and therefore the mechanism by which humans gaze at the path and how they perceive the correct information is unclear. Therefore, it is important to figure out their fixation point. The fixation model that was first proposed in relation to human driving is the "Tangent Point", which is shown in Figure 1.6 [39]. Tangent Point is a point on the inner side of the lane where the gaze direction of the driver becomes tangential with respect to the lane edge. The effectiveness of Tangent Point has been verified by some studies [40, 41], whereas recent studies show that "Future Path Point" is more effective in explaining the gaze point of drivers [25, 42–47]. Future Path Point is an arbitrary point on the desired path, e.g. center of the lane. In particular, Kountouriotis et al. showed that drivers cannot perform steering control correctly while they gaze at points other than Future Path Point [48]. Therefore, drivers can perceive the correct path information when they fixate on the point on the future path or 'Where you want to go'. Simultaneously, they can also perceive Visual Direction information from the future path point. As a result, Future Path Point is considered to be effective in explaining driver gazing behavior. Note that, in this study, Look-ahead fixations are not considered. Look-ahead fixations are

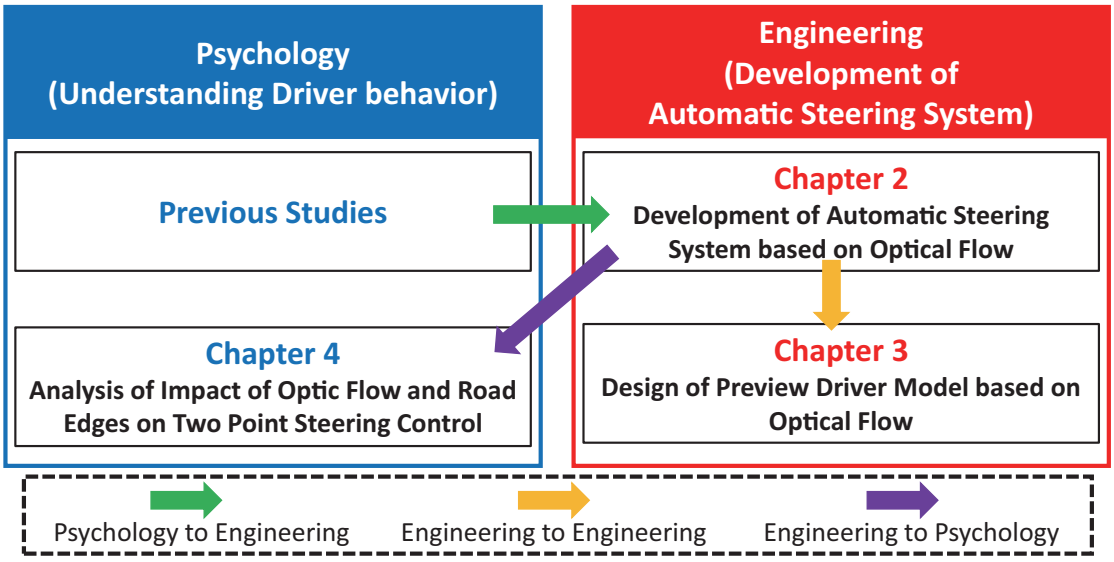

Figure 1.7: Flow of this thesis

defined that the drivers make an eccentric fixation towards the road further up, such as looking at occlusion point, road signs, and so on [49–51]. This behavior is considered as high-level tasks, such as trajectory planning, not to engage the visual guidance of online steering control; therefore, we do not consider this behavior in this study.

In general, retinal flow is an important information for human locomotion. In particular, optic or retinal flow is effective for modifying the direction perception in situations where the road curvature changes and the road is featureless [35, 52]. However, although the fact that flow information is important for locomotion has been established in the field of Psychology, there are few cases to directly implement it into vehicle control [53–56]. In this thesis, a vehicle control method based on optic flow information is proposed in order to construct a method that can reproduce the human locomotor behavior.

In this thesis, we use both “Optic Flow” and “Optical Flow”, which are used as metrics of Psychology and Engineering, respectively. In addition, we do not distinguish between “Optic Flow” (or Optical Flow) and “Retinal Flow”, and we call them both optic flow (or optical flow) in this thesis.

1.4 Composition of This Thesis

The composition of this thesis is as follows. The flow of this thesis is shown in Figure 1.7.

In Chapter 2, we develop a mathematical model of optical flow acquired from a camera image. We derive the FoE point group, which is the source point of optical flow, then we verify whether or not FoE can represent the direction of self-motion correctly as an aspect of Engineering, and confirm the effectiveness of the optical flow model for automated steering control. Next, we propose a nonlinear control theory of optical flow based on Lyapunov function referring to the results of FoE. The proposed method is tested through vehicle simulations and experiments. We confirm the effectiveness of the optical flow model as the control performance, and confirm that the proposed steering control method based on optical flow can reproduce human-like driving behavior.

In Chapter 3, an engineering steering control method, namely the preview/predictive driver model, is interpreted based on the optical flow theory derived in Chapter 2. The preview/predictive driver model is a famous driver model that express the gaze-steering behavior of drivers. We can interpret the model in detail by using the knowledge of optical flow, which is a visual characteristic. In addition, we apply the idea of optical flow to the preview/predictive driver model in order to construct the new driver model, considering the driver visual characteristic. The proposed model is verified through vehicle simulations in order to confirm its effectiveness.

In Chapter 4, we try to figure out the relationship between steering performance and optic flow information with respect to driver gazing, referring to the results in Chapter 2. In Chapters 2 and 3, we apply the knowledge acquired from the aspect of Psychology to Engineering, whereas in this chapter, we apply the results of the aspect of Engineering to the psychological experiments. From the simulation results of Chapter 2, it is seen that there is a relationship between the distance of gaze point of the driver and optic flow at that point. Therefore, the driver's visual-steering behavior is tested within the scope of the Two-point steering control model. The two-point model is a driver model that represents general driver visual-steering behavior in which they perceive some information from the far and near regions in the entire vision. In this driver model, we construct a special environment in the simulator that can selectively mask either the optical flow or the road edge information. Then, we verify how these two information affects the steering performance of the driver.

Finally, we summarize all the results of these studies as the conclusion and describe the future research in Chapter 5.

Chapter 2

Development of Automatic Steering System based on Optical Flow

2.1 Introduction

In the recent automobile societies, car ownership around the world has been increasing each year. Because of this, the social need for safety has also been increasing. As a consequence, advanced technologies such as driving support, preventive safety, and crash safety have been developed. Practical applications of driving support among these technologies are already available, such as the lane keeping assist (LKA) and adaptive cruise control (ACC). However, these automated driving systems which do not include human factors sometimes give drivers feeling of discomfort and distrust since the operation calculated by the systems is the difference from the behavior of the human drivers. Therefore, it is desired to develop comfortable driving support systems experienced by expert drivers. In this chapter, we introduce a human-oriented system for an automatic steering system which is a part of the driving support systems. We simulate the human factor between the driver's visual information processing and steering technique.

In terms of longitudinal control which includes the acceleration and deceleration, there are a number of studies which have focused on braking behavior in car-following situations. Lee proposed the longitudinal control method based on time-to-collision (TTC) associated with driver's visual input [57]. Goodrich and Boer characterized human braking behavior in the phase plane of TTC and time headway (THW) [58]. The risk perception of the lead vehicle in car-following situations was investigated based on both visual cues of TTC and THW [59]. Wada et al. proposed K_{dB} as an index related to the driver's risk

perception and implemented it into collision avoidance systems [60]. Their findings have implied that the drivers perceive the timing of the brake initiation and deceleration based on their perceptual risk. These longitudinal control methods are constructed based on an index of driver's perceptual information modeled by the experimental results, and they have been effective in driving assistance systems. On the other hand, there are also a lot of studies about lateral steering control based on driver behavior. Although each visual cue is not consistent, either of lateral deviation in the predictive point of the vehicle [61] and Visual Direction with/without cognitive model [62, 63] is used for steering control. All of them are based on driver's visual cue, and they have shown that these visual cues are effective for a driver steering model.

As a basis of human factors in this study, we focus on optical flow which is one of the visual information that drivers perceive as described in detail in Section 1.3 [18,19]. Optical flow is the velocity vector generated on the retina of the humans. Drivers perceive the flow pattern that integrates the motions generated by the vehicle motion and extra-retinal signals such as eye and neck motion, as shown in Figure 2.1. One of characteristics of optical flow is effective for drivers to perceive the direction of self-motion based on the focus of expansion (FoE), which is the source point of optical flow [21, 28–33]. Gibson showed that we can reach the target point by matching to the direction of self-motion. Although studies are being actively carried out on the optical flow itself, few have examined introducing optical flow into some system directly. In general, control methods based on image information are divided into two groups: position-based control, which uses the position and attitude of the control object obtained from image information; and image-based control, which does not explicitly deal with the position and attitude but rather directly defines the state quantity and control purpose on the image plane [64, 65]. Inou et al. considered a position-based method using optical flow [53, 54]. The merit of making position-based control is that the control method becomes simpler and easy interpretable models, whereas it is not human-like method since the information in the image plane is converted others. On the other hand, some studies have examined using image-based control for posture stabilization [66, 67]. Optical flow is generally used for human locomotion, however, flow information has not been applied to tracking control for automated vehicles.

In this chapter, we derive the mathematical model of FoE and confirm it has the effectiveness for perceiving the direction of self-motion. Then, we present the design of

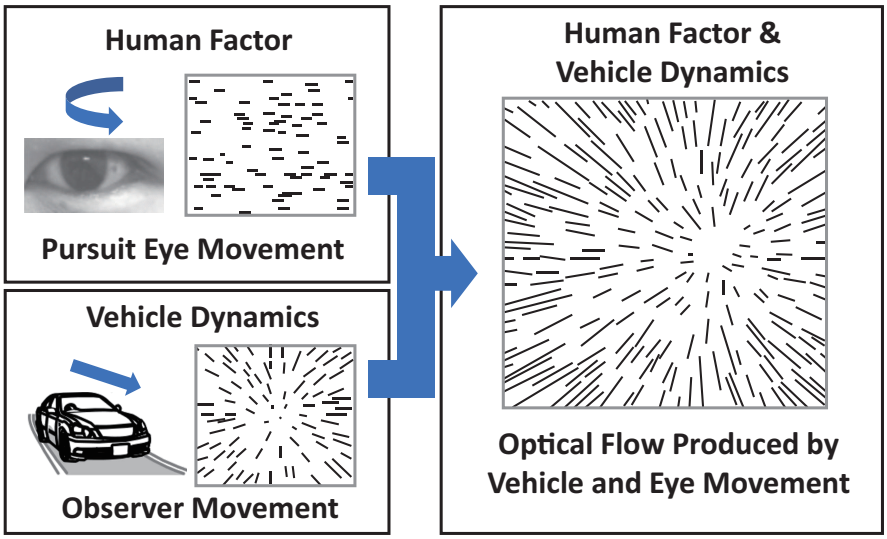

Figure 2.1: Retinal flow pattern integrating vehicle dynamics and eye movement

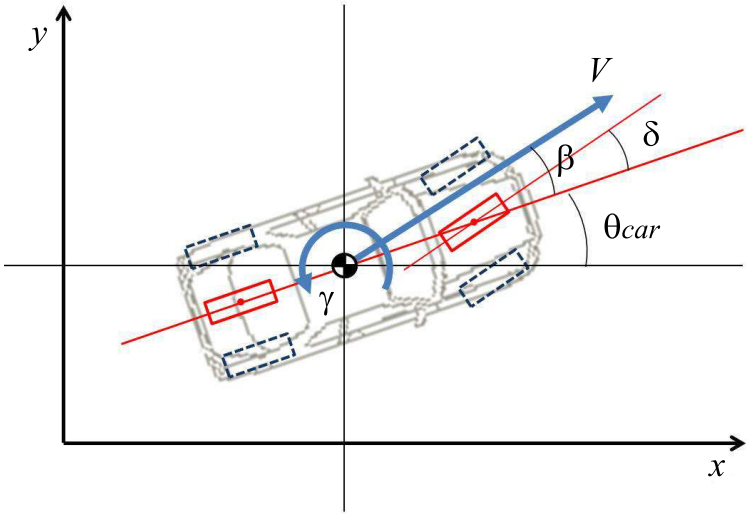

Figure 2.2: Single-track model

an automatic steering controller for the purpose of tracking control based on optical flow. Finally, we confirmed the effectiveness of the proposed method through a vehicle simulation.

2.2 Vehicle Dynamics

In this study, we used a single-track model for the vehicle dynamics, as shown in Figure 2.2 [68]. This is a motion model of the vehicle where the right and left wheels at the front and rear are concentrated on the intersection of the longitudinal axis and axletree

equivalently. The vehicle motion at the center of gravity is as follows:

$$\frac{d}{dt}\begin{bmatrix} x \\ y \\ \theta_{car} \end{bmatrix} = \begin{bmatrix} \cos(\theta_{car}+\beta) & 0 \\ \sin(\theta_{car}+\beta) & 0 \\ 0 & 1 \end{bmatrix}\begin{bmatrix} V \\ \gamma \end{bmatrix}, \tag{2.1}$$

where x, y are the position of the vehicle coordinates, θ_{car} is the yaw angle, β is the slip angle, V is the velocity, and γ is the yaw rate of the vehicle.

The dynamics is described as follows:

$$\frac{d}{dt}\begin{bmatrix} \beta \\ \gamma \end{bmatrix} = \begin{bmatrix} A & B \\ C & D \end{bmatrix}\begin{bmatrix} \beta \\ \gamma \end{bmatrix} + \begin{bmatrix} E \\ F \end{bmatrix}\delta, \tag{2.2}$$

where

$$\begin{bmatrix} A & B \\ C & D \end{bmatrix} = \begin{bmatrix} -\frac{2(K_f+K_r)}{mV} & -\frac{mV+\frac{2}{V}(l_fK_f-l_rK_r)}{mV} \\ -\frac{2(l_fK_f-l_rK_r)}{I_{car}} & -\frac{2(l_f^2K_f+l_r^2K_r)}{I_{car}V} \end{bmatrix},$$

$$\begin{bmatrix} E \\ F \end{bmatrix} = \begin{bmatrix} \frac{2K_f}{mV} \\ \frac{2l_fK_f}{I_{car}} \end{bmatrix}.$$

K_f, K_r are the cornering stiffness of the front and rear axles, l_f, l_r are the distances from the vehicle's center of gravity to the front and rear tire axles, m is the mass, and I_{car} is the moment of inertia of the vehicle. Here, we assume that K_f and K_r are constant, that is, the road condition is invariant. Also the velocity V is constant and a turning radius is large to use the single-track model.

2.3 Focus of Expansion

The Focus of Expansion (FoE) is the source point of optical flow and shows the direction of the vehicle's motion. In this section, we provide the derivation of the FoE using a camera in order to confirm whether the FoE successfully gives us the correct direction of self-motion.

2.3.1 Modeling of Focus of Expansion

We derive a mathematical model of the FoE generated on a camera. If a mathematical formula of the FoE can be built, the direction of the vehicle's motion can be perceived. We assume that the rolling, pitching, and vertical motions are neglectable because we consider

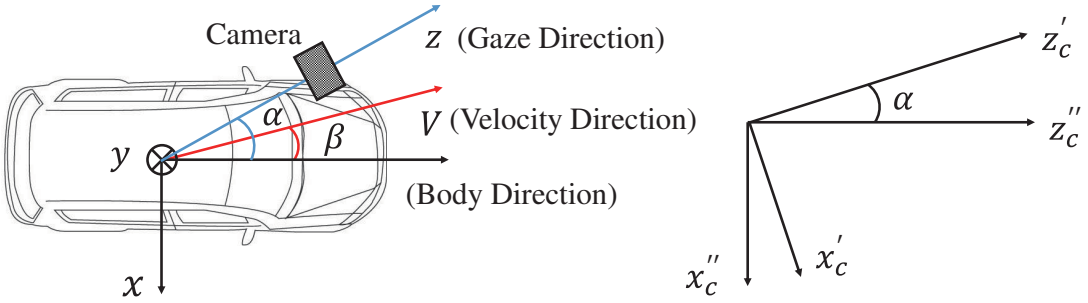

Figure 2.3: Vehicle coordinates (camera: α [rad], $\phi = 0$ [rad])

the ideal situation where the vehicle velocity is constant, the turning radius is large, and there are no irregularity and gradient on the running road. Therefore, we can only derive the FoE in the horizontal direction because a vehicle only moves in the direction by the vehicle steering.

Figure 2.3 shows the vehicle coordinates $[x_c'', y_c'', z_c'']^T$ and gaze coordinates $[x_c', y_c', z_c']^T$. The camera is located at the center of the vehicle and gazes in the direction of the angle α that is between the vehicle axis and target direction. Because this camera movement is equivalent to the human behavior that is eye and neck movements toward the target point, we can derive the FoE in the same manner as for human behavior. As an additional condition, the elevation angle ϕ of the camera is set to 0 deg.

We transform the position of the target to the image plane $[X, Y]^T$ by perspective transformation:

$$\begin{bmatrix} X \\ Y \end{bmatrix} = f \begin{bmatrix} \frac{x_c'}{z_c'} \\ \frac{y_c'}{z_c'} \end{bmatrix}, \tag{2.3}$$

where f is the focal length of the camera.

Optical flow on the image plane can be expressed as follows:

$$\begin{bmatrix} u \\ v \end{bmatrix} = \frac{d}{dt} \begin{bmatrix} X \\ Y \end{bmatrix} = f \begin{bmatrix} \frac{\dot{x}_c' z_c' - x_c' \dot{z}_c'}{z_c'^2} \\ \frac{\dot{y}_c' z_c' - y_c' \dot{z}_c'}{z_c'^2} \end{bmatrix}, \tag{2.4}$$

where u, v are the horizontal and vertical optical flows, respectively.

We change the vehicle coordinates $[x_c'', y_c'', z_c'']^T$ to the gaze coordinates $[x_c', y_c', z_c']^T$ for looking around y_c'' axis by α:

$$\begin{bmatrix} x_c' \\ y_c' \\ z_c' \end{bmatrix} = \begin{bmatrix} \cos\alpha & 0 & -\sin\alpha \\ 0 & 1 & 0 \\ \sin\alpha & 0 & \cos\alpha \end{bmatrix} \begin{bmatrix} x_c'' \\ y_c'' \\ z_c'' \end{bmatrix}. \tag{2.5}$$

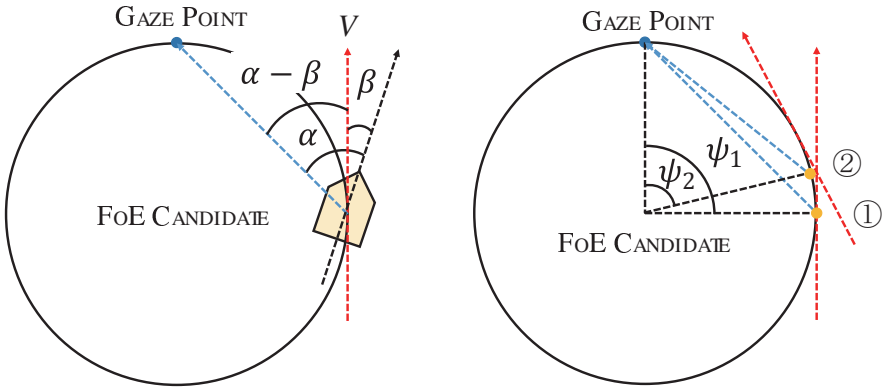

Figure 2.4: Situation where FoE and target point are matched

The velocity of the target points in the vehicle coordinates $[x_c'', y_c'', z_c'']^T$ is given as follows:

$$\begin{bmatrix} \dot{x}_c'' \\ \dot{y}_c'' \\ \dot{z}_c'' \end{bmatrix} = \begin{bmatrix} V_x \\ V_y \\ V_z \end{bmatrix} + \begin{bmatrix} \Omega_x \\ \Omega_y \\ \Omega_z \end{bmatrix} \times \begin{bmatrix} x_c'' \\ y_c'' \\ z_c'' \end{bmatrix}, \tag{2.6}$$

where $\boldsymbol{V}$, $\boldsymbol{\Omega}$ are the translation and angular velocity, respectively.

Since the rolling, pitching, and vertical motions are neglectable, $\boldsymbol{V}$ and $\boldsymbol{\Omega}$ of Equation (2.6) are presented as follows:

$$\begin{bmatrix} V_x \\ V_y \\ V_z \end{bmatrix} = \begin{bmatrix} -V\sin\beta \\ 0 \\ -V\cos\beta \end{bmatrix}, \quad \begin{bmatrix} \Omega_x \\ \Omega_y \\ \Omega_z \end{bmatrix} = \begin{bmatrix} 0 \\ \gamma + \dot{\beta} \\ 0 \end{bmatrix}. \tag{2.7}$$

Using Equation (2.7), Equation (2.6) can be rewritten as follows:

$$\begin{bmatrix} \dot{x}_c'' \\ \dot{y}_c'' \\ \dot{z}_c'' \end{bmatrix} = \begin{bmatrix} -V\sin\beta + (\gamma + \dot{\beta})z_c'' \\ 0 \\ -V\cos\beta - (\gamma + \dot{\beta})x_c'' \end{bmatrix}. \tag{2.8}$$

By substituting Equations (2.5) and (2.8) into Equation (2.4), we get the following:

$$u = f\frac{\left\{(\gamma + \dot{\beta} - \dot{\alpha})z_c' + V\sin(\alpha - \beta)\right\}z_c' - x_c'\left\{-(\gamma + \dot{\beta} - \dot{\alpha})x_c' - V\cos(\alpha - \beta)\right\}}{z_c'^2}. \tag{2.9}$$

The FoE, whose horizontal optical flow is zero, can be given by $u = 0$. Then, the following equation is obtained:

$$\left(x_c' + \frac{V\cos(\alpha - \beta)}{2(\gamma + \dot{\beta} - \dot{\alpha})}\right)^2 + \left(z_c' + \frac{V\sin(\alpha - \beta)}{2(\gamma + \dot{\beta} - \dot{\alpha})}\right)^2 = \left(\frac{V}{2(\gamma + \dot{\beta} - \dot{\alpha})}\right)^2. \tag{2.10}$$

Then, we consider a condition that the FoE and target point are matched as shown in Figure 2.4. In the left figure, the angle between the velocity direction and gaze direction

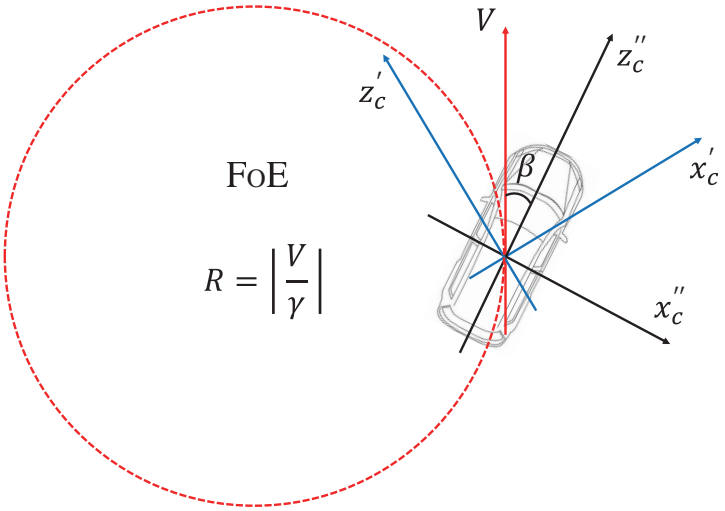

Figure 2.5: FoE (camera: α [rad], $\phi = 0$ [rad])

is given by $\alpha - \beta$ because the angle between the vehicle axis and velocity direction is β. In the right figure, we describe point ② of the vehicle position from point ① after the minute time dt. If the subscripts correspond to each position, the following relations hold:

$$\frac{1}{2}\psi_i = \alpha_i - \beta_i \ (i = 1, 2). \tag{2.11}$$

Equation (2.11) changes during the minute time dt:

$$\frac{1}{2}\lim_{dt\to 0}\frac{\psi_2 - \psi_1}{dt} = \lim_{dt\to 0}\frac{\alpha_2 - \alpha_1}{dt} - \lim_{dt\to 0}\frac{\beta_2 - \beta_1}{dt}. \tag{2.12}$$

We assume $\lim_{dt\to 0}\frac{\psi_2-\psi_1}{dt} = \gamma$; thus, Equation (2.12) can be rewritten as follows:

$$\frac{1}{2}\gamma = \dot{\alpha} - \dot{\beta}. \tag{2.13}$$

By substituting Equation (2.13) into Equation (2.10), we get the following:

$$\left(x_c' + \frac{V\cos(\alpha - \beta)}{\gamma}\right)^2 + \left(z_c' + \frac{V\sin(\alpha - \beta)}{\gamma}\right)^2 = \left(\frac{V}{\gamma}\right)^2. \tag{2.14}$$

As a result, the FoE shows a circular orbit as shown in Figure 2.5. This result corresponds to the vehicle motion on a steady turning circle with a radius V/γ. This result means that the FoE correctly shows the direction of the vehicle's motion. Furthermore, the FoE without the use of a camera also corresponds to this result [54].

In the above derivation, Equation (2.13) is only satisfied when the target point matches the FoE. However, because we control the FoE to match the target point, the former does

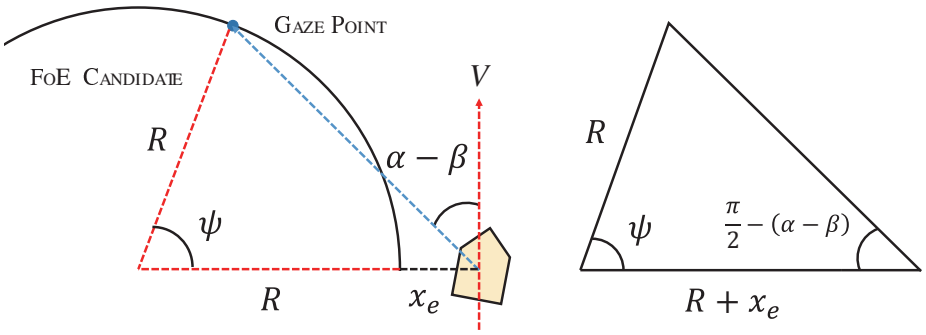

Figure 2.6: Situation where FoE and target point are not matched

not normally correspond to the latter. Therefore, when they are not matched, it is necessary that Equation (2.13) be approximately satisfied. Figure 2.6 shows a geometric relation where the vehicle has a deviation x_e from the target orbit. We use this to approximately derive Equation (2.13).

The right side of Figure 2.6 shows a triangle that connects the center of the vehicle, the target point, and the center of the FoE candidate. The geometric constraint is determined by the laws of sines as follows:

$$\frac{R + x_e}{\sin\left(\frac{\pi}{2} + X_1 - \frac{\psi}{2}\right)} = \frac{R}{\sin\left(\frac{\pi}{2} - X_1 - \frac{\psi}{2}\right)}, \tag{2.15}$$

where $X_1 = \alpha - \beta - \frac{\psi}{2}$.

Equation (2.15) is expressed as follows:

$$X_1 = \tan^{-1}\left(\frac{x_e}{2R + x_e}\frac{1}{\tan\frac{\psi}{2}}\right). \tag{2.16}$$

As a result,

$$\frac{1}{2}\psi = \alpha - \beta - \tan^{-1}\left(\frac{x_e}{2R + x_e}\frac{1}{\tan\frac{\psi}{2}}\right). \tag{2.17}$$

If $R \gg x_e$ is satisfied, Equation (2.17) equals Equation (2.11). When this situation is satisfied, we can confirm the effectiveness of the FoE ,which represents the direction of the vehicle's motion.

2.3.2 Interpretation of Model of Eye Movement

We derived the mathematical model of eye movement in Equation 2.13. In the process of derivation, we made one constraint that drivers continuously look at the fixed point on the

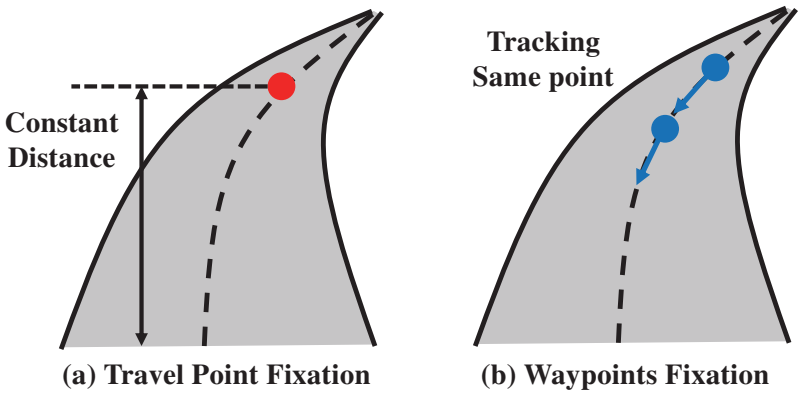

Figure 2.7: Differences between Travel Point Fixation and Waypoints Fixation

target path. Then, the derived FoE is the same as the vehicle motion. We need to confirm whether or not this model is valid as compared with the experimental results.

In some literature about driver fixation behavior in the measurement experiment [44, 45, 47], the driver fixation behavior is divided into two strategies, as shown in Figure 2.7. First is 'Travel Point Fixation' such as when looking at Tangent Point, as shown in Figure 1.6. Next is 'Waypoints Fixation' which is the same as the assumption in this study. The differences between both fixation strategies trigger the generation of the differences of optokinetic nystagmus (OKN). OKN is a small-amplitude eye movement characterized by alternating a slow phase (pursuit) and a quick phase (saccade) movements. In particular, slow phase of OKN during driving is generated by optic flow. The lateral component of OKN during gazing at Tangent Point is similar to zero because the gazing point in the curve situation is fixed. On the other hand, it is measured as approximately the same as the half of vehicle's yaw rate when fixating at Future Path Point. Referring to some experiments [44, 47], OKN has half value of the vehicle's yaw rate when there is no any constraint for drivers. Therefore, drivers fixation strategy is considered as the both of Future Path Point and Waypoints Fixation Strategy.

This eye movement measured in the experiments is similar to the assumption in this study; therefore, we deal with the Equation 2.13 as the actual human eye movement.

2.4 Design of Nonlinear Controller

In this section, we present the derivation of a nonlinear controller to track circular turning. The aim of a controller is to match the FoE generated by the current vehicle state to the

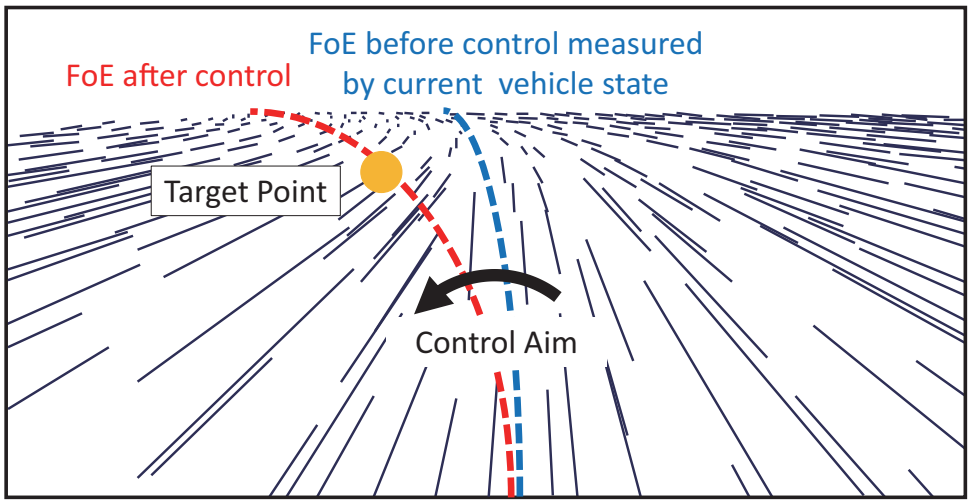

Figure 2.8: Aim of controller

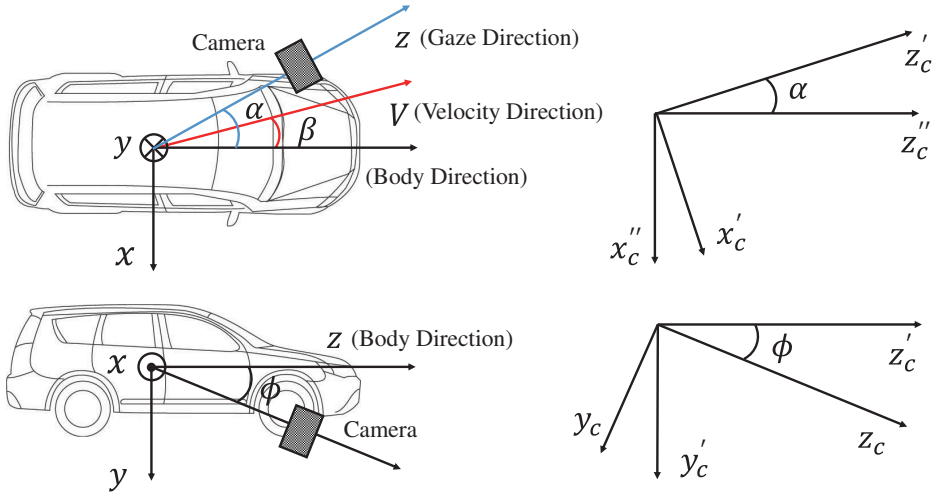

Figure 2.9: Vehicle coordinates (camera: α [rad], $\phi \neq 0$ [rad])

target path when the camera is towards the arbitrary point on the target path, as shown in Figure 2.8. We define the gaze coordinates $[x_c, y_c, z_c]^T$ as when the camera gazes in the direction of the angles α and ϕ, as shown in Figure 2.9. α is the angle between the vehicle axis and the target point. ϕ is the elevation angle and is constant.

We transform the position of the target to the image plane $[X, Y]^T$ by perspective transformation:

$$\begin{bmatrix} X \\ Y \end{bmatrix} = f \begin{bmatrix} \frac{x_c}{z_c} \\ \frac{y_c}{z_c} \end{bmatrix}. \tag{2.18}$$

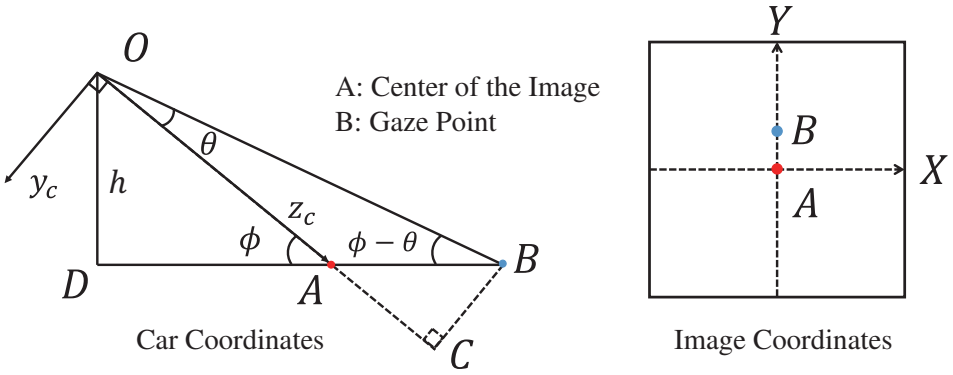

Figure 2.10: Gaze point coordinates

Optical flow on the image plane can be expressed as follows:

$$\begin{bmatrix} u \\ v \end{bmatrix} = \frac{d}{dt}\begin{bmatrix} X \\ Y \end{bmatrix} = f\begin{bmatrix} \frac{\dot{x}_c z_c - x_c \dot{z}_c}{z_c^2} \\ \frac{\dot{y}_c z_c - y_c \dot{z}_c}{z_c^2} \end{bmatrix}. \tag{2.19}$$

We change the coordinates $[x'_c, y'_c, z'_c]^T$ to the gaze coordinates $[x_c, y_c, z_c]^T$ for looking around the x'_c axis by ϕ:

$$\begin{bmatrix} x_c \\ y_c \\ z_c \end{bmatrix} = \begin{bmatrix} 1 & 0 & 0 \\ 0 & \cos\phi & -\sin\phi \\ 0 & \sin\phi & \cos\phi \end{bmatrix}\begin{bmatrix} x'_c \\ y'_c \\ z'_c \end{bmatrix}. \tag{2.20}$$

Equation (2.20) can be differentiated to obtain:

$$\begin{bmatrix} \dot{x}_c \\ \dot{y}_c \\ \dot{z}_c \end{bmatrix} = \begin{bmatrix} 1 & 0 & 0 \\ 0 & \cos\phi & -\sin\phi \\ 0 & \sin\phi & \cos\phi \end{bmatrix}\begin{bmatrix} \dot{x}'_c \\ \dot{y}'_c \\ \dot{z}'_c \end{bmatrix}. \tag{2.21}$$

The differential of Equation (2.5) is given as follows:

$$\begin{bmatrix} \dot{x}'_c \\ \dot{y}'_c \\ \dot{z}'_c \end{bmatrix} = -\dot{\alpha}\begin{bmatrix} \sin\alpha & 0 & \cos\alpha \\ 0 & 0 & 0 \\ -\cos\alpha & 0 & \sin\alpha \end{bmatrix}\begin{bmatrix} x''_c \\ y''_c \\ z''_c \end{bmatrix} + \begin{bmatrix} \cos\alpha & 0 & -\sin\alpha \\ 0 & 1 & 0 \\ \sin\alpha & 0 & \cos\alpha \end{bmatrix}\begin{bmatrix} \dot{x}''_c \\ \dot{y}''_c \\ \dot{z}''_c \end{bmatrix}. \tag{2.22}$$

First, we derive the horizontal optical flow u by the image plane coordinates. By substituting Equations (2.5), (2.8), (2.20), and (2.22) into Equation (2.21), we obtain the following:

$$\dot{x}_c = (\Omega_y - \dot{\alpha})(-y_c \sin\phi + z_c \cos\phi) + V\sin(\alpha - \beta). \tag{2.23}$$

$$\dot{z}_c = \cos\phi\left\{-(\Omega_y - \dot{\alpha})x_c - V\cos(\alpha - \beta)\right\}. \tag{2.24}$$

Based on Equations (2.7), (2.13), (2.23), and (2.24), Equation (2.19) can be rewritten as follows:

$$u = \frac{f\gamma}{2}\left(\frac{x_c^2}{z_c^2} + 1\right)\cos\phi + \frac{fV\cos(\alpha-\beta)\cos\phi}{z_c}\frac{x_c}{z_c} + \frac{fV\sin(\alpha-\beta)}{z_c} - \frac{f\gamma}{2}\frac{y_c}{z_c}\sin\phi. \quad (2.25)$$

By substituting Equation (2.18) into Equation (2.25), we get the following:

$$u = \frac{f\gamma}{2}\left(\frac{X^2}{f^2} + 1\right)\cos\phi + \frac{V\cos\phi}{z_c}X\cos(\alpha-\beta) + \frac{fV\sin(\alpha-\beta)}{z_c} - \frac{\gamma}{2}Y\sin\phi. \quad (2.26)$$

We define a situation of choosing the target to be as shown in Figure 2.10. Then, z_c can be expressed as follows:

$$z_c = OC = OB\cos\theta = \frac{h\cos\theta}{\sin(\phi-\theta)}, \quad (2.27)$$

where h is the height of the camera.

As shown in Figure 2.10, the angle θ between the target point and center of the camera coordinates is given as follows:

$$\theta = \tan^{-1}\frac{BC}{OC} = \tan^{-1}\frac{y_c}{z_c}. \quad (2.28)$$

By using Equation (2.18), Equation (2.28) can be rewritten as follows:

$$\theta = \tan^{-1}\frac{Y}{f}. \quad (2.29)$$

Although θ is variable, $\dot{\theta}$ is zero except for discontinuous parts because we select the target point segmentally.

By substituting Equation (2.27) into Equation (2.26), we get the following:

$$\begin{aligned} u &= \frac{f\gamma}{2}\left(\frac{X^2}{f^2} + 1\right)\cos\phi + \frac{V\cos\phi\sin(\phi-\theta)}{h\cos\theta}X\cos(\alpha-\beta) \\ &\quad + \frac{fV\sin(\phi-\theta)}{h\cos\theta}\sin(\alpha-\beta) - \frac{\gamma}{2}Y\sin\phi. \end{aligned} \quad (2.30)$$

We can derive the horizontal optical flow u by using solely the mesuared information. Next, we determine the control method by using a Lyapunov function to converge the vehicle to the target point [69]. A candidate Lyapunov function is given as follows:

$$V_1 = \frac{1}{2}u^2. \quad (2.31)$$

Equation (2.31) converges to zero if the derivative of the function satisfies the following:

$$\frac{dV_1}{dt} = -k_1 u^2 \leq 0, \tag{2.32}$$

where k_1 is a positive feedback gain.

Because d^2V_1/dt^2 is bounded, dV_1/dt becomes uniformly continuous. Thus, we can accomplish $\lim_{t\to\infty} \frac{dV_1}{dt} \to 0$ by Barbalat's lemma, that is, $u \to 0$. The terms to satisfy Equations (2.31) and (2.32) are given below:

$$\frac{du}{dt} = -k_1 u = -k_1 \frac{dX}{dt}, \tag{2.33}$$

where we use Equation (2.19) to describe the variable of the image plane.

We can achieve $u \to 0$ by deriving a controller that satisfies Equation (2.33). Based on Equations (2.2), (2.30), and (2.33), the nonlinear controller can be derived as follows:

$$\begin{aligned} \delta &= \frac{1}{g(X,Y)}\left[-\left\{\frac{\gamma X\cos\phi}{f} + G\cos(\alpha-\beta) + k_1\right\}\frac{dX}{dt}\right. \\ &\quad \left. +\frac{\gamma}{2}\sin\phi\frac{dY}{dt} + w(\alpha,\beta,\gamma,X,Y)\right], \end{aligned} \tag{2.34}$$

where

$$\begin{aligned} G &= \frac{V\cos\phi\sin(\phi-\theta)}{h\cos\theta} \\ H &= \frac{fV\sin(\phi-\theta)}{h\cos\theta} \\ g(X,Y) &= F\left\{\frac{f}{2}\left(\frac{X^2}{f^2}+1\right)\cos\phi - \frac{Y}{2}\sin\phi\right\} \\ w(\alpha,\beta,\gamma,X,Y) &= \frac{\gamma}{2}GX\sin(\alpha-\beta) - \frac{\gamma}{2}H\cos(\alpha-\beta) \\ &\quad -(C\beta+D\gamma)\left\{\frac{f}{2}\left(\frac{X^2}{f^2}+1\right)\cos\phi - \frac{Y}{2}\sin\phi\right\}. \end{aligned}$$

Here, in the simulation condition of Section 2.6, $g(X,Y)$ does not vanish because this term shows the situation when the camera is nearly directed below. When the vehicle does not achieve tracking, the FoE represented by Equation 2.14 is not matched to the target path, and optical flow on a point on the FoE in Equation 2.14 is not zero. If we choose the point on the FoE (Equation 2.14) in the image plane $[X,Y]^T$ for the controller, the vehicle converges to the point because $u \to 0$.

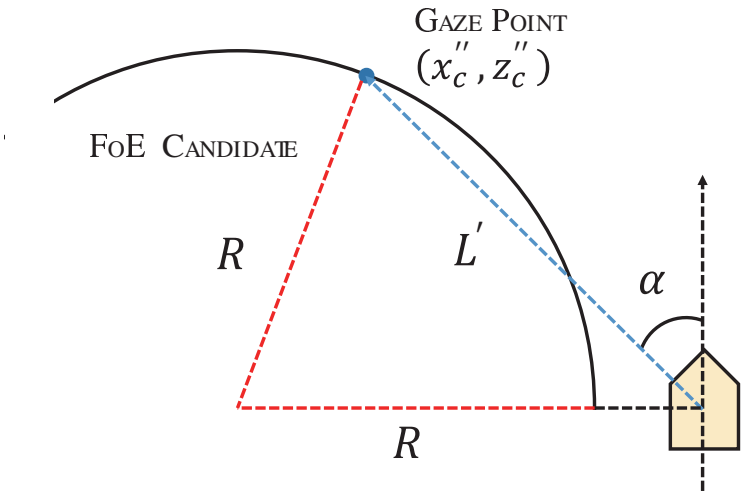

Figure 2.11: Relationship between vehicle and target point

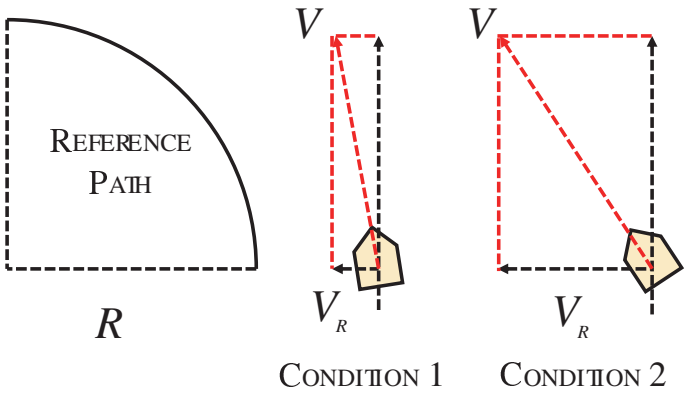

Figure 2.12: V_r condition

2.5 Evaluation of Convergence Performance

When the horizontal optical flow u of the target point converges to zero by applying the nonlinear controller, the convergence performance must be analyzed. In this section, we omit most of the proof because the convergence performance was almost the same as that in [54]. Figure 2.11 shows the geometric relation when the vehicle is far from the target orbit. The gaze point (x_c'', z_c'') is located on the target path. We assume the condition of $\beta = 0$ and $\phi = 0$ deg for simplicity. In addition, we use Equation (2.5) because optical flow of the target points is equivalent to a situation where the camera gazes frontward. Because $\phi = 0$ deg, the gaze coordinates $[x_c, y_c, z_c]^T$ are equal to the coordinates $[x_c', y_c', z_c']^T$. Thus,

Equation (2.25) is rewritten as follows:

$$u = f\frac{x_c''^2 + z_c''^2}{(x_c'' \sin\alpha + z_c'' \cos\alpha)^2}\left(\frac{\gamma}{2} + \frac{x_c''}{x_c''^2 + z_c''^2}V\right). \tag{2.35}$$

When we consider the geometric condition and accomplish $u \to 0$, Equation (2.35) is given as follows:

$$\frac{\gamma}{2} - \frac{\sin\alpha}{L'}\sqrt{V_r^2 + (R'\gamma)^2} = 0, \tag{2.36}$$

where L' is the distance between the vehicle and target point, and V_r is the radius component of the vehicle velocity.

The geometric constraint condition is determined from the law of cosines:

$$R^2 = R'^2 + L'^2 - 2R'L'\cos\left(\frac{\pi}{2} - \alpha\right). \tag{2.37}$$

Equations (2.36) and (2.37) express the geometric relation of the vehicle and target orbit under the condition of $u \to 0$. We investigated the behavior of Equations (2.36) and (2.37) to evaluate the geometric convergence performance. We considered two conditions because Equation (2.36) is affected by V_r.

<Condition 1 : $V_r \approx 0$>

If the current turning radius is large enough, V_r can be approximated as zero as shown in Figure 2.12. Using Equations (2.36) and (2.37), we get the following:

$$R^2 - R'^2 = 0. \tag{2.38}$$

If the vehicle accomplish $u \to 0$, the current turning radius R' converges to the target radius R.

<Condition 2 : $V_r \neq 0$>

If the current radius is small, V_r cannot be ignored as shown in Figure 2.12. Using Equations (2.36) and (2.37), we get the following:

$$R^2 - R'^2 = \frac{L'}{R'}\left(\frac{V_r}{\gamma}\right)^2 \sin\alpha = \frac{x_c''}{R'}\left(\frac{V_r}{\gamma}\right)^2. \tag{2.39}$$

As a result, if V_r cannot be ignored, the requirement that the current turning radius R' converges to target radius R is met by performing the following:

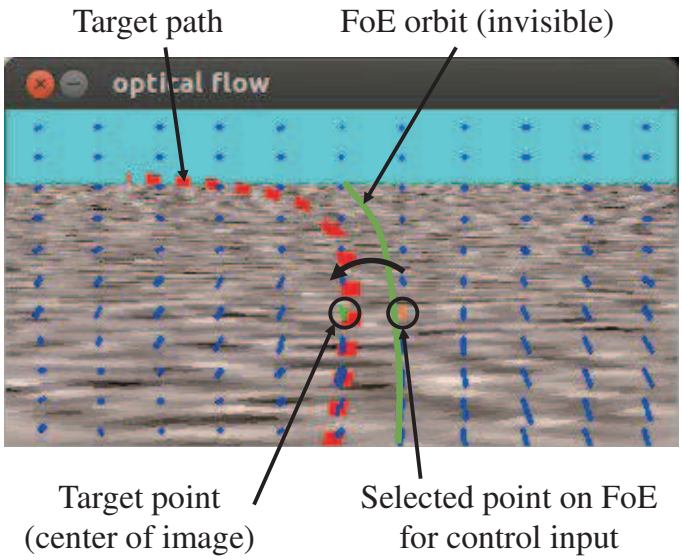

Figure 2.13: OpenGL simulator

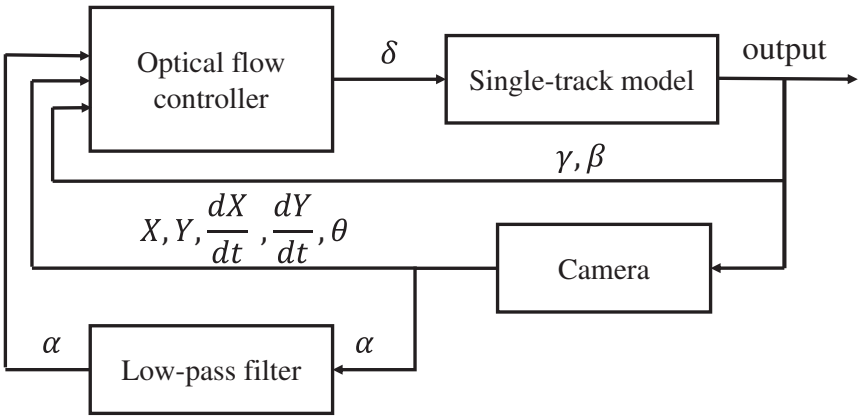

Figure 2.14: Control system

(I) Add Equation (2.39) to the nonlinear controller Equation (2.34).

(II) Choose the target point so that x_c'' becomes sufficiently small.

2.6 Simulation

We confirmed the effectiveness of the proposed method through vehicle simulations. We performed two simulations: (I) comparison of the target fixation points and (II) comparison of the fixation distances.

We used a simulator constructed in OpenGL and Gunnar Farneback's algorithm [70] utilizing OpenCV to detect optical flow. Figure 2.13 shows an appearance of the simulator. The dashed red line, which is the circular orbit from the bottom center to the top left of the image, is the target path. Optical flow was calculated from 11×11 pixels located on the image. We chose one pixel from these pixels as the target point (green point). The camera is towards this point which means the target point is ideally at the center of the image. A point on the FoE represented by Equation 2.14 is chosen for control input. The row of this point is the same as it of the target point. When the target path and calcutated pixel matched, we chose the pixel. However, when the target path and calculated pixel did not match, we continued using the previous selected pixel. When multiple calculated pixels matched the target path, we selected the pixel that was farthest from the vehicle. A general method is recognizing the feature point and calculating optical flow of the feature point. However, because the processing time is longer in order to calculate all pixels in the general method, we use the fixed points in this study. The target path needs to have some thickness in order to match the fixed points because this method does not recognize the feature point. When we accomplish $u \to 0$ by using the proposed method, the FoE orbit matched the target path.

When we determine the target point, the gaze angle α is determined by the geometric relation. Using Equations (2.18) and (2.20), the gaze angle α is given as follows:

$$\alpha = \tan^{-1} \frac{x'_c}{z'_c} = \tan^{-1} \left(\frac{X}{-Y \sin \phi + f \cos \phi} \right). \tag{2.40}$$

We applied the low-pass filter of the time constant T to the gaze angle α because α is discrete when we change the target point. The initial vehicle velocity was located in the tangential direction on the target path, and the initial deviation was zero. In the simulation, we compared the root-mean-squared error and standard deviation of the control performance. Figure 2.14 shows a block diagram of the control system.

There are some methods in order to evaluate driver and control steering performance, such as Steering Bias as steering accuracy, Root Mean Squared Error (RMSE) as steering precision, and Steering Wheel Jerk or Steering Correction as driver fatigue and ride quality. In this section, we use RMSE to evaluate control performance itself and to compare the driver's characteristics.

Table 2.1: Simulation parameters

m	1753.0 [kg]	V	30 [km/h]
l_f	1.437 [m]	h	0.3 [m]
l_r	1.413 [m]	ϕ	3.0 [deg]
K_f	47,500.0 [N/rad]	T	1.2 [s]
K_r	80,000.0 [N/rad]	k_1	1320.0
I_{car}	3559.43 [kgm^2]	ΔT	30 [ms]

Table 2.2: Assumed camera specifications

Imaging sensor	CCD, 1/1.8
Resolution	1664×1224 [pixel]
Pixel size	4.40×4.40 [μm]
Frame rate	30
Focal length f	5.0 [mm]

2.6.1 Comparison of Target Fixation Points

Various studies have shown that the novice and experienced drivers differ in various ways. For instance, novice drivers generally have underdeveloped vehicle control skills [71, 72], adjust visual search less effectively to the environmental situation [73], rely less on peripheral vision [74, 75], show less variability in fixation patterns [76], tend to direct their gaze more often to the immediate near region [77–81]. In particular, the last point, which the fixation point of expert drivers is longer than that of novice drivers, is important to correct tracking since expert drivers choose the target point well for accuracy steering control [54]. Therefore, in this simulation, we compared the situations when the camera gazed at the target path and just forward, that is, $\alpha = 0$. The latter situation represented the driver selecting the wrong point for his or her will. In the next section, we confirm the difference through a simulation between the distance of the target points of expert and novice drivers.

In the simulation, the vehicle followed a 150R steady circle for approximately 15 s. The vehicle velocity was 30 km/h. Tables 2.1 and 2.2 list the simulation and assumed camera parameters. ΔT is a sampling period of the controller. Figures 2.15 and 2.16 show the simulation results. We confirmed the effectiveness of the proposed method and the difference in performance under the two conditions. The simulation result was better when the camera gazed at the target path than straight forward.

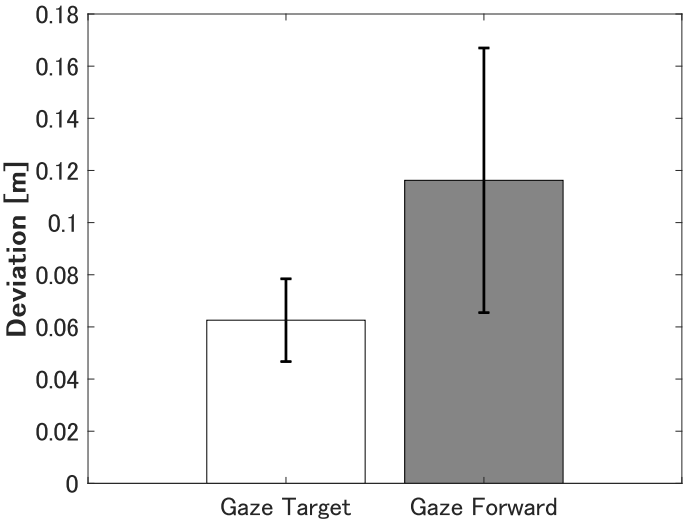

Figure 2.15: Results of comparison of target point

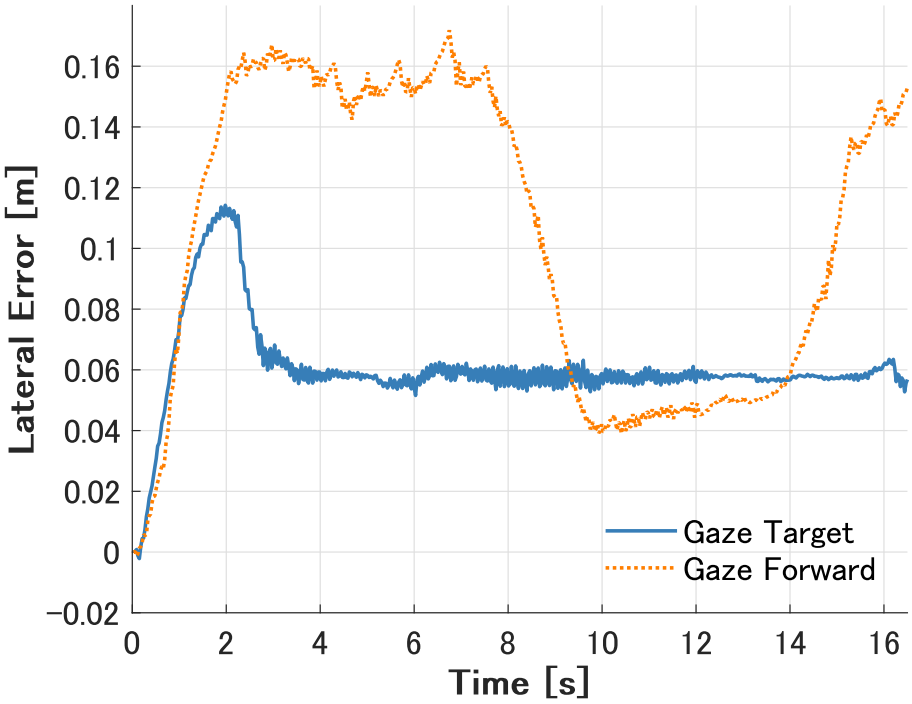

Figure 2.16: Results of comparison of target point (time vs. error)

2.6.2 Comparison of Fixation Distances

We demonstrated that tracking could be performed with a high degree of accuracy when the gaze was maintained on the target. Next, we confirm the difference through a simulation between the distance of the target points of expert and novice drivers. In general, expert drivers select a point farther than novice drivers [77–81]. Therefore, we changed the elevation angle ϕ in the simulation to compare the tracking performance by the fixation

Table 2.3: Distance to fixation point

ϕ [deg]	2.0	2.5	3.0	3.5	4.0	4.5	5.0
L [m]	4.31	3.59	3.30	3.05	3.26	2.96	2.84

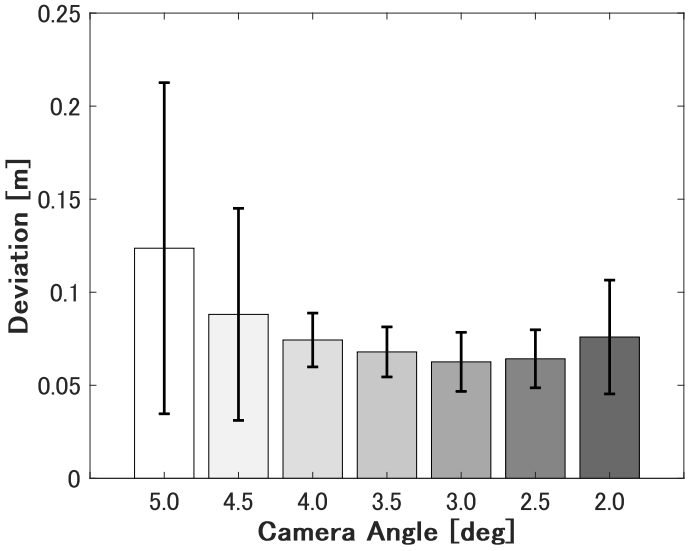

Figure 2.17: Results of comparison of fixation distance

distance.

The simulation conditions were the same as in the previous simulation except for the angle ϕ. We compared the angle ϕ from 2.0 deg to 5.0 deg in increments of 0.5 deg. Figures 2.17-2.19 show the simulation results. Table 2.3 lists the average distance L of each angle, where $DB = L$ as shown in Figure 2.10. Based on these results, the tracking performance improved as the fixation point becomes far away. Thus, the proposed controller correctly simulated the driver behavior. Here, the driver behavior is defined as the characteristics with respect to the vehicle motion that varies with gaze point. When ϕ was less than 2.5 deg, the tracking accuracy became worse. This may have been caused by an increase in pixel errors during the image processing. In addition, L was larger at $\phi = 4.0$ deg than at $\phi = 3.5$ deg. This may be because the vehicle motion was oscillating based on the large standard deviation.

2.6.3 Simulation in Higher Velocity

We show that the controller of the optical flow model is effective in higher velocity. Since optical flow is calculated by the difference of the previous period of image data and the current one, we must shorten the sampling period of the image data. Here, we show the

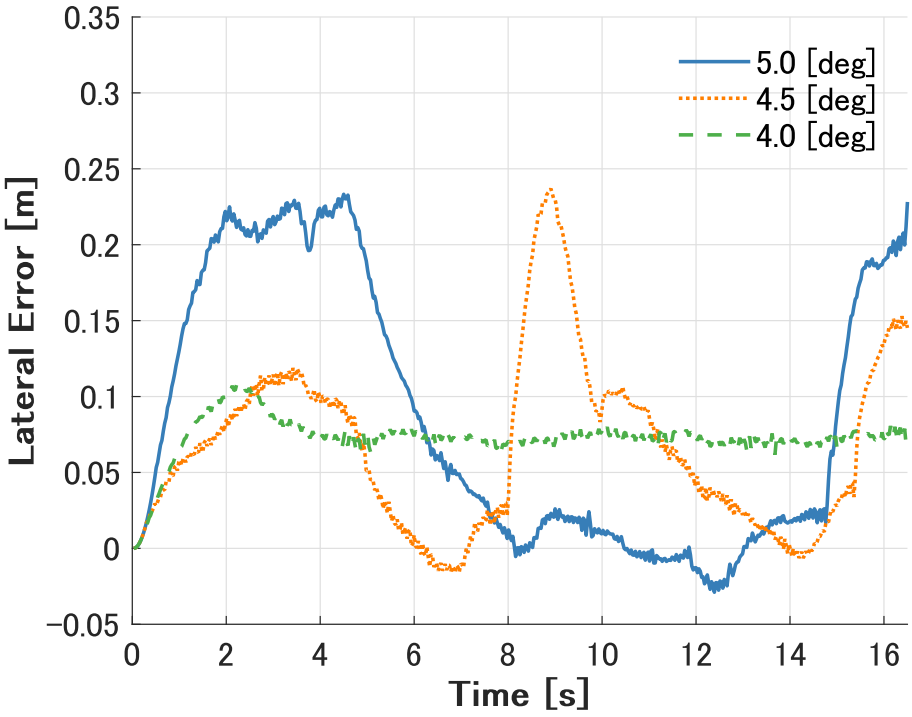

Figure 2.18: Results of comparing of fixation distance 1 (time vs. error)

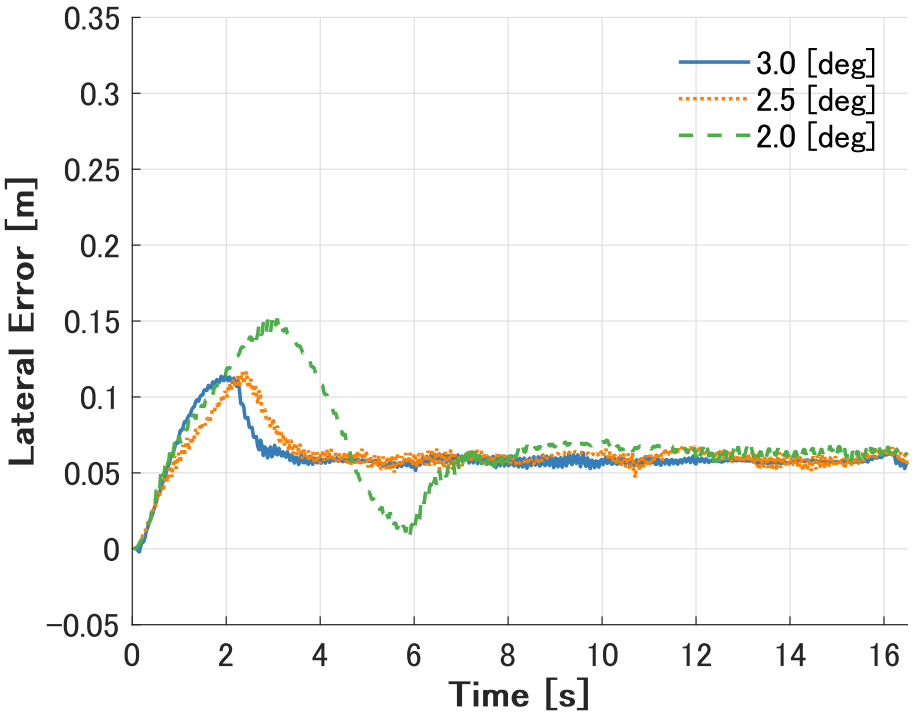

Figure 2.19: Results of comparing of fixation distance 2 (time vs. error)

result of the faster case where the velocity V is 60 and 70 km/h as shown in Figure 2.20. The sampling period is 10 ms compared with 30 ms of Simulation 1 and 2. $\phi = 3.0$

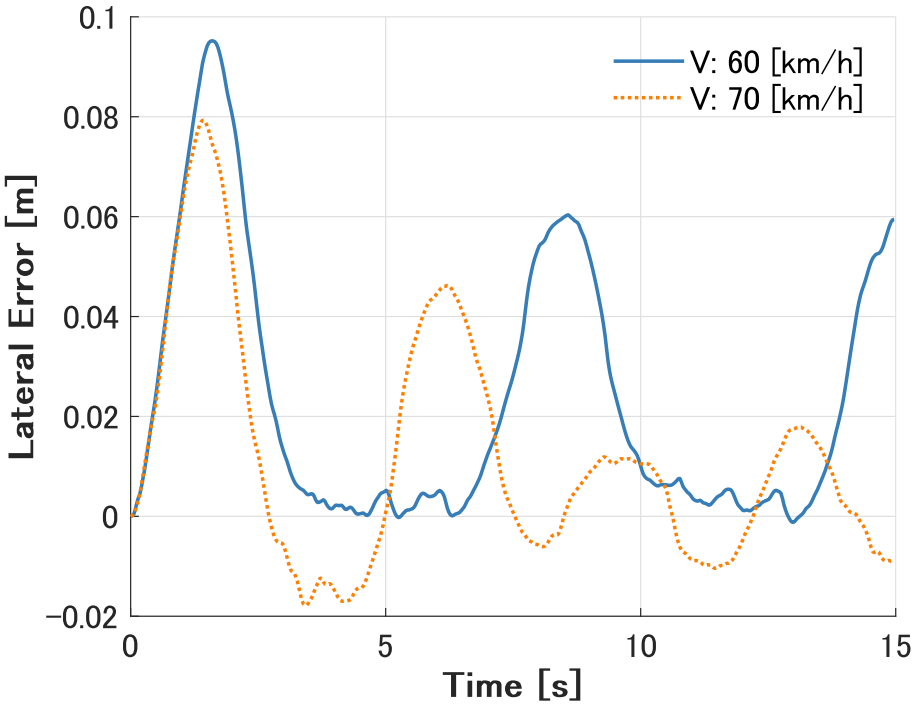

Figure 2.20: Results of higher velocity (time vs. error)

deg. When V is 60 km/h, the result has higher accuracy compared with the case of 30 km/h in Section 2.6.2. When V is 70 km/h, we can understand that the result becomes oscillatory. We also confirmed that the vehicle is more oscillatory in faster case than 70 km/h. Therefore, we can conclude that the proposed controller based on the optical flow model is effective in the higher velocity when the sampling period is short. The possibility of Kalman filter to interpolate the sampling periods has not been tried yet. This is a future subject.

2.7 Design of Nonlinear Controller in Fixed Camera

In this section, we present the derivation of a nonlinear controller to track circular turning when the camera is fixed. In the simulation, it is easy to move the camera toward to the target point, whereas there are some restrictions in the real world. If we use a pan-tilt camera ideal motion like gaze behavior of human drivers is achieved, however, it is not realistic since we need additional control. Firstly, we show the controller when we assume that the camera attached to the vehicles is fixed. Next, we present the controller considering the camera motion simulating human's eye and neck movements in the fixed camera.

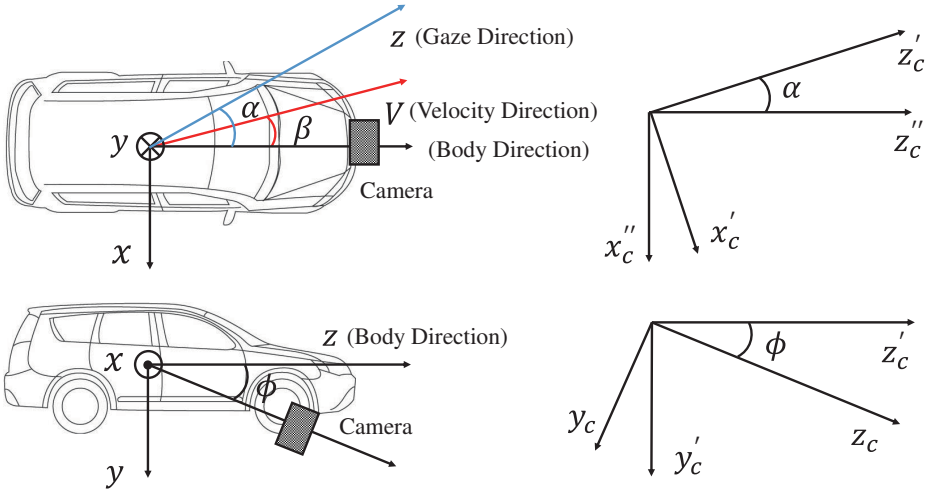

Figure 2.21: Vehicle coordinates (camera: $\alpha = 0$ [rad], $\phi \neq 0$ [rad])

2.7.1 Nonlinear Controller in Fixed Camera

We define the gaze coordinates $[x_c, y_c, z_c]^T$ where the camera gazes in the direction of angle ϕ, as shown in Figure 2.21. The elevation angle ϕ is constant. We assume that the azimuth angle $\alpha = 0$ [rad] because it is difficult to move a camera towards the target path; that is, the camera attached to the vehicle is fixed. We abbreviate the derivation process of optical flow. Optical flow on the fixed camera coordinate is follows:

$$\begin{aligned} u &= f\gamma\left(\frac{X^2}{f^2}+1\right)\cos\phi + \frac{V\cos\phi\sin(\phi-\theta)}{h\cos\theta}X\cos\beta \\ &\quad -f\frac{V\sin(\phi-\theta)}{h\cos\theta}\sin\beta - \gamma Y\sin\phi, \end{aligned} \tag{2.41}$$

where we use the condition of $\alpha = \dot{\alpha} = 0$.

Next, we determine the control method by using a Lyapunov function to converge the vehicle to the target point [69]. A candidate Lyapunov function is the same as the one in Section 2.4, then the nonlinear controller with the fixed camera can be derived as follows:

$$\begin{aligned} \bar{\delta} &= \frac{1}{g(X,Y)}\left[M(\beta,\gamma,\delta)\sin\phi\frac{dY}{dt} + w(\beta,\gamma,\delta,X,Y)\right. \\ &\quad \left.-\left\{\frac{2X\cos\phi}{f}M(\beta,\gamma,\delta) + G\cos\beta + k\right\}\frac{dX}{dt}\right], \end{aligned} \tag{2.42}$$

where

$$
\begin{aligned}
G &= \frac{V\cos\phi\sin(\phi-\theta)}{h\cos\theta} \\
H &= \frac{fV\sin(\phi-\theta)}{h\cos\theta} \\
I &= f\cos\phi\left(\frac{X^2}{f^2}+1\right)-Y\sin\phi \\
g(X,Y) &= \frac{E\left(f\cos\phi\left(\frac{X^2}{f^2}+1\right)-Y\sin\phi\right)}{T}
\end{aligned}
$$

$$
\begin{aligned}
J &= g(X,Y)-FI(B+1)+AEI \\
K &= AI^2-CI(B+1) \\
L &= -DI(B+1) \\
M(\beta,\gamma,\delta) &= E\delta-A\beta+(1-B)\gamma \\
w(\beta,\gamma,\delta,X,Y) &= \{J-E(GX\sin\beta+H\cos\beta)\}\,\delta \\
&\quad +(A\beta+B\gamma)(GX\sin\beta+H\cos\beta)+K\beta+L\gamma,
\end{aligned}
$$

where we assume that the steering angle δ is a first-order lag system of the input, and the steering angle is given as follows:

$$
\dot{\delta} = -\frac{1}{T}\delta+\frac{1}{T}\bar{\delta}, \tag{2.43}
$$

where T is the time constant.

2.7.2 Nonlinear Controller Considering Camera Motion

In the previous subsection, we derived the nonlinear controller by assuming a fixed camera. However, this assumption is problematic. We discuss this problem in this subsection and present a solution to the fixed camera.

When we assume a fixed camera, because $\alpha = \dot{\alpha} = 0$, Equation (2.10), which implies the FoE, can be expressed as follows:

$$
\left(x_c'+\frac{V\cos\beta}{2(\gamma+\dot{\beta})}\right)^2+\left(z_c'-\frac{V\sin\beta}{2(\gamma+\dot{\beta})}\right)^2=\left(\frac{V}{2(\gamma+\dot{\beta})}\right)^2. \tag{2.44}
$$

We can understand that Equation (2.44) represents an orbit that is about 50% of the circular orbit of the original FoE expressed by Equation (2.14). Therefore, the controlled

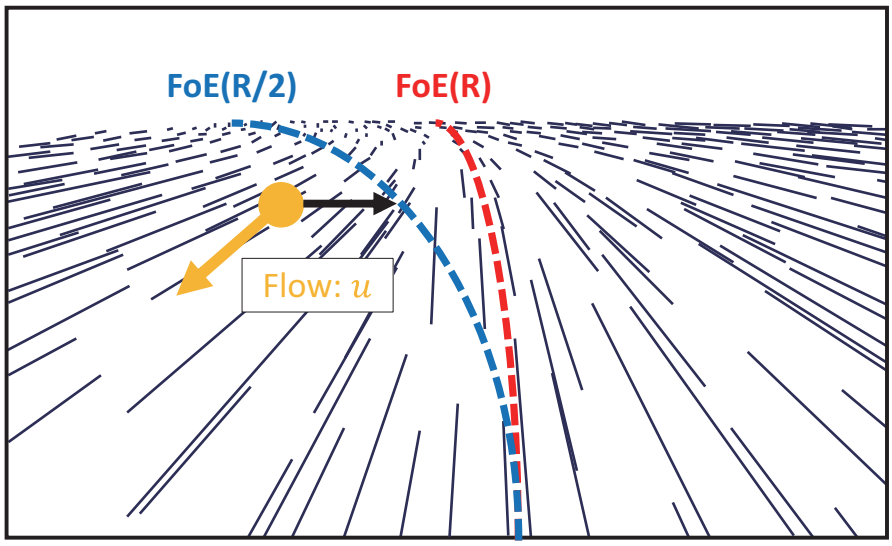

Figure 2.22: Convergence to FoE (R/2)

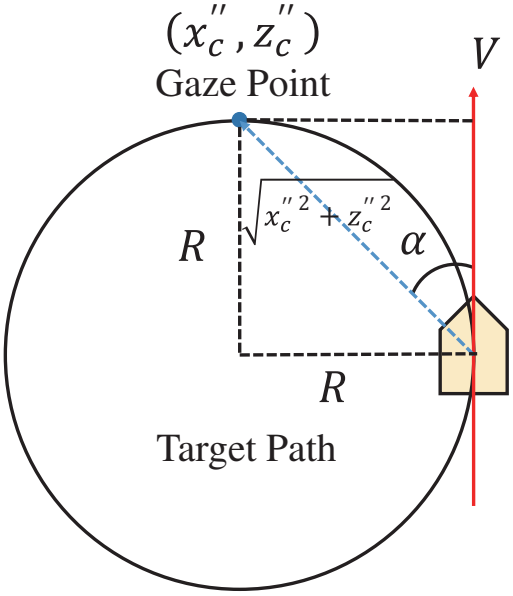

Figure 2.23: Geometric relationship when vehicle is on target path

vehicle cannot converge to the target path, whereas we could converge optical flow of the target point to the FoE, as shown Figure 2.22. In this figure, we define the original FoE expressed by Equation (2.14) and that by Equation (2.44) as FoE (R) and FoE (R/2), respectively.

In this subsection, to resolve this problem, we propose a solution based on the convergence to the target path. We assume the condition of $\beta = 0$ [rad] and $\phi = 0$ [rad]

for simplicity. Because $\phi = 0$ [rad], the gaze coordinates $[x_c, y_c, z_c]^T$ are equal to the vehicle coordinates $[x_c'', y_c'', z_c'']^T$. Thus, Equation (2.25) can be rewritten in $[x_c'', y_c'', z_c'']^T$ coordinate as follows:

$$u = -f\frac{x_c''^2 + z_c''^2}{z_c''^2}\left(\gamma - \frac{x_c''}{x_c''^2 + z_c''^2}V\right), \tag{2.45}$$

where we assume $\alpha = \dot{\alpha} = 0$, and γ represents the yaw rate of the vehicle, but γ in Equation (2.45) denotes the yaw rate of the target point as seen from the vehicle. Thus, we reversed a sign of yaw rate γ.

Figure 2.23 shows the geometric relation when the vehicle corresponds to the target path. In Figure 2.23, when we focus on the relationship of the triangle formed by the center of the target path, the vehicle's center of gravity, and the gaze point, the geometric term using the cosine formula is expressed as follows:

$$\frac{x_c''}{x_c''^2 + z_c''^2} = \frac{\sin\alpha}{\sqrt{R^2 + R^2 - 2R^2\cos 2\alpha}} = \frac{1}{2R}. \tag{2.46}$$

By substituting Equation (2.46) and $V = R\gamma$ into Equation (2.45), we obtain the following:

$$\tilde{u} = -f\left(1 + \tan^2\alpha\right)\frac{\gamma}{2}. \tag{2.47}$$

Consequently, when we gaze at the target point on the path, optical flow of the point has a deviation including the yaw rate. When we can converge u to $\tilde{u}$, we can achieve the ideal control. Therefore, the control method in the fixed camera is represented as follows:

$$\begin{aligned}\bar{\delta} \;=\; & \frac{1}{g(X,Y)}\Bigg[M(\beta,\gamma,\delta)\sin\phi\frac{dY}{dt} + w(\beta,\gamma,\delta,X,Y) \\ & -\left\{\frac{2X\cos\phi}{f}M(\beta,\gamma,\delta) + G\cos\beta + k\right\}\frac{dX'}{dt}\Bigg]\end{aligned} \tag{2.48}$$

where $\frac{dX'}{dt} = u - \tilde{u}$. We choose the target point (X, Y) and optical flow u on the image, and obtain optical flow $\tilde{u}$ from the image plane or by the calculation of Equation (2.47). This means that $\tilde{u}$ is optical flow represented by Equation 2.14 and u is assumed to be the camera motion towards the target point. As a result, the vehicle converges to the target point because $u \to \tilde{u}$, as shown in Figure 2.24. That is, the vehicle can track to the target path.

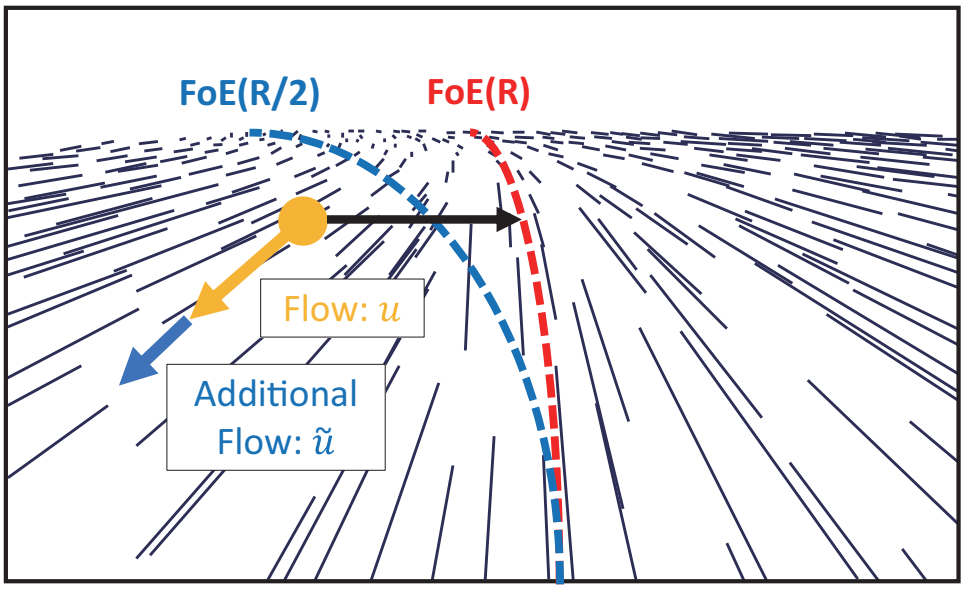

Figure 2.24: Convergence to FoE (R)

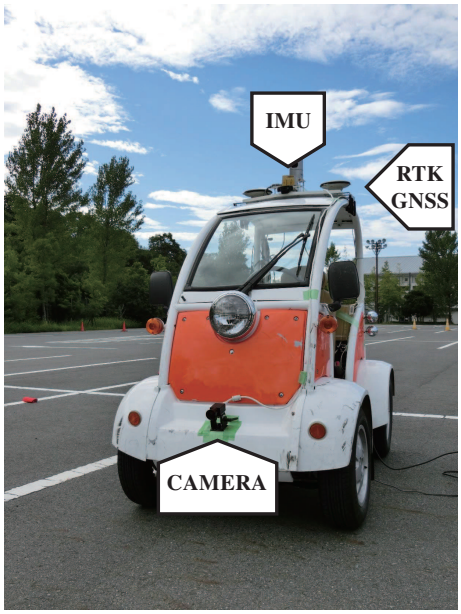

Figure 2.25: Robocar with camera, IMU, and RTK-GNSS

2.8 Experiment

In this section, we apply the proposed nonlinear controller to an automatic steering control system and confirm the efficiency of the proposed controller.

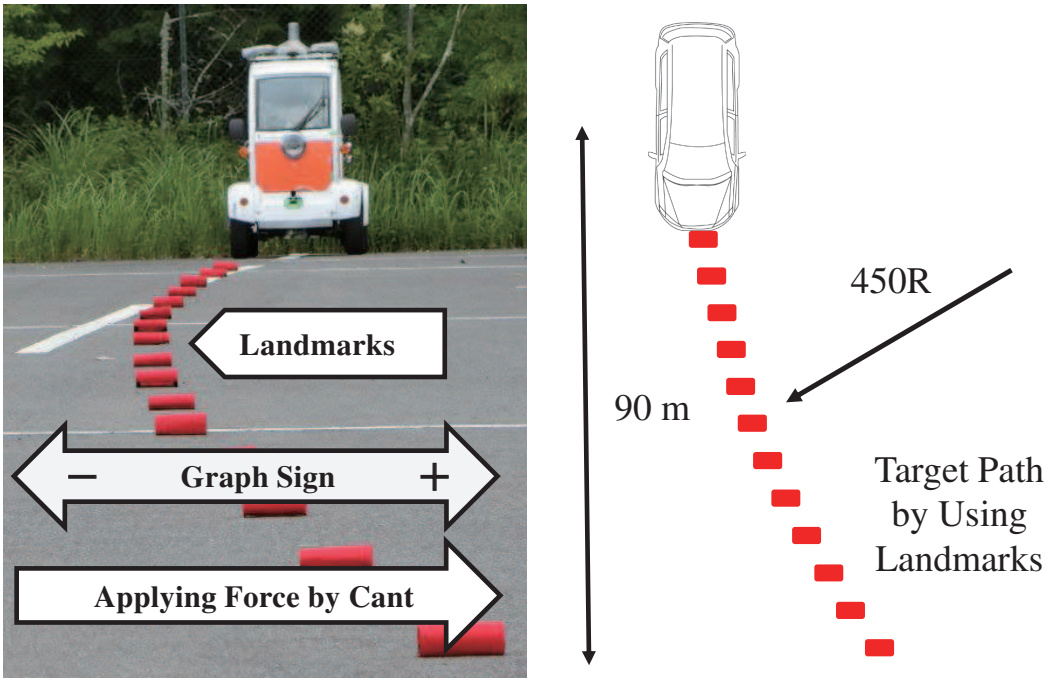

Figure 2.26: Overview of target path

Table 2.4: Robocar parameters and experimental conditions

m	440.0 [kg]	I_{car}	185.196 [kgm^2]
l_f	0.69 [m]	T	70 [ms]
l_r	0.61 [m]	V	10 and 20 [km/h]
K_f	5,600.0 [N/rad]	h	0.5 [m]
K_r	10,000.0 [N/rad]	ϕ	10.0 [deg]

Table 2.5: Camera specifications

Imaging sensor	CCD, 2/3
Resolution	1664 × 1224 [pixel]
Pixel size	4.40 × 4.40 [μm]
Frame rate	30
Focal length f	5.0 [mm]

2.8.1 Experimental Setup

Robocar made by ZMP Inc. is used in this experiment. On Robocar, a camera, inertia measurement unit (IMU), and RTK-GNSS are installed, as shown in Figure 2.25. The camera is attached to the vehicle tip. IMU is attached to Robocar to estimate the roll, pitch, and yaw angles and rates for the control input. RTK-GNSS is installed to estimate the running path for analyzing performance. In this experiment, we assume $\beta = 0$ because it is difficult to measure the slip angle β. This assumption is not a problem since the turning

Table 2.6: Control Gain k

Proposed method	1100.0
Comparative method	1250.0

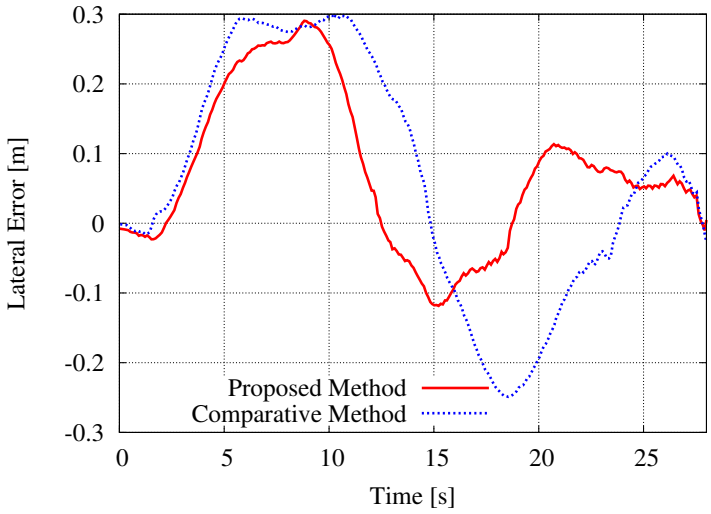

Figure 2.27: Results of lateral error in 20 [km/h]

radius is large. Table 2.4 lists the Robocar parameters and the experimental conditions. Table 2.5 lists the camera parameters. We created the target path indicating the circular orbit of radius 450R by using landmarks as shown in Figure 2.26. The controlled Robocar tracks to the target path of approximately 90 [m]. We use Gunnar Farneback's algorithm [70] utilizing OpenCV to detect optical flow of the target.

2.8.2 Experimental Results

We confirmed the effectiveness of the proposed method Equation (2.48) as compared to the comparative method Equation (2.42). The control gains of each method are shown in Table 2.6. We show the results of the lateral errors and optical flow, as shown in Figures 2.27, 2.28, and 2.29. In Figures 2.27 and 2.28, a positive value implies that Robocar runs towards the inside of the circular orbit, and there is cant such as applying force in the positive value direction as shown in Figures 2.26. At the beginning of the 3 [s] of Figures 2.29, we neglect the value of optical flow because of the acceleration section. A low-pass filter is used for removing observation noises from these results.

From Figures 2.27 and 2.28, we confirmed that the convergence performance of the proposed method was better than that of the comparative method. The maximum lateral

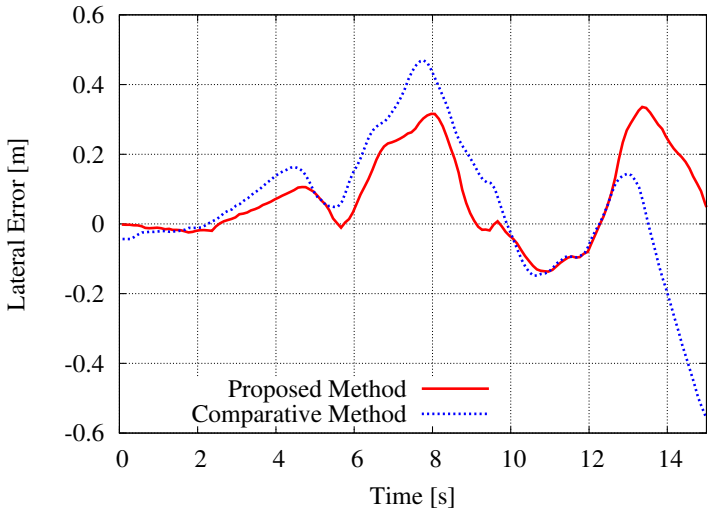

Figure 2.28: Results of lateral error in 10 [km/h]

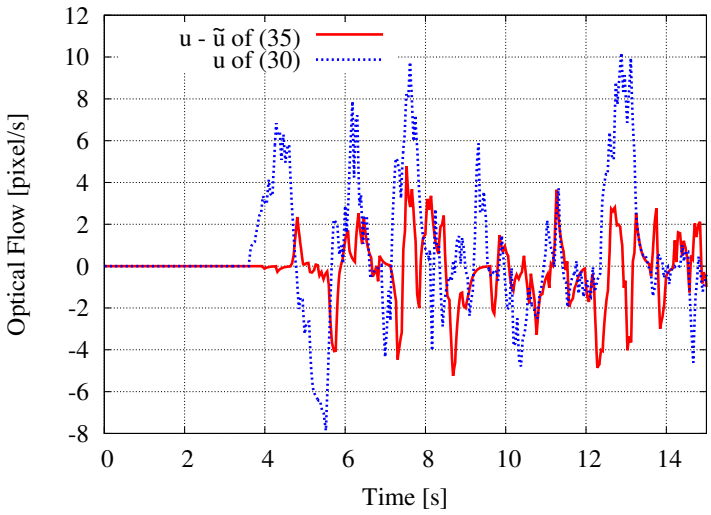

Figure 2.29: Results of optical flow in 20 [km/h]

error of the proposed method, as shown in Figure 2.27, was about 35 [cm]. The following may be reasons that Robocar cannot converge to the target path accurately: The control distance was short, and an exact observation of optical flow was difficult. On the other hand, the latter half of the lateral error of the comparative method was unstable. If optical flow of the target converged to FoE (R/2), the controlled vehicle moved towards the outside of the target path. Therefore, Robocar had a large lateral error towards the negative values. Moreover, we confirmed that the result of 10 [km/h] had a tendency similar to that of 20 [km/h], as shown in Figure 2.28. The convergence performance was improved as compared to the relatively high velocity since the observation of optical flow was more

accurate. Thus, if we can measure optical flow exactly, we can apply the optical flow control to a vehicle having a relatively high velocity.

Figure 2.29 shows the control input of optical flow of 20 [km/h] in each control method. From the result of the proposed method, we inferred that the target point matched FoE (R) because the value of $u - \tilde{u}$ converged to zero. Furthermore, the control input of the proposed method was more stable than the input of the comparative method. This reason can be considered to improve robustness because the proposed method utilizes two optical flows. If optical flow u of the target has noises, the control input is modified by the deviation flow $\tilde{u}$.

Thus, the proposed method showed an improvement in the convergence performance and the stability of optical flow. Therefore, we conclude that the proposed method is effective.

2.9 Conclusions

We derived the FoE and proposed an image-based automatic steering system based on optical flow. Using this control method, we confirmed that the proposed controller simulates the driver steering behavior with respect to the distance toward to the target point through vehicle simulations. In addition, we proposed a nonlinear controller considering camera motion for applying an optical flow model to in-vehicle control systems. Then, experimental results were presented. From the results of the vehicle experiments, we found that the proposed method was more accurate than our existing method. These results show the optical flow steering model is effective for the automated steering systems. However, when the target path is changed to a path such as a clothoid path, a serpentine curve, and a double-lane-change path, it is difficult to apply the optical flow model because the convergence of the model is limited to a steady circle. Thus, we need to integrate other information in terms of driver's visual cue such as Visual Direction into the optical flow model.

Appendix 2.A Detail Design of a Controller

Here, we derive the nonlinear controller in detail. We rewrite Equations (2.2), (2.30), and (2.33).

$$\frac{d}{dt}\begin{bmatrix} \beta \\ \gamma \end{bmatrix} = \begin{bmatrix} A & B \\ C & D \end{bmatrix}\begin{bmatrix} \beta \\ \gamma \end{bmatrix} + \begin{bmatrix} E \\ F \end{bmatrix}\delta, \tag{A.1}$$

$$\begin{aligned} u &= \frac{f\gamma}{2}\left(\frac{X^2}{f^2}+1\right)\cos\phi + \frac{V\cos\phi\sin(\phi-\theta)}{h\cos\theta}X\cos(\alpha-\beta) \\ &\quad + \frac{fV\sin(\phi-\theta)}{h\cos\theta}\sin(\alpha-\beta) - \frac{\gamma}{2}Y\sin\phi, \end{aligned} \tag{A.2}$$

$$\frac{du}{dt} = -k_1 u = -k_1\frac{dX}{dt}. \tag{A.3}$$

The derivative of the horizontal optical flow is as follows:

$$\begin{aligned} \frac{du}{dt} &= \frac{f\dot{\gamma}}{2}\left(\frac{X^2}{f^2}+1\right)\cos\phi + \frac{\gamma X\dot{X}}{f}\cos\phi + G\dot{X}\cos(\alpha-\beta) \\ &\quad -\frac{\gamma}{2}GX\sin(\alpha-\beta) + \frac{\gamma}{2}H\cos(\alpha-\beta) - \frac{\dot{\gamma}}{2}Y\sin\phi - \frac{\gamma}{2}\dot{Y}\sin\phi. \end{aligned} \tag{A.4}$$

By substituting Equation (A.1) and (A.4) into Equation (A.3), we get the following:

$$\begin{aligned} &\dot{X}\left\{\frac{\gamma X\cos\phi}{f} + G\cos(\alpha-\beta) + k_1\right\} - \frac{\gamma}{2}\dot{Y}\sin\phi \\ &+(C\beta + D\gamma + F\delta)\left\{\frac{f}{2}\left(\frac{X^2}{f^2}+1\right)\cos\phi - \frac{Y}{2}\sin\phi\right\} \\ &-\frac{\gamma}{2}GX\sin(\alpha-\beta) + \frac{\gamma}{2}H\cos(\alpha-\beta) = 0, \end{aligned} \tag{A.5}$$

where

$$\begin{aligned} G &= \frac{V\cos\phi\sin(\phi-\theta)}{h\cos\theta} \\ H &= \frac{fV\sin(\phi-\theta)}{h\cos\theta}. \end{aligned}$$

By arranging the above equation, we get the nonlinear controller as following:

$$\begin{aligned} \delta &= \frac{1}{g(X,Y)}\left[-\left\{\frac{\gamma X\cos\phi}{f} + G\cos(\alpha-\beta) + k_1\right\}\frac{dX}{dt}\right. \\ &\quad \left. + \frac{\gamma}{2}\sin\phi\frac{dY}{dt} + w(\alpha,\beta,\gamma,X,Y)\right], \end{aligned} \tag{A.6}$$

where

$$\begin{aligned} g(X,Y) &= F\left\{\frac{f}{2}\left(\frac{X^2}{f^2}+1\right)\cos\phi - \frac{Y}{2}\sin\phi\right\} \\ w(\alpha,\beta,\gamma,X,Y) &= \frac{\gamma}{2}GX\sin(\alpha-\beta) - \frac{\gamma}{2}H\cos(\alpha-\beta) \\ &\quad -(C\beta+D\gamma)\left\{\frac{f}{2}\left(\frac{X^2}{f^2}+1\right)\cos\phi - \frac{Y}{2}\sin\phi\right\}. \end{aligned}$$

Chapter 3

Design of Preview Driver Model based on Optical Flow

3.1 Introduction

Automated driving systems have been released in the last few years to improve vehicle dynamics performances, enhance the active safety, and reduce driver load. A previous study [13] revealed that the elements required for the development of these technologies in order to investigate vehicle stability performance are the driver, the vehicle, and the environment. Since the driver's subjective evaluation is affected primarily by the vehicle dynamics, it is essential to incorporate driver modeling in such systems. In particular, in the early days of this research field of driver steering many researchers proposed several typical models.

Many driving models that focus on the preview or predictive behavior of the driver have been proposed, because the driver gazes at a future desired path while driving. Kondo [82] first proposed a model of this type. The lateral deviation with regard to the preview point is used for the control object in this model. In addition, the model was expanded to the preview driver model by Yoshimoto [61], who used a predictive point determined by the velocity and the acceleration of the vehicle. The control object of these models was a single point on the predictive location. On the other hand, an optimal preview control, where the control input is determined by multiple points within the preview window, was proposed by Macadam for improving the control performance and reproducing driver behavior [83]. The cost function of this optimal model includes the lateral deviations from the multiple preview points. This model is well known a rela-

tively general driver model that can reproduce driver behavior quite well and it has been implemented in a commercial software product called CarSim [84]. Macadam's model uses only the lateral deviations for the P controller in the cost function. However, the application to this optimal preview driver model of the lateral deviations by adding an instantaneous yaw error feedback method [85] and the PD controller in the cost function [86] were proposed. These expanded optimal preview driver models can reproduce the driver's steering behavior and are effective in practical use, e.g., for lane keeping, by using the PID controller [87]. These studies above used the lateral deviation from the predictive point as the control object. In contrast, a preview driver model based on Tangent Point [88] as the control object was also proposed, because the driver can perceive the current curvature of the vehicle's path by using Tangent Point [89]. The effectiveness is verified by introducing these preview driver models into various vehicle dynamics [90]. In recent decades, there are some expanded models based on the preview/predictive driver model: first is with Model Predictive Model for the effective controller [91, 92], second is including a neuromuscular dynamics to capture the interaction between the vehicle and the driver [93, 94], the aim of other studies is to identify the individual driver based on the model parameters [95, 96].

In our previous works [53, 54, 97, 98], we focused on optical flow, which is the visual information that drivers perceive. In general, humans can reach the target point "where I want to go" by matching it to the FoE [18, 19]. Therefore, by introducing this human behavior into vehicle control systems, we constructed automated steering systems based on two types of method: position-based control [53, 54] and image-based control [97, 98]. We confirmed that in these control methods the optical flow model can reproduce driver steering behavior [97] and showed its effectiveness for application in real environments [53, 98].

A comparison of the preview driver model and the optical flow model shows that they have characteristics in common: both are based on the driver's preview behavior and reproduce the driver's steering behavior such as the steering input and the vehicle trajectory. Therefore, in this study we analyzed the preview driver model from the viewpoint of optical flow. Although many conventional preview models have been proposed, we selected the single point model using the predictive point [61], because the purpose of the optimal preview driver model is to improve the control performance and not to express driver behavior. In addition, we propose a new preview driver model that utilizes our knowledge

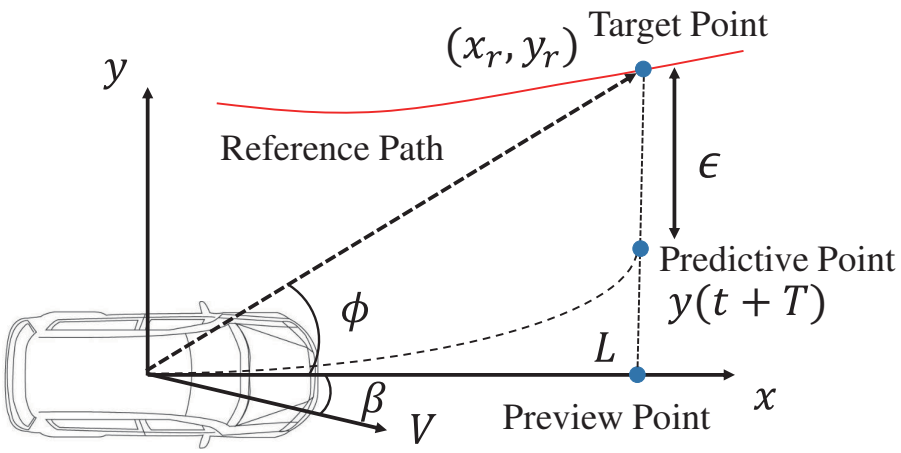

Figure 3.1: Definition of second-order preview driver model

of optical flow. Then we confirm the effectiveness of the proposed method as compared with the conventional preview driver model through a vehicle simulation.

3.2 Conventional Preview Driver Model

The preview driver model is a control method that considers driver-vehicle interaction. In this model, we set a preview point viewed from the vehicle, and the model controls the lateral deviation between a predictive point of the vehicle and the target point on a target path with respect to the preview point.

In this study, we consider a second-order preview driver model in which the predictive point of the vehicle is expressed as the velocity and the acceleration of the vehicle [61]. We define the states of this model, as shown in Figure 3.1. The target point and the y-coordinate of the predictive point are expressed as (x_r, y_r) and $y(t+T)$, respectively; then, the lateral deviation ϵ with regard to the preview point is

$$\epsilon = y_r - y(t+T). \tag{3.1}$$

The predictive point $y(t+T)$ changed by Taylor expansion by a second order approximation can be described as

$$y(t+T) = y(t) + \dot{y}(t)T + \frac{1}{2}\ddot{y}(t)T^2. \tag{3.2}$$

Next, we show the predictive point as determined by using vehicle information. We assume that $\boldsymbol{i}, \boldsymbol{j}$ are each unit vectors on the (x, y) coordinates and the vehicle velocity V

is constant; then, the velocity vector of the vehicle is given as

$$\dot{\boldsymbol{R}} = (V\cos\beta)\boldsymbol{i} + (V\sin\beta)\boldsymbol{j}. \tag{3.3}$$

Differentiating Equation (3.3), we obtain the acceleration vector as

$$\ddot{\boldsymbol{R}} = \left\{-V(\gamma+\dot{\beta})\sin\beta\right\}\boldsymbol{i} + \left\{V(\gamma+\dot{\beta})\cos\beta\right\}\boldsymbol{j}, \tag{3.4}$$

where γ denotes the yaw rate, β represents the slip angle of the vehicle, $\dot{\boldsymbol{i}} = \gamma\boldsymbol{j}$, and $\dot{\boldsymbol{j}} = -\gamma\boldsymbol{i}$.

Using Equations (3.2), (3.3), and (3.4), we can show the y-coordinate of the predictive point with respect to the preview distance ($L = TV\cos\beta$) as

$$y(t+T) = y(t) + TV\sin\beta + \frac{T^2}{2}V(\gamma+\dot{\beta})\cos\beta = y(t) + L\beta + \frac{L^2}{2V}\gamma, \tag{3.5}$$

where we assume a situation where $\beta \ll 1$ and $\dot{\beta} \simeq 0$, because the slip angle is small when the steering of the vehicle is not steep, the turning radius is sufficiently large, and no irregularities and gradients exist on the road along which it is traveling. We apply these assumptions to the following derivation processes, except for definitions.

Substituting Equation (3.5) into Equation (3.1), we can rewrite the lateral deviation with the second-order model as

$$\epsilon = y_r - \left(L\beta + \frac{L^2}{2V}\gamma\right), \tag{3.6}$$

where we define $y(t) = 0$, because this deviation is viewed from the vehicle.

In general, driver behavior can be expressed as the PD controller including the dead time of control, so that the preview driver model is frequently constructed with the same controller. However, in this study the design of the PD controller was aimed at providing an easier expression of this model. Therefore, the control method of the preview driver model is represented as

$$\overline{\delta} = K_P\epsilon + K_D\dot{\epsilon}. \tag{3.7}$$

Differentiating Equation (3.6), we obtain

$$\dot{\epsilon} = \dot{y}_r - \dot{L}\left(\beta + \frac{\gamma L}{V}\right) - \frac{L^2}{2V}\dot{\gamma}. \tag{3.8}$$

Then, we derive $\dot{y}_r$ to analyze Equation (3.8). In general, the preview time T and velocity V are assumed to be constant in this model. Thus, the preview distance L also

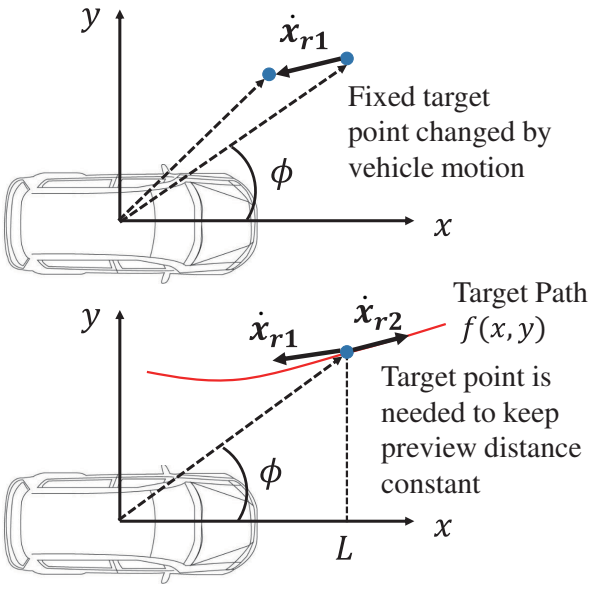

Figure 3.2: Two types of velocity in preview driver model

becomes constant. Therefore, the target velocity $\dot{\boldsymbol{x}}_{\boldsymbol{r}} = [\dot{x}_r, \dot{y}_r]^T$ is expressed as two types of velocity, as shown in Figure 3.2. The first velocity, $\dot{\boldsymbol{x}}_{\boldsymbol{r1}} = [\dot{x}_{r1}, \dot{y}_{r1}, \dot{z}_{r1}]^T$, is the target velocity viewed from the vehicle coordinates. The second velocity, $\dot{\boldsymbol{x}}_{\boldsymbol{r2}} = [\dot{x}_{r2}, \dot{y}_{r2}, \dot{z}_{r2}]^T$, is along the target path to maintain a constant preview distance. The velocity $\dot{\boldsymbol{x}}_{\boldsymbol{r1}}$ is expressed as

$$\frac{d}{dt}\begin{bmatrix} x_{r1} \\ y_{r1} \\ z_{r1} \end{bmatrix} = \begin{bmatrix} -V\cos\beta \\ -V\sin\beta \\ 0 \end{bmatrix} + \begin{bmatrix} 0 \\ 0 \\ -(\gamma+\dot{\beta}) \end{bmatrix} \times \begin{bmatrix} x_r \\ y_r \\ z_r \end{bmatrix} = \begin{bmatrix} -V\cos\beta + (\gamma+\dot{\beta})y_r \\ -V\sin\beta - (\gamma+\dot{\beta})x_r \\ 0 \end{bmatrix}. \tag{3.9}$$

As the preview distance is constant, the velocity $\dot{x}_{r2}$ is described as

$$\dot{x}_{r2} = -\dot{x}_{r1} = V\cos\beta - (\gamma+\dot{\beta})y_r. \tag{3.10}$$

When the target path viewed from the vehicle coordinates is denoted by $f(x, y)$, the velocity $\dot{y}_{r2}$ is given as

$$\dot{y}_{r2} = \dot{x}_{r2}\left.\frac{\partial f}{\partial x}\right|_{x=x_r} = \left\{V\cos\beta - (\gamma+\dot{\beta})y_r\right\}\left.\frac{\partial f}{\partial x}\right|_{x=x_r}. \tag{3.11}$$

Using Equations (3.9), (3.10), and (3.11), we can obtain the target velocity $\dot{\boldsymbol{x}}_{\boldsymbol{r}}$

$$\frac{d}{dt}\begin{bmatrix} x_r \\ y_r \end{bmatrix} = \frac{d}{dt}\begin{bmatrix} x_{r1}+x_{r2} \\ y_{r1}+y_{r2} \end{bmatrix} \approx \begin{bmatrix} 0 \\ -V\beta - \gamma x_r + (V-\gamma y_r)\left.\frac{\partial f}{\partial x}\right|_{x=x_r} \end{bmatrix}. \tag{3.12}$$

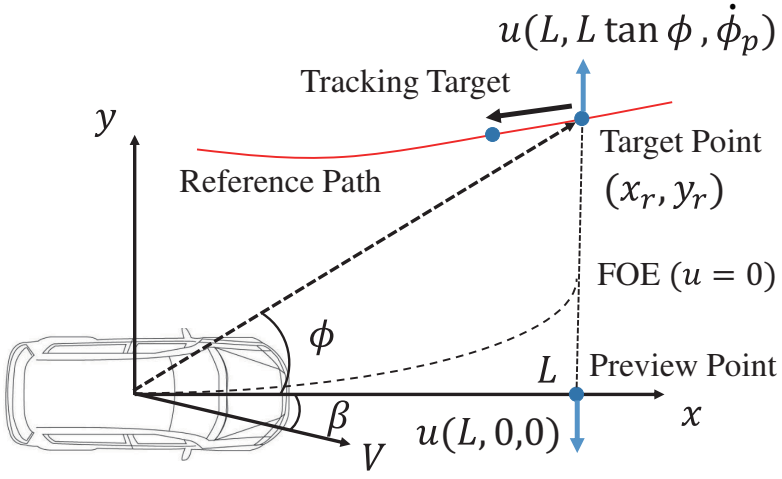

Figure 3.3: Definition of optical flow model

Substituting Equation (3.12) into Equation (3.8), we can rewrite Equation (3.8) as

$$\dot{\epsilon} = L\left(-\gamma - \frac{V}{L}\beta\right) + (V - \gamma L\tan\phi)\left.\frac{\partial f}{\partial x}\right|_{x=x_r} - \frac{L^2}{2V}\dot{\gamma}, \tag{3.13}$$

where we assume $x_r = L$, $y_r = L\tan\phi$, and $\dot{L} = 0$ according to the definition of the preview driver model.

Using Equations(3.6) and (3.13), we can obtain the PD controller with the second-order preview driver model

$$\bar{\delta} = K_P\left[y_r - \left(L\beta + \frac{L^2}{2V}\gamma\right)\right] + K_D\left[L\left(-\gamma - \frac{V}{L}\beta\right) + (V - \gamma L\tan\phi)\left.\frac{\partial f}{\partial x}\right|_{x=x_r} - \frac{L^2}{2V}\dot{\gamma}\right]. \tag{3.14}$$

3.3 Preview Driver Model based on Optical Flow

In this section, we derive optical flow and analyze the conventional preview driver model using optical flow modeling. Using the results, we propose a preview driver model based on optical flow.

3.3.1 Modeling of Optical Flow

In this subsection, we construct optical flow based on the study reported in Inou's paper [53, 54]. We consider the definition of optical flow as a variable value of a change in the target angle because optical flow in this section is assumed to be generated in the

retina coordinate and it is easier to interpret models than that in Section 2. Figure 3.3 also shows the vehicle coordinates used to construct optical flow. We assume that rolling, pitching, and vertical motions are negligible, because we consider the same situation as in the slip angle assumption in Section 3.2. Therefore, we can derive only the azimuth angle direction of optical flow, because the vehicle moves only in the direction in which it is steered. The angle between the vehicle and the target point is represented as

$$\phi = \tan^{-1} \frac{y_r}{x_r}. \tag{3.15}$$

As the azimuth angle direction of optical flow is expressed as a change in the angle, we differentiate Equation (3.15) and obtain

$$u = \frac{d\phi}{dt} = \frac{x_r \dot{y}_r - \dot{x}_r y_r}{x_r^2 + y_r^2}. \tag{3.16}$$

Before arguing the details of optical flow, Equation 3.16 is compared with optical flow defined in the image plane in order to confirm optical flow in this chapter has the relationship with optical flow in Chapter 2. Equation 3.16 can be rewritten as

$$u = \frac{1}{1 + \frac{y^2}{x^2}} \frac{1}{x^2} \left(x_r \dot{y}_r - \dot{x}_r y_r \right) = \frac{\cos^2 \theta}{x^2} \left(x_r \dot{y}_r - \dot{x}_r y_r \right). \tag{3.17}$$

When the angle θ between the vehicle direction and the target point direction is small, Equation 3.17 is equivalent to Equation 2.4 generated in the image plane.

We show the target velocity viewed from the vehicle coordinates. In Equation (3.12), we considered the relative velocity, which is the combination of the target velocity and the velocity along the target path, as mentioned in Section 3.2, because the preview distance is determined to be constant. However, in this derivation process we consider only the target velocity, because we consider the assumption that the driver continues to gaze at the fixed target point:

$$\frac{d}{dt} \begin{bmatrix} x_r \\ y_r \\ z_r \end{bmatrix} = \begin{bmatrix} -V \cos\beta \\ -V \sin\beta \\ 0 \end{bmatrix} + \begin{bmatrix} 0 \\ 0 \\ -\dot{\phi}_{vp} \end{bmatrix} \times \begin{bmatrix} x_r \\ y_r \\ z_r \end{bmatrix} = \begin{bmatrix} -V \cos\beta + \dot{\phi}_{vp} y_r \\ -V \sin\beta - \dot{\phi}_{vp} x_r \\ 0 \end{bmatrix}, \tag{3.18}$$

where $\dot{\phi}_{vp}$ represents the yaw rate combined with the vehicle motion and the driver's eye movement. In this paper, we consider that the driver's eye and neck movements are integrated and call them the eye movement. It is considered that optical flow that driver perceives is a combination value of the vehicle motion and his/her eye movement; that is, we must construct optical flow using a combination of parameters.

For this reason, $\dot{\phi}_{vp}$ is expressed as

$$\dot{\phi}_{vp} = \gamma + \dot{\beta} + \dot{\phi}_p, \tag{3.19}$$

where $\dot{\phi}_p$ indicates the pursuit eye movement, where the eye movement is assumed to be smooth. We derive $\dot{\phi}_p$ in detail in Subsection 3.3.4.

By using Equation (3.19), Equation (3.18) is rewritten as

$$\frac{d}{dt}\begin{bmatrix} x_r \\ y_r \end{bmatrix} = \begin{bmatrix} -V\cos\beta + (\gamma + \dot{\beta} + \dot{\phi}_p)y_r \\ -V\sin\beta - (\gamma + \dot{\beta} + \dot{\phi}_p)x_r \end{bmatrix}. \tag{3.20}$$

Substituting Equation (3.20) into Equation (3.16), we can obtain optical flow considering the vehicle and the driver models as

$$u(x_r, y_r, \dot{\phi}_p) = -(\gamma + \dot{\beta} + \dot{\phi}_p) + \frac{V}{x_r^2 + y_r^2}(-x_r\sin\beta + y_r\cos\beta), \tag{3.21}$$

where optical flow is described by $u(x_r, y_r, \dot{\phi}_p)$ in the following derivation.

If we choose the target point (x_r, y_r) for calculating, we can obtain the azimuth angle direction of optical flow of the target point by using Equation (3.21).

3.3.2 Analyzing Preview Driver Model based on Optical flow

We now analyze the preview driver model based on optical flow. First, we assume the eye movement $\dot{\phi}_p = 0$, which means the driver's eye and neck are always turned toward the vehicle heading direction and the target point $(x_r, y_r) = (L, 0)$. Thus, optical flow represented by Equation (3.21) is described as

$$u(L, 0, 0) \quad = \quad -\gamma - \frac{V}{L}\beta. \tag{3.22}$$

By using Equation (3.22), the conventional preview driver model of Equation (3.14) is rewritten as

$$\overline{\delta} = K_P\left[y_r - \left(L\beta + \frac{L^2}{2V}\gamma\right)\right] + K_D\left[Lu(L, 0, 0) + (V - \gamma L\tan\phi)\left.\frac{\partial f}{\partial x}\right|_{x=x_r} - \frac{L^2}{2V}\dot{\gamma}\right]. \tag{3.23}$$

From this result, we can understand that the conventional preview driver model controls optical flow on the preview point $(L, 0)$ in the differential term.

3.3.3 Modeling of Preview Driver Model based on Optical Flow

In our previous works on optical flow control [53, 54, 97, 98], we chose the target point, and the azimuth angle direction of optical flow at the point converged to zero. Then, the vehicle could achieve tracking to the target path. The zero flow point of the optical flow is called the FoE (Focus of Expansion), and the fact that the FoE shows the direction of the vehicle or human motion is well known. When the target point matches the FoE it means that the point corresponds to the direction of self-motion, and therefore, tracking control is achieved. In addition, we showed that this control method can express driver behavior by changing the gaze distance [97]. In our previous works, it was shown that for expressing driver behavior with respect to the distance toward to the target point, the following knowledge terms are important

(I) The convergence of optical flow of the target point to zero.
(II) The eye movement tracks the target point.

In term (II), when the vehicle runs in a steady circle, the FoE, which the driver perceives, shows the same orbit as the tracking path as he/she continues to gaze at the point on the path. However, the FoE shows a half radius orbit of the target steady circle if we ignore the eye movement, e.g., $\dot{\phi}_p = 0$. Therefore, the effectiveness of the control method is lacking, since the FoE does not reflect the correct direction of self-motion.

In Equation (3.23), the eye movement $\dot{\phi}_p$ is assumed to be zero and the conventional preview driver model includes optical flow not on the point of the target path but on the preview point. Therefore, this control method does not satisfy terms (I) and (II) for expressing driver behavior. For this reason, when the turning radius is small and the vehicle runs at a higher velocity, this system is not constructed based on the driver's subjective evaluation. Thus, we construct a new preview driver model that includes terms (I) and (II).

In the proposed preview driver model based on optical flow, we apply a geometric condition concerning the relationship between the vehicle and the target point for the differential term in the conventional controller. The geometric condition is given as

$$y_r = x_r \tan \phi. \tag{3.24}$$

By using Equation (3.9), the differentiation of Equation (3.24) is represented as

$$\dot{y_r} = \dot{x_r}\tan\phi + x_r\dot{\phi}_p\frac{1}{\cos^2\phi} = (-V\cos\beta + \gamma y_r)\tan\phi + x_r\dot{\phi}_p\frac{1}{\cos^2\phi}, \quad (3.25)$$

where $\frac{d\phi}{dt}$ becomes $\dot{\phi}_p$, because we assume continued tracking of the target point.

As $x_r = L$ and $y_r = L\tan\phi$, Equation (3.25) is rewritten as

$$\begin{aligned}\dot{y_r} &= -V\cos\beta\tan\phi + L\gamma\tan^2\phi + \frac{L}{\cos^2\phi}\dot{\phi}_p + (V\sin\beta - V\sin\beta) + (L\gamma - L\gamma)\\ &= -\frac{L}{\cos^2\phi}\left\{-(\gamma+\dot{\phi}_p) + \frac{V}{L}\sin(\phi-\beta)\cos\phi\right\} + L\left(-\gamma - \frac{V}{L}\beta\right). \quad (3.26)\end{aligned}$$

By substituting Equation (3.26) into Equation (3.8), the differentiation of the lateral deviation with the second-order model is

$$\begin{aligned}\dot{\epsilon} &= -\frac{L}{\cos^2\phi}\left\{-(\gamma+\dot{\phi}_p) + \frac{V}{L}\sin(\phi-\beta)\cos\phi\right\}\\ &\quad + L\left(1+\frac{\dot{L}}{V}\right)\left(-\gamma - \frac{V}{L}\beta\right) - \frac{L^2}{2V}\dot{\gamma}. \quad (3.27)\end{aligned}$$

By using Equation (3.27), the proposed control method of Equation (3.7) is expressed as

$$\begin{aligned}\overline{\delta} &= K_P\left[y_r - \left(L\beta + \frac{L^2}{2V}\gamma\right)\right] + K_D\left[-\frac{L}{\cos^2\phi}\left\{-(\gamma+\dot{\phi}_p)\right.\right.\\ &\quad \left.\left. + \frac{V}{L}\sin(\phi-\beta)\cos\phi\right\} + L\left(1+\frac{\dot{L}}{V}\right)\left(-\gamma - \frac{V}{L}\beta\right) - \frac{L^2}{2V}\dot{\gamma}\right]. \quad (3.28)\end{aligned}$$

Next, we evaluate the new control method of Equation (3.28) using optical flow of Equation (3.21). If we assume $x_r = L$ and $y_r = L\tan\phi$ in Equation (3.21), we obtain optical flow on the target point considering the eye movement as

$$u(L, L\tan\phi, \dot{\phi}_p) = -(\gamma+\dot{\phi}_p) + \frac{V}{L}\sin(\phi-\beta)\cos\phi. \quad (3.29)$$

By using Equations (3.22) and (3.29), Equation (3.28) is rewritten as

$$\begin{aligned}\overline{\delta} &= K_P\left[y_r - \left(L\beta + \frac{L^2}{2V}\gamma\right)\right] + K_D\left[-\frac{L}{\cos^2\phi}u(L, L\tan\phi, \dot{\phi}_p)\right.\\ &\quad \left. + L\left(1+\frac{\dot{L}}{V}\right)u(L,0,0) - \frac{L^2}{2V}\dot{\gamma}\right]. \quad (3.30)\end{aligned}$$

Thus, a new preview driver model that includes optical flow considering the eye movement on the target point is constructed. This model can satisfy terms (I) and (II).

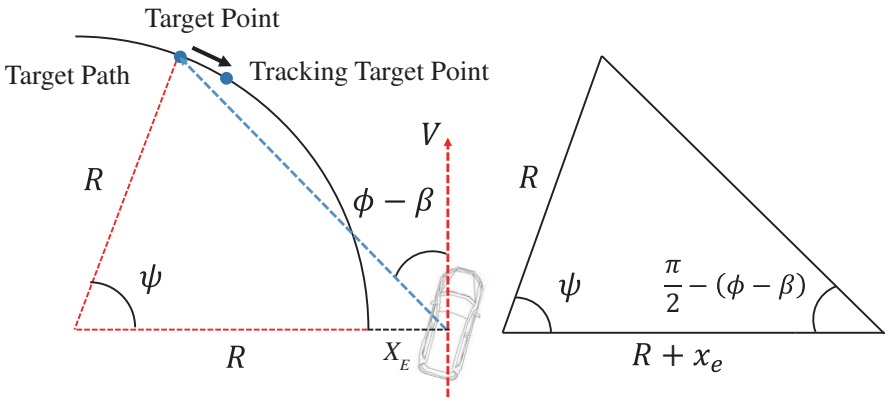

Figure 3.4: Relationship between target path and vehicle

3.3.4 Deriving Eye Movement in Steady Circle

In this subsection, we derive the eye movement for a steady circle in detail. We assume a condition where the vehicle has a lateral deviation x_e from the target steady circle with radius R, as shown in Figure 3.4. The right hand side of Figure 3.4 shows a triangle that connects the center of the vehicle, the target point, and the center of the steady circle. The geometric constraint is determined by the laws of sines as

$$\frac{R + x_e}{\sin\left(\frac{\pi}{2} + X_1 - \frac{\psi}{2}\right)} = \frac{R}{\sin\left(\frac{\pi}{2} - X_1 - \frac{\psi}{2}\right)}, \tag{3.31}$$

where $X_1 = \phi - \beta - \frac{\psi}{2}$.

From Equation (3.31), X_1 is described as

$$X_1 = \tan^{-1}\left(\frac{x_e}{2R + x_e}\frac{1}{\tan\frac{\psi}{2}}\right). \tag{3.32}$$

As a result,

$$\frac{1}{2}\psi = \phi - \beta - \tan^{-1}\left(\frac{x_e}{2R + x_e}\frac{1}{\tan\frac{\psi}{2}}\right). \tag{3.33}$$

By differentiating Equation (3.33), the eye movement $\dot{\phi}_p$ is presented as

$$\frac{1}{2}\dot{\psi} = -\dot{\phi}_p - \dot{\beta} - \frac{1}{1 + \left(\frac{x_e}{2R+x_e}\frac{1}{\tan\frac{\psi}{2}}\right)^2}\left[\frac{2R\dot{x}_e}{(2R + x_e)^2}\frac{1}{\tan\frac{\psi}{2}} - \frac{x_e}{2R + x_e}\frac{\dot{\psi}}{2\sin^2\frac{\psi}{2}}\right], \tag{3.34}$$

where the differentiation of ϕ becomes $\dot{\phi}_p$, because we do not consider the vehicle motion in this derivation. We need to pay attention to the sign of $\dot{\phi}_p$.

When the vehicle is sufficiently close to the target path, we can assume $R \gg x_e$; thus, each element in Equation (3.34) is approximated as

$$\frac{x_e}{2R + x_e} \simeq 0 \tag{3.35}$$

$$\frac{2R\dot{x}_e}{(2R + x_e)^2} \simeq \frac{\dot{x}_e}{2R} \tag{3.36}$$

$$\dot{\psi} \simeq \gamma. \tag{3.37}$$

By using Equations (3.35)-(3.37), Equation (3.34) is rewritten as

$$\dot{\phi}_p = -\frac{1}{2}\gamma - \dot{\beta} - \frac{\dot{x}_e}{2R\tan\frac{\psi}{2}}. \tag{3.38}$$

In addition, we can assume $\dot{\beta} \simeq 0, \dot{x}_e \simeq 0$ during tracking of the steady circle; then, Equation (3.38) is given as

$$\dot{\phi}_p = -\frac{1}{2}\gamma. \tag{3.39}$$

We can derive the eye movement in Equation (3.39). This eye movement constraint is considered the correct result, because it corresponds to the experimental results for the driver measurement [45].

3.3.5 Modified Preview Driver Model based on Optical Flow

By substituting Equation (3.38) into Equation (3.28) and using Equations (3.22) and (3.29), the proposed preview driver model that includes optical flow considering the eye movement on the target point is

$$\begin{aligned}\bar{\delta} = K_P\left[y_r - \left(L\beta + \frac{L^2}{2V}\gamma\right)\right] + K_D\Bigg[-\frac{L}{\cos^2\phi}\frac{\dot{x}_e}{2R\tan\frac{\psi}{2}} \\ -\frac{L}{\cos^2\phi}u\left(L, L\tan\phi, -\frac{\gamma}{2}\right) + L\left(1 + \frac{\dot{L}}{V}\right)u(L, 0, 0) - \frac{L^2}{2V}\dot{\gamma}\Bigg].\end{aligned} \tag{3.40}$$

We mention control law of Equation (3.40) in comparison with Equation (3.23). We compare only the differential term. The first term represents the information of the target path. The second term represents optical flow of the target point which considers

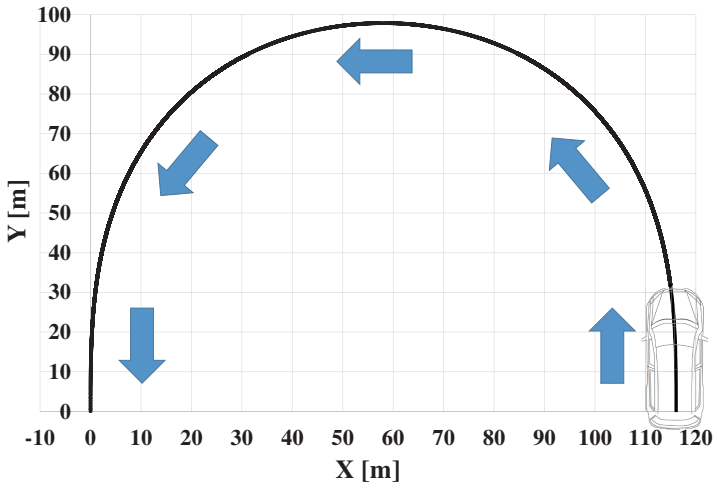

Figure 3.5: Overview of clothoid path

the eye movements. The second term and $\dot{L}$ in the third term are derived by assuming continuously tracking the target point.

If we choose the target point (x_r, y_r) and use the controller of Equation (3.40), the vehicle can track the target path and in particular the FoE of the vehicle matches that point.

3.4 Simulation I

In this section, we confirm the effectiveness of the proposed preview driver model (Prop1, Equation (3.40)) through a vehicle simulation. We used the single-track model described in Section 2.2 and following first-order lag system.

$$\dot{\delta} = -\frac{1}{\Delta T}\delta + \frac{1}{\Delta T}\bar{\delta}, \tag{3.41}$$

where ΔT denotes the time constant.

3.4.1 Overview of Simulation

In this simulation, we show the results when the vehicle aims to track the clothoid path at velocity 60 km/h. The overviews of the target path are as shown in Figures 3.5 and 3.6. Furthermore, we used image processing to detect the target point, since we will conduct in-vehicle experiments using a camera in the future. The target point $[x_r, y_r, z_r]^T$

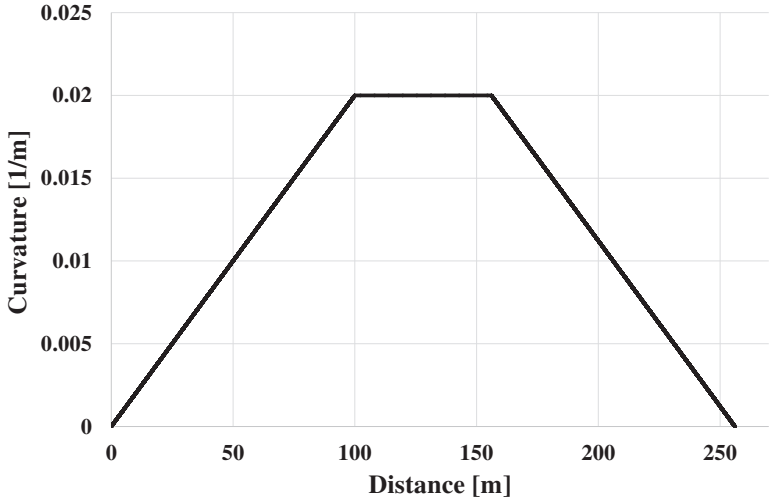

Figure 3.6: Curvature of clothoid path

Table 3.1: Control gain (prop1)

Method	K_P	K_D
Prop1	2.9	0.06

is transformed to the image plane $[X, Y]^T$ as

$$\begin{bmatrix} X \\ Y \end{bmatrix} = f \begin{bmatrix} \frac{y_r}{x_r} \\ \frac{z_r}{x_r} \end{bmatrix}. \tag{3.42}$$

We assumed that the lateral velocity $\dot{x}_e$ for the target path is sufficiently small; thus, the value of the first item in the differential term in Equation (3.40) was determined to be zero. The vehicle's initial posture was set in the tangential direction of the target path. The control gain is as shown in Table 3.1. Table3.2 and Table 3.3 list the vehicle parameters and the assumed camera parameters, respectively. h is the set height of the camera. As the preview time T is appropriate for 0.5-1.5 s (L = 8.3-25 m) [86], we set the preview time within this range. $\dot{L}$ is calculated from the difference of the preview distance caused by tracking the target point.

3.4.2 Results of Simulation I

We show the results of the lateral error of the vehicle for the target path, optical flow, preview distance, and control input $\overline{\delta}$ in Figures 3.7-3.10, respectively. Optical flow, as shown in Figure 3.8, is calculated by $u(L, L\tan\phi, -\frac{\gamma}{2})$ to evaluate the value that the driver perceives during driving.

Table 3.2: Vehicle parameters

m	1753.0 kg
l_f	1.437 m
l_r	1.413 m
K_f	47,500.0 N/rad
K_r	80,000.0 N/rad
I_{car}	3559.43kgm^2
ΔT	50.0 ms
h	1.5 m

Table 3.3: Assumed camera specifications

Imaging sensor	CCD, 1/1.8
Resolution	1664×1224 pixel
Pixel size	4.40×4.40 μm
Frame rate	30
Focal length f	5.0 mm

Figure 3.8 shows optical flow has more oscillatory values. When the target point is updated from a near point to a far one, the preview distance becomes discontinuous. This is the reason why the value of optical flow is not stable. This result means the target clothoid path does not correspond to the FoE, which is a steady circle, regardless of whether the vehicle converges to the path or not. If the target path is a steady circle and the vehicle completely converges to the target path, the target point on the path does not become discontinuous although the point is updated from the near point to the far one. Therefore, the control input also becomes oscillatory values, and the vehicle trajectory shows the large deviation.

For this reason, we can confirm that the preview driver model that includes tracking of the target point suffers a discontinuous problem when the target point is changed from the near point to the far one. In particular, when the target is a path having a changing curvature, the control input does not become stable.

3.5 Preview Driver Model based on Optical Flow with Virtual Following

In the previous simulation described in Section 3.4, we set the target point on the path and used the control law of Equation (3.40) while continuing to track the point. However, the control input becomes oscillatory because of discontinuous. This is the reason why

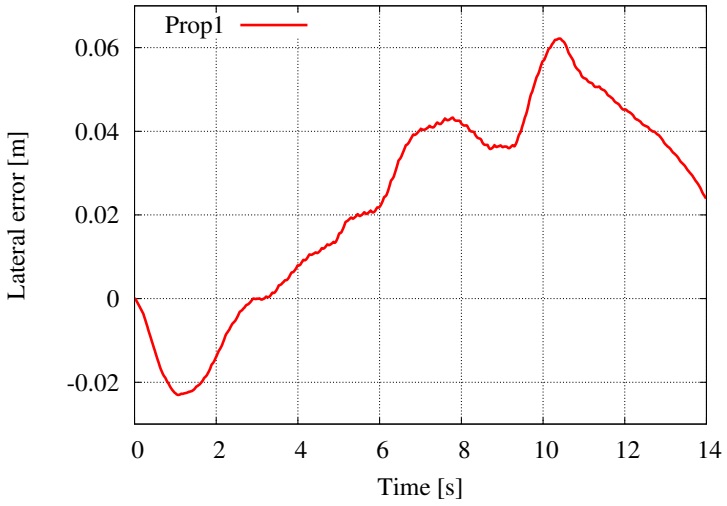

Figure 3.7: Results for lateral error (Prop1)

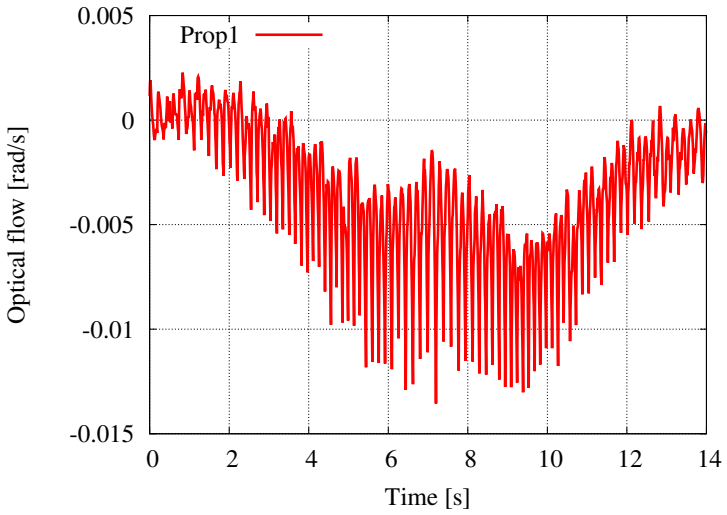

Figure 3.8: Results for optical flow (Prop1)

the control input becomes discontinuous when the target point is changed. Such situations frequently occur in real environments. Therefore, we propose a new preview driver model based on optical flow that does not need to continue tracking the target path when the preview distance is the same as in the conventional preview driver model; that is, constant. Information of $\dot{L}$ is lacking because $\dot{L}$ cannot be calculated in Equation (3.40) when the

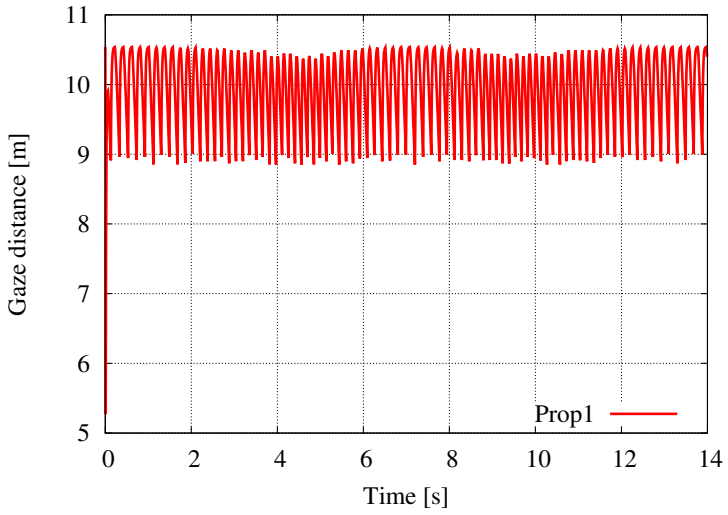

Figure 3.9: Results for gaze distance (Prop1)

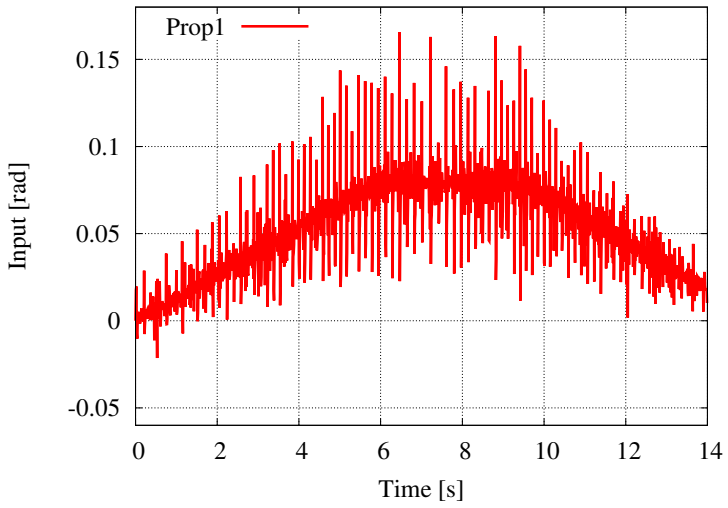

Figure 3.10: Results for input (Prop1)

preview distance is constant. Thus, we introduce Equation (3.20) into Equation (3.40):

$$\begin{aligned}\overline{\delta} &= K_P\epsilon + K_D\left[-\frac{L}{\cos^2\phi}\frac{\dot{x}_e}{2R\tan\frac{\psi}{2}} - \frac{L}{\cos^2\phi}u\left(L, L\tan\phi, -\frac{\gamma}{2}\right)\right. \\ &\quad \left. + \frac{\gamma}{2V}L^2\tan\phi\, u(L,0,0) - \frac{L^2}{2V}\dot{\gamma}\right]. \end{aligned} \tag{3.43}$$

As a result, the preview driver model based on optical flow with virtual following, which means that we continue to set the constant preview distance, is derived. The con-

ventional preview driver model is shown again as

$$\overline{\delta} = K_P\epsilon + K_D\left[(V - \gamma L\tan\phi)\left.\frac{\partial f}{\partial x}\right|_{x=x_r} + Lu(L,0,0) - \frac{L^2}{2V}\dot{\gamma}\right]. \tag{3.44}$$

We show the difference in comparison with control laws of Equations (3.43) and (3.44). We compare only the differential term. The first terms $\left(-\frac{L}{\cos^2\phi}\frac{\dot{x}_e}{2R\tan\frac{\psi}{2}},\ (V - \gamma L\tan\phi)\left.\frac{\partial f}{\partial x}\right|_{x=x_r}\right)$ of both equations represent the information of the target path. The fourth term in Equation (3.43) and the third term in Equation (3.44) represent the same information $\left(-\frac{L^2}{2V}\dot{\gamma}\right)$ and are derived by the prediction of the second-order model. The third term $\left(\frac{\gamma}{2V}L^2\tan\phi\ u(L,0,0)\right)$ in Equation (3.43) and the second term ($Lu(L,0,0)$) in Equation (3.44) represent optical flow on the preview point, but the former term includes the continuous tracking of the target point. The second term $\left(-\frac{L}{\cos^2\phi}u\left(L, L\tan\phi, -\frac{\gamma}{2}\right)\right)$ in Equation (3.43) is optical flow of the target point. In particular, we can confirm that this optical flow is considered with eye movement $\dot{\phi}_p = -\frac{\gamma}{2}$, and therefore, it is necessary to show the correct FoE. If the vehicle perfectly converges to the target path, the information of the target path, which is the differential first term in Equation (3.43), becomes zero. However, the path information is considered in the second term, because this includes the assumption of a steady circle with radius R.

3.6 Simulation II

In this section, we confirm the effectiveness of the proposed preview driver model with virtual following (Prop2, Equation (3.43)) by comparing it with the conventional preview driver model (Conv, Equation (3.44)) through a vehicle simulation.

3.6.1 Overview of Simulation II

We used the same simulation conditions as in Simulation I, except for the control gains. The control gains are as shown in Table 3.4. The control gains were determined for minimizing the maximum lateral error. The preview time T was set to be 0.6 s (L = 10 m).

Table 3.4: Control gain

Method	K_P	K_D
Conv	4.6	0.08
Prop2	5.2	0.2

3.6.2 Results of Simulation II

We show the comparison results of the lateral error, optical flow, lateral acceleration, lateral jerk, and control input $\overline{\delta}$ in Figures 3.11-3.15, respectively. The lateral acceleration and the lateral jerk are used for analyzing the ride quality of the driver [99, 100]. We show the maximum lateral error, the Root Mean Squared (RMS) lateral error and maximum optical flow, and RMS optical flow in Table 3.5.

Figure 3.11 shows that the convergence performance of the proposed method is better than that of the conventional method. The ride quality of the proposed method is also more comfortable, since the vibration of the vehicle is smoother, and the maximum value of the lateral acceleration and jerk are small, as shown in Figures 3.13 and 3.14.

In the results for optical flow, the value of the proposed method is slightly larger than that of the conventional method; however, both values are converged to zero. The reason why the values are the same is that the tracking path and the preview point of both methods are almost the same. Now, we calculate the elevation angle direction of optical flow to evaluate its azimuth angle direction, since optical flow perceived by the driver is synthesized using the elevation and the azimuth values. Thus, we can evaluate the convergence of optical flow from the viewpoints of the driver's perception. The elevation angle direction of optical flow v and synthesized optical flow uv are given as

$$v = \frac{d}{dt}\left(\tan^{-1}\frac{z}{x}\right) = \frac{\dot{z}x - z\dot{x}}{x^2 + z^2} \tag{3.45}$$

$$uv = \sqrt{u^2 + v^2}. \tag{3.46}$$

The parameters are determined as $x = L$, $z = h$, $\dot{z} = 0$, and $\dot{x} = -V + L\gamma\tan\phi$ as the definition of the preview driver model, and the elevation angle direction of optical flow $|v|$ becomes 0.2396 rad/s by using the maximum yaw rate from a calculated simulation condition. Thus, synthesized optical flow uv is 0.2396 rad/s in the results of both Conv and Prop2. Therefore, the driver cannot perceive the azimuth angle direction of optical flow u, since synthesized optical flow uv is not changed as compared with the elevation

Table 3.5: Simulation results: Conv and Prop2

	Conv	Prop2
Abs Maximum Error [m]	0.0373	0.0300
RMS Error [m]	0.0213	0.0164
Abs Maximum Flow [rad/s]	0.0029	0.0040
RMS Flow [rad/s]	0.0012	0.0017

angle direction of optical flow v, that is, the target point converging to the FoE for the driver.

The reason for the improved control performance and ride quality of the proposed method is that the proposed model can control FoE, which reflects the current vehicle motion, in the differential term, as described in subsection 3.3.3. For this, the proposed model can use two types of information: lateral deviation in the proportional term and FoE in the differential term, whereas the conventional method use only lateral deviation. The additional reason for the improved controller is considered to be the low gain property. In both the proposed model of Equation (3.43) and the conventional method of Equation (3.44), both differential terms have information of the target path. However, there is a difference in Equation (3.44) has static information, which is the assumption of a steady circle of radius R, and Equation (3.44) has dynamic information, which is $\partial f/\partial x$ on the target point. If the curvature of the target path is changed such that it follows the clothoid path, the control input of of Equation (3.44) is more oscillatory than that of of Equation (3.43). For this reason, the proposed method becomes a low gain controller, so that this model improves the control performance and ride quality. These results show that we can confirm that the preview driver model that includes knowledge of optical flow improves the control performance and ride quality.

3.7 Conclusions

In this study, we discussed the preview driver model and optical flow. Using our knowledge of optical flow, we analyzed the preview driver model and understood that optical flow used in the conventional preview driver model is not on the target point but on the preview point. Therefore, we proposed a new preview driver model that includes optical flow on the target point and the term of the following the target point. We confirmed through the vehicle simulations that the proposed control method shows a better control

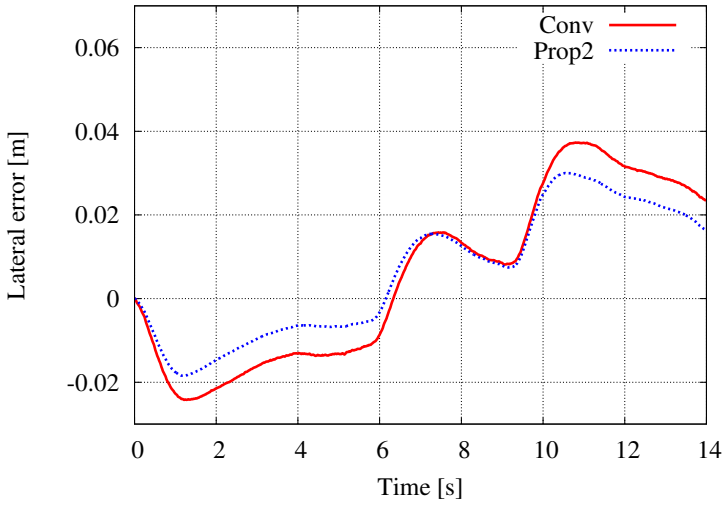

Figure 3.11: Results of comparison of lateral error (Conv and Prop2)

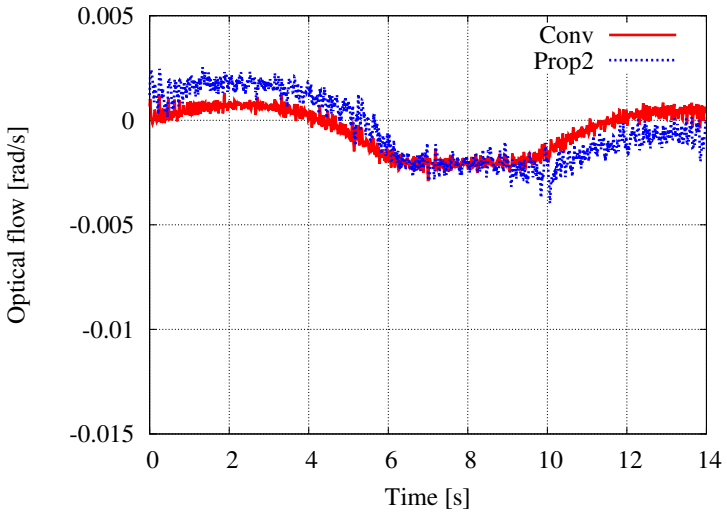

Figure 3.12: Results of comparison of optical flow (Conv and Prop2)

performance and ride quality than that of the conventional preview driver model. In addition, the previous optical flow model is limited in a situation where the vehicle is aimed to track a steady circle only, because the target point converges to the FoE, which is a steady circle [53, 54, 97, 98]. However, the proposed model can be applied to various situations, because the control object is the lateral error related to the preview point, although the FoE assumption is included.

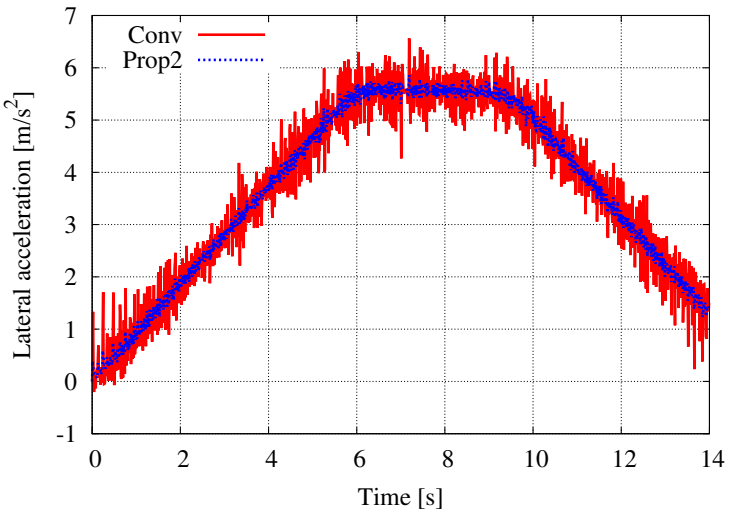

Figure 3.13: Results of comparison of lateral acceleration (Conv and Prop2)

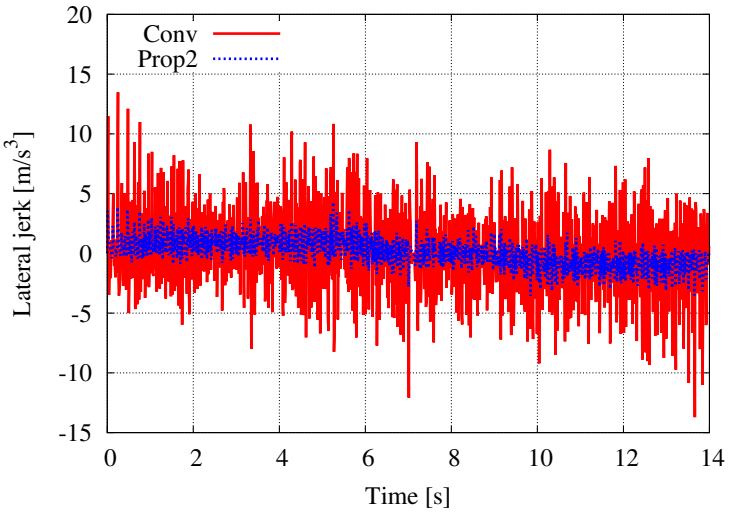

Figure 3.14: Results of comparison of lateral jerk (Conv and Prop2)

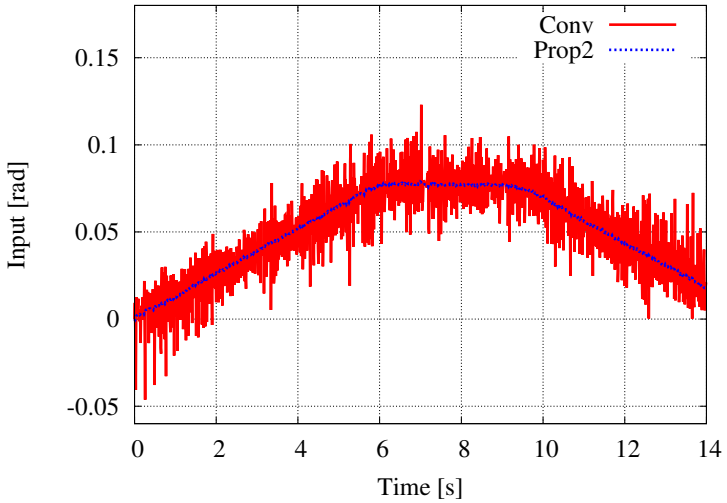

Figure 3.15: Results of comparison of input (Conv and Prop2)

Chapter 4

Analysis of Impact of Optic Flow and Road Edges on Two Point Steering Control

4.1 Introduction

Humans use multiple sources of visual information to steer when driving down winding roads [36, 37]. However, models of steering control can recreate some aspects of steering behaviours using solely two control points: typically, a far point (which provides a preview of future changes in direction), and a near point (which indicates current position-in-lane [89, 101, 102]. The key principles of two-point control models have been tested by examining driver behaviour when far (preview) or near (position-in-lane) information has been selectively removed. When far road information is removed, steering actions become less smooth because drivers rely upon near road information to correct errors after they have occurred and thereby prevent large position-in-lane errors from accruing [103–107]. Conversely, when near road information is removed drivers find it difficult to correct for positional errors, leading to larger deviations from the desired path, whilst still managing to maintain smooth steering to match the future road curvature (for in-depth discussions of this evidence the reader is referred to [107]). The behavioural relationship is assumed to be a basic control model which is divided into guidance control using far vision (Figure 4.1, Guidance) and compensatory control using near vision (Figure 4.1, Compensatory). Whilst the weightings of the components displayed in Figure 4.1 will vary depending on the nature of the steering task, the general principles appear to be well supported and acts as the basis of many current steering models [102, 108–112].

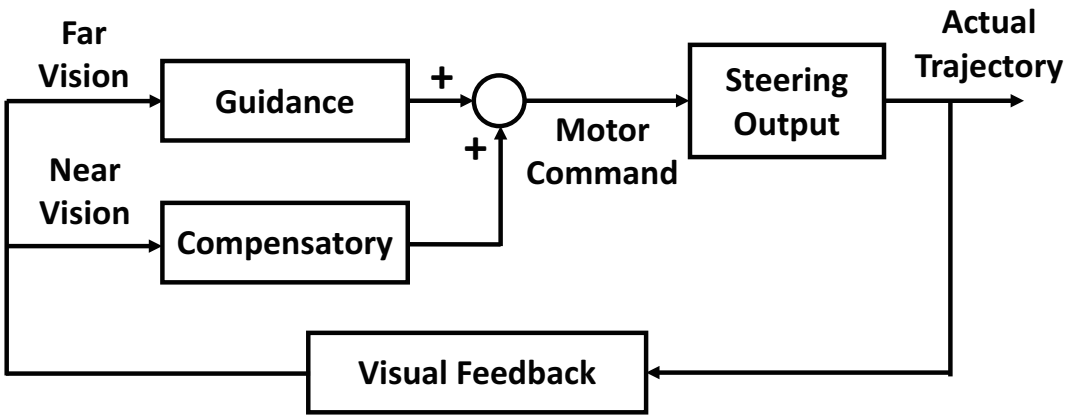

Figure 4.1: A two point control model. When steering using the far point the driver is able to match the future road curvature but unable to eliminate positional error, leading to steering which is smooth but inaccurate. Conversely, when relying on just the near point the driver is able to eliminate positional error but unable to respond in advance to changes in curvature, leading to steering which is jerky but accurate.

Given the widespread prevalence of such two-point steering models it is worth noting that the precise sources of near and far information are often only weakly specified. Road environments are rich sources of information, containing a large set of features from near and far regions that could contribute to estimates of position in lane and the future steering requirements. The characteristic two-point control behaviours (Figure 4.1) have been elicited using displays that only contained 'windows' of perspective correct road-edges [103–105, 113] and components are sometimes refined even further to include elements solely containing splay angle information [114, 115]. In theoretical accounts it is often assumed that angular inputs would be obtained from these road-edges. However, the precise mechanisms for extracting this information are unclear. Computational driver models during curve following tend to use angular inputs determined by the vehicle direction and points on the road centre rather than signals obtained directly from road-edges [89, 102, 108–110]; although in some cases the near point has been implemented as dependent on road-edge information [48]. These accounts do not disentangle use of road-edge information from the other perceptual inputs that are available when looking where you are going (such as gaze direction, or retinal flow [37]). One issue when determining the role of the visible road-edges is that they not only supply useful information about the steering that has been taking place, but they also place hard constraints upon the future steering requirements. Consequently, when removing road edges it can be difficult to determine whether individuals rely more on remaining perceptual inputs, because removing

road edges can fundamentally change the nature of the steering task (e.g. when steering is unconstrained human behaviour can be modelled using single point control [116]). One way of preserving the steering task (maintaining a position on the road) but weakening the inputs supplied by road-edges is to selectively remove road-edges in either near or far regions. The driver's reliance on alternative sources of information (such as optic flow) can then be compared across the same lane following task [107].

The two-point control models of steering referred to so far rely solely on a near point and far point to produce trajectories similar in quality (i.e. similar smoothness and variability) to those produced by humans. However, just because the trajectories produced are broadly similar to human data, it cannot be concluded that human drivers are not using other sources of visual information to ensure that steering control remains robust. Other sources may provide redundancy if visual conditions become degraded and/or unreliable. Indeed, skilful control of steering has been demonstrated in a wide range of visual environments, including many where roads (and critically road edge information) is weak or absent [48]. There are many potential informational inputs available to human drivers navigating visually rich environments [37, 117], and evidence across multiple studies suggest that humans exploit the redundancy in perceptual information, using a combination of the available signals to provide reliable and robust steering control [24, 26, 36, 118]. In particular, humans are highly sensitive to optic flow [28], and there is evidence that optic flow information provides information distinct from that supplied by the road-edges [107, 119]. Using Land & Horwood's method [103] of adjusting 1 deg viewing windows, Chatziastros et al. [104] found that adding road texture (i.e. optic flow information) reduced lateral deviation uniformly across all viewing segment conditions. Indeed, humans appear to use optic flow as a control source even when current and future steering requirements are solely determined by salient road-edges [107, 119, 120]. Furthermore, specific components of flow appear to interact with near and far information in different ways [107], prompting Mole and colleagues to call for two-point models to be developed that incorporate flow information.

In contrast with models identifying the importance of read edge information, there are also steering control solutions that predominantly rely upon optic flow [19] or retinal flow (the flow pattern available to an animal that looks where it wants to go [30, 121]). Recently a driver model has been reported that is able to generate human-like steering trajectories along roads using a form of retinal flow signal rather than road edge information [97].

Importantly, Okafuji et al.'s control model seemed most accurate when the inputs were obtained from far regions rather than near regions. Whilst the model steered successfully, it only used flow signals from around the fixation point (rather than the global flow field as used by humans when steering [107, 119]. It seems, then, that accurate models of human steering control will somehow need to combine the signals derived from optic flow and road edges perhaps in a two-point control model that allows for additional perceptual inputs. An issue when trying develop such a two-point control model is that the contribution of flow and road edge information to near and far points remains unclear. Whilst Chatziastros et al. [104] found that the presence of a flow signal made the same contribution across varying road-edge conditions (i.e. there was no interaction), they only added texture to the road surface (not the entire scene) which may have limited the availability of flow information from the visual periphery. There is evidence that optic flow and road-edge information can interact [107], but only under specific conditions where the flow signals are biased with respect to the road edges. The extent to which the presence of optic flow within near and far zones is used to support accurate steering control remains to be tested.

The current experiment examines whether flow and road edge information can be simply modelled with a two-level steering control model. In particular, the aim is to examine whether the use of optic flow varies depending whether the signal comes from near or far regions and whether the impact of optic flow interacts with the presence of road edge information. Using a driving simulator, near or far portions of optic flow and/or road-edge information were selectively masked. In line with studies that selectively removed road-edge information [103–107], it was expected that removing far road edges would produce steering that is lagged with respect to upcoming changes in the road (reduced anticipation), whereas removing near road edges would reduce steering accuracy. Crucially, selective removal of optic flow information from near and far regions, alongside road edge information, tested whether there were interactions between these sources of information. In order to control for the potential differential patterns of eye-movements elicited by the various visual conditions gaze was directed to a fixation point placed at the centre of the road ahead (see method for more details).

Whilst removing near or far road edge information provides a pure test of whether each source is being used, this form of manipulation does effectively force the driver to rely on alternative sources to control steering. Another way of examining reliance on

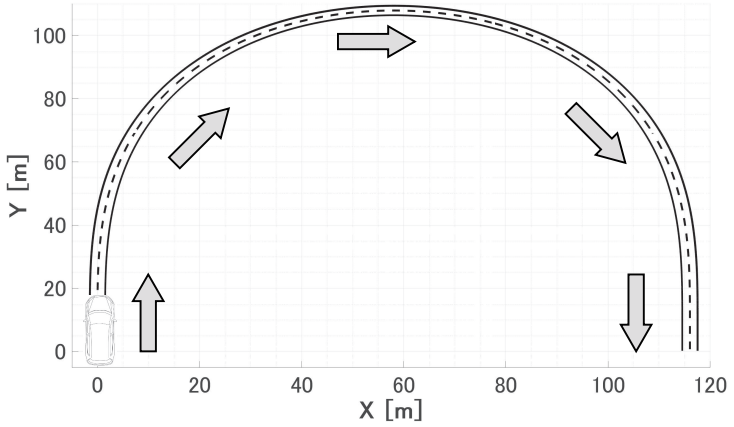

Figure 4.2: Clothoid - Steady Circle - Clothoid (*CSC*) course

perceptual information is keeping the availability constant but changing the utility across conditions. Therefore, we also wished to examine whether there were more subtle interactions between optic flow and road edges depending on whether near and far information was more or less useful for the steering task. Even when driving along simple sections of road (such as a straight leading into a bend) the extent to which far road information will be a useful input to steering control can vary (e.g. far road information is less important when maintaining steering on a straight road section, than on a bend of varying curvature). To examine this issue we used two steering situations that frequently occur during routine driving (described further in the method section: Course Design), and which varied the task requirements: i) a clothoid bend with changing and constant curvature sections (Figure 4.2, 4.3) and ii) a double lane-change manoeuvre (Figure 4.4, 4.5). Trajectories during both tasks were subdevided to examine phases based on the particular steering requirements. The road sections that could lead the driver to stabilise the wheel angle at a set value (straight road for the lane change task; or constant curvature bend for the clothoid task), might be predicted to cause drivers to predominantly rely on information from near regions (to stabilise steering). These sections were contrasted with phases that require the driver to respond to future changes in road (the point when the lane change occurs or the change in bend curvature for the clothoid) where the driver may rely more on information from far regions (anticipating future steering requirements). Our aim was to determine whether both optic flow and road edges contributed to steering during these particular phases of control, and whether there were interactions between the sources.

We considered two main hypotheses: whether the region of the scene (near or far) supplying optic flow information altered steering (H1), and whether there were interac-

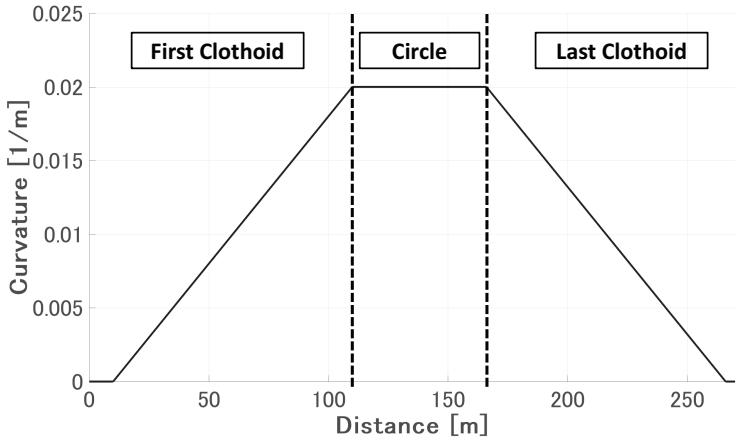

Figure 4.3: The three phases of *CSC* course

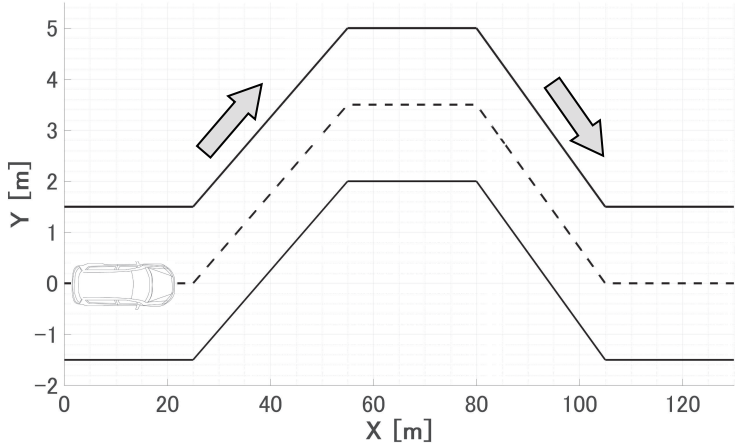

Figure 4.4: Double lane change (*DLC*)

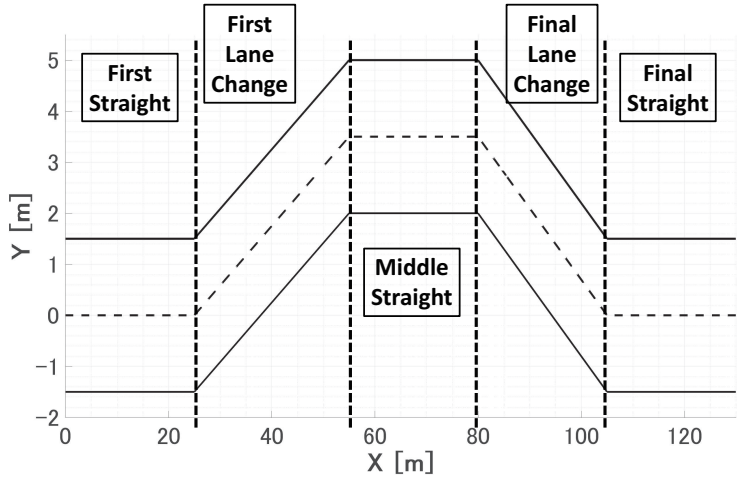

Figure 4.5: The five phases of *DLC* course

tions between the regions supplying optic flow and the road-edge information (H2).

H1. Optic Flow affects Steering Control:
Optic flow from the near region contains larger flow vectors than far regions [122] and peripheral viewing of these vectors may best support the driver in detecting travel direction [123], in which case masking flow from the near region (Figure 4.6; C7-9 Near Flow Mask) will have the biggest effect upon steering (H1A). In contrast, it might instead be predicted that flow from around the point of fixation would be most useful for controlling steering [97, 121] in which case masking far regions (Figure 4.6; C4-6) will have the greatest influence over steering (H1B). Finally, masking either region of the ground will reduce the overall quality of optic flow, and it may be that the global pattern of optic flow is the main predictor of steering (H1C) [119]. If this is the case we would expect steering accuracy to deteriorate whenever there was a flow mask irrespective of where the mask fell (Figure 4.6; C4-9).

The first set of hypotheses are mutually exclusive, and are concerned with which regions of flow influence steering (independent of road edges). However, an interaction between flow and road-edges could take many different forms depending on which hypothesis within H1 is most supported. The second set of hypotheses considers the two most extreme cases provided under the two point control framework.

H2. The effect of Optic Flow on steering control depends on road-edges:
If optic flow is incorporated into the estimate of near and far points we might expect that the utility of flow depends on the proximity to these points, in which case optic flow from a region should be most useful when the corresponding road-edge in the same region is also visible. If this is the case we would expect steering to be more accurate when the congruent flow and road regions are visible (Figure 4.6, C5 & C9) compared to when the incongruent flow and road regions are visible (Figure 4.6, C8 & C6), even though there should be a similar quantity of road and flow information across the whole visual scene (H2A).

Alternatively, optic flow may provide useful information for two-point control independent of road edge information (i.e. provide redundancy). If this is the case we might expect similar steering patterns in conditions with incongruent flow and road masks (Fig-

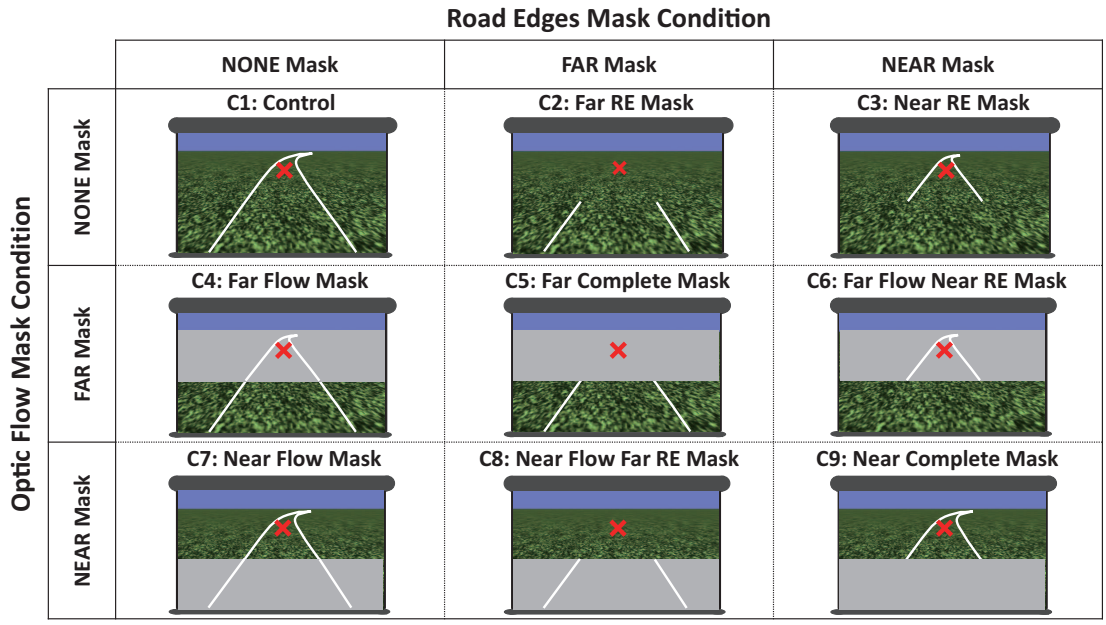

Figure 4.6: A schematic representation of the nine experimental conditions showing the various combinations of Optic Flow Mask (None, Far or Near) and Road Edge Mask (None, Far or Near). The X symbol indicates the presence of a fixation cross positioned over the road centre that drivers were required to look at throughout trials (note that the cross has been artificially enlarged in this figure, the actual fixation cross was optically much smaller relative to the display).

ure 4.6, C8 & C6) to congruent masks (Figure 4.6, C5 & C9) because of similar quantity of road and flow information (H2B).

4.2 Methods

4.2.1 Participants

A sample of 20 University students and staff (2 males and 18 females, 21-33 yrs, mean = 27.4 yrs) took part in this study. All participants had normal vision (participants did not need glasses) or corrected-to-normal vision (participants wore glasses). All held a full driving license (mean time since test = 7.85 yrs). Participants received £10 for taking part in the study. All participants gave written informed consent and the study was approved by the University of Leeds, School Psychology Research Ethics Committee (Reference number: 17-0216), and complied with all guidelines as set out in the declaration of Helsinki.

4.2.2 Apparatus

Virtual environments were generated using using WorldViz Vizard 3.0 (WorldViz, Santa Barbara, CA) on a PC with Intel i7 3770 (3.40 GHz), and projected (EPSON EH-TW5210) with matte-black surroundings. The projections subtended 1.96 m × 1.12 m and was perspective correct from a viewing distance of 1 m and an eye-height of 1.2 m (field of view 88.84° × 55.5°). The display refresh rate was synchronised with data recording at 60 Hz. Steering was controlled using a force-feedback wheel (Logitech G27, Logitech, Fremont, CA), which was linearly mapped onto rate of change of heading through a minimum step size of 0.36 deg/s. The wheel applied a centre-return spring force to ensure that the wheel was re-centred at the end of trials (when participants released the wheel). This meant the wheel was centred and ready for the next trial. The force was constant and was not tied to vehicle dynamics therefore participants did not require extensive training to learn how forces changed according to the vehicle state. The steering dynamics used a point mass model that was not matched to a particular vehicle. All participants were given practice before the actual experiments and rapidly became familiar with the simple simulator model and the mapping of movements of the wheel onto the directional changes that occurred.

4.2.3 Stimuli

Course Design

Driving in the real-world typically consists of negotiating straight sections of road connected by a series of bends. The nature of the bends will change the balance between stabilisation of lane position and anticipation of upcoming changes in steering. Two different courses were created to examine steering when the balance between stabilisation and anticipation components were altered. Both courses had an initial 10 m straight section, with the driver starting in the road centre. Path direction (left or right bend) was randomised from trial to trial to ensure that trials were not so repetitive that participants learnt the motor action required to steer each bend.

The first course was a 'U'-shaped bend (Figure 4.2) consisting of alternating Clothoid - Steady Circle - Clothoid (*CSC*). Okafuji et al. [124] used a similar course to show that optic flow control with path information (i.e. an array of points specifying the desired

trajectory) was able to keep closer to a marked trajectory than a traditional lateral deviation control model. During data analysis steering trajectories along *CSC* were separated into the 'first clothoid' (increasing curvature), 'steady circle' (constant curvature), and the 'last clothoid' (decreasing curvature), to isolate the segments where greater anticipation should have been required (compared to the steady circle phase). In this task, we expect that far preview information would be most useful during the first clothoid and the last clothoid (where far preview information indicates that there is an upcoming change in steering wheel angle required), rather than the middle constant curvature period (Steady Circle; drivers need to maintain a constant wheel angle) (Figure 4.3).

The second course consisted of a Double Lane Change (*DLC*) which is consistent with ISO 3881-1 (Figure 4.4) [125]. This type of course has been successfully used to discriminate between different driver steering behaviours [87]. Since *DLC* has discrete changes in heading angle there are sections where anticipation should be more useful (i.e. immediately before the lane change) than when holding course on the straight sections where compensatory control may be predominant (Figure 4.5). This course differs from *CSC* in a number of ways. Not only does it place greater emphasis on anticipation prior to the lane change, but because of steering dynamics there is no way for drivers to generate trajectories that exactly match the centre of the road at all points in time (effectively trying to fit a sinusoidal path to square-wave-like signal). As such the driver will be attempting to gauge when they should initiate steering to generate a trajectory that leads to a road position that is closest to the centre of the lane.

Gaze Fixation Requirements

During an experiment that used similar displays with constant curvature bends, Mole et al. [107] found that removing far road edges (see next section: Optic Flow and Road Edges Mask) affected driver's gaze patterns, with participants re-orienting their gaze lower in the scene toward the remaining visible portion of the near road. Eye-movements will alter retinal flow information, so it is possible that participants are less able to use flow information if they are not looking proximal to where they wish to travel [121]. To avoid systematic differences between conditions due to changes in eye-movements (whilst also minimising between-participant differences that would be caused by varied eye-movement strategies), we controlled for eye-movements by asking participants to look, throughout each trial, at a red cross displayed in the road centre approximately 16.1 m (1.2 s) ahead

of the participant. In previous research we have found that participants usually look on the region 1-2 s ahead, and we have used this method to control gaze patterns when investigating the other visual factors influencing steering behaviours [37, 43, 48].

It could be argued that constraining gaze in this way prevents the visual system from optimally sampling the information available in the optic array, whilst also imposing cognitive load costs on the driver. The problem of course with free gaze is that the loss of control potentially confounds exploration of the data depending on the behaviours adopted by the participants. The decision to require gaze fixation of a point on the road ahead was driven by the nature of the two-point model that we were investigating since it explicitly uses such a point as an input. Whilst freely fixating a point on the road ahead is likely to be somewhat different from being forced to fixate a fixation cross drawn in the world, the loss of ecological validity was felt to be more than outweighed by the improved experimental control provided.

Optic Flow and Road Edges Mask

The simulated virtual environment consisted of a green tinted texture, with a 3 m wide road demarcated with white road-edges (see Figure 4.6). Our virtual environments were designed so that two primary sources of information were made available to control steering: optic flow and road-edges. In order to assess the importance of each source to two-point control, we selectively applied a flow or road-edge mask to near or far portions of the scene (see Figure 4.6). Two masked areas were determined based on the half distance (8.0 m) of the fixation point distance. This distance was chosen so that the far mask would remove crucial preview information (such as direction of the upcoming bend). Previous studies have applied masks which simultaneously cover road and flow information [106], but no study has applied road or flow masks independently or applied masks whilst controlling for changes in gaze. A 3 ($FlowMask_{No}$; $FlowMask_{Fr}$; $FlowMask_{Nr}$) $\times$ 3 ($REMask_{No}$; $REMask_{Fr}$; $REMask_{Nr}$) design leads to 8 conditions that include one or two mask combinations, and one mask-free condition (i.e. $FlowMask_{No}$ and $REMask_{No}$, the control condition). Whilst it would have been possible to also introduce complete masks to both information sources, masking both near and far road edge regions then made it impossible to perform the steering task. For ease of analysis (to keep factors balanced) we did not include a condition where both far and near flow regions were masked.

Task Instructions

Participants were instructed to fixate the red cross displayed on the screen and "attempt to steer a central trajectory, keeping to the middle of the road"; to steer "as smoothly and as accurately as you can". We were aware that instructing the participants to keep to the road centre may have reduced natural 'cutting the corner' behaviour, however we wanted to use this instruction since it then allows precise measurement of steering bias relative to this centre point, and is especially useful for examining systematic steering biases with reference to the same ideal trajectory (zero bias) for all participants. As per previous studies [107,119,120] simulated locomotor speed was kept constant at 13.41 m/s (30 mph) throughout all trials to avoid any differences between trials, conditions and/or participants. This meant that participants were not required to use the foot pedals for longitudinal control.

4.2.4 Procedure

Participants were given 10 practice trials on each of the two courses (20 trials in total) in order to become familiar with the driving simulator dynamics, steering tasks, and mask conditions, and to minimise major learning effects throughout the experiment. During practice trials participants were exposed to each condition for a single trial (only the control condition was repeated) in the order C1, C5, C9, C7, C4, C3, C2, C8, C6, C1 (see Figure 4.6 for condition labels). In the experiment proper, trials were randomly interleaved, and participants experienced 6 trials per condition [48, 107, 119], resulting in 54 trials per course. The trial durations were 10s for DLC and 19s for CSC, resulting in a block running time of 9 mins and 17.1mins respectively. Participants first performed the CSC task and then the DLC task. Participants took a 5 minute break between tasks.

4.2.5 Analysis

The hypotheses outlined in the introduction require steering metrics which predominantly capture anticipatory and compensatory steering behaviours. Steering wheel angle, and position and orientation in the world were recorded per frame, allowing driver performance to be examined with respect to the ideal trajectory (road centre, as per instructions), or with respect to key environmental events (such as approaching a large change in road di-

rection). The first 0.84 s (50 frames) of each trial were stationary to allow the participant to prepare for the next trial and re-centre the wheel.

Three main measures of steering performance were calculated:

1. *Steering Bias* (*SB*) provides a signed measure of **accuracy** and was calculated using the average deviation of position away from the road centre for each frame of each trial (in metres). It is a signed measure of error and for the clothoid bends positive values indicate steering biased toward the inside road edge (a behaviour referred to as 'oversteering') whereas negative values indicate steering biased toward the outside of the bend ('understeering'). Note that the labels understeering and oversteering should not be confused with the terms 'oversteer' and 'understeer' commonly used to describe the steering properties of real vehicles on roads (and the associated requirements for the driver to compensate for these properties). The *DLC* task did not have a single direction of bend so rather than indicating over/understeering the sign indicates systematic bias toward the left (negative) or right (positive) road edges during these trials.

$$SB = \frac{1}{N}\sum_{i=1}^{N}(Vehicle\ Position - Centre\ Line) \tag{4.1}$$

2. *Root-Mean-Squared Error* (*RMSE*) provides a measure of **precision** of each trajectory relative to the road centre in order to capture the extent of lateral deviation across each trial (in metres). Larger values of this unsigned measure indicate trials where the driver spent longer periods deviating further from the road centre.

$$RMSB = \sqrt{\frac{1}{N}\sum_{i=1}^{N}(Vehicle\ Position - Centre\ Line)^2} \tag{4.2}$$

3. *Initiation Point* provides a measure of lag/anticipation (in seconds) on the *DLC* roads. Steering performance leading up to the first lane change was isolated (the later bends are potentially contaminated by prior steering making it is difficult to obtain a "pure" measure of the timing responses) and the time at which drivers made their first large steering turn was calculated. The time at which a 1 degree change in steering occurred since this approximates to a 10% change in heading angle. For *CSC* there was not a single point that the Initiation Point could be measured from (because the change in heading was incremental) so it was not considered as a useful metric to calculate.

SB and *RMSE* are calculated per each phase to analyse the steering performance depending on the tracking path. For both *CSC* and *DLC* tasks a 3 ($REMask_{No}$, $REMask_{Fr}$, $REMask_{Nr}$) × 3 ($FlowMask_{No}$, $FlowMask_{Fr}$, $FlowMask_{Nr}$) repeated measures ANOVA were conducted on each of the steering metrics. Bonferroni corrections were made for any post-hoc comparisons. For ease of understanding, main effects and interactions are reported in Tables 4.1, 4.2, and key contrasts that explain interactions are depicted in figures. When sphericity assumptions were violated Huynh-Feldt corrections (when $\epsilon > .75$) or Greenhouse-Geisser corrections (when $\epsilon < .75$) were used [126].

4.3 Results

The two steering tasks (*CSC* and *DLC*) were designed to put different demands on the drivers, whilst also varying the potential utility of prospective information sources for steering control. Each task was analysed separately to see whether similar patterns of steering were apparent independent of particular task characteristics.

4.3.1 CSC Steering Task

To determine the influence of road edges and optic flow when steering curved roads we divided each trial into three phases: 1) First Clothoid (0.84 − 9.50 s), 2) Steady Circle (9.50 − 14.17 s), 3) Last Clothoid (14.17 − 19.00 s). The first clothoid was a tightening bend, the middle phase was a bend of constant curvature, and the last clothoid was a straightening bend (Figure 4.2). A 3 (REMask) × 3 (FlowMask) ANOVA was run on steering bias measures from across the whole trial, and also for each phase (main effects and interactions are reported in Table 4.1).

Steering Bias

Average trajectory plots across REMask and FlowMask conditions for three phases of CSC path are shown in Figure 4.7 and 4.8. These results are related to main effects that are reported in Table 4.1. When no masks were in place (all optic flow and road-edge information was present) steering was relatively unbiased during the first two phases of the trial, but then oversteering (corner cutting) occurred during the final phase as the road straightened (Figures 4.9-4.13). This is consistent with a number of other studies

showing a propensity for human drivers to cut corners [42, 127]. From Figures 4.9, 4.10 it can be observed that removing either flow or road-edge information altered trajectories, leading to an increased propensity for understeering. Across the whole course (Figure 4.10) this resulted in significant main effects for manipulations of optic flow and road edges, but not a significant interaction (see Table 4.1). Removing either region led to increased understeering compared to when there were no masks ($FlowMask_{No\ vs\ Fr}: p < .001; FlowMask_{No\ vs\ Nr}: p < .001; REMask_{No\ vs\ Fr}: p = .003; REMask_{No\ vs\ Nr}: p = .001$).

On closer inspection of the individual phases of steering, it seems that masking road or flow information had differential effects on steering depending on the task requirements. During the First Clothoid phase, $REMask_{Fr}$ caused the greatest bias ($REMask_{No\ vs\ Fr}: p = .003; REMask_{No\ vs\ Nr}: p = .132$) (Figure 4.11), presumably because without this information it is not possible to predict whether the future path curved to the left or right (path direction was randomised from trial to trial). During the Steady Circle phase (Figure 4.12) both flow masks and only $REMask_{Nr}$ caused significantly greater understeering (compared to the no mask condition) (see Table 4.1; $FlowMask_{No\ vs\ Nr}: p < .001; FlowMask_{No\ vs\ Fr}: p < .001; REMask_{No\ vs\ Nr}: p = .001; REMask_{No\ vs\ Fr}: p = .091$). During the Last Clothoid phase (Figure 4.13) masking either flow or road edges reduced oversteering compared to when there was no mask (Table 4.1). Interestingly, during the Last Clothoid phase there is also an interaction (Table 4.1), caused by FlowMask$_{Fr}$ and FlowMask$_{Nr}$ reducing oversteering relative to $FlowMask_{No}$ during $REMask_{No}$ ($FlowMask_{No\ vs\ Nr}: p < .001; FlowMask_{No\ vs\ Fr}: p = .001$) and $REMask_{Fr}$ ($FlowMask_{No\ vs\ Nr}: p = .002; FlowMask_{No\ vs\ Fr}: p < .001$), but not $REMask_{Nr}$ ($FlowMask_{No\ vs\ Nr}: p = 1; FlowMask_{No\ vs\ Fr}: p = .097$).

Root-Mean-Squared Error

The steering bias metric usefully distinguished between performance accuracy across the display conditions, identifying systematic shifts in position relative to the road centre. It is possible, however, that non-systematic directional changes in position would not be captured by steering bias (since positive and negative errors could effectively cancel one another out). An alternative metric of lateral deviation (relative to the road centre) is Root-Mean-Squared Error (*RMSE*; Figure 4.14). *RMSE* was calculated for the whole course to act as a metric of variability, whereby larger values reflect a trajectory that was further

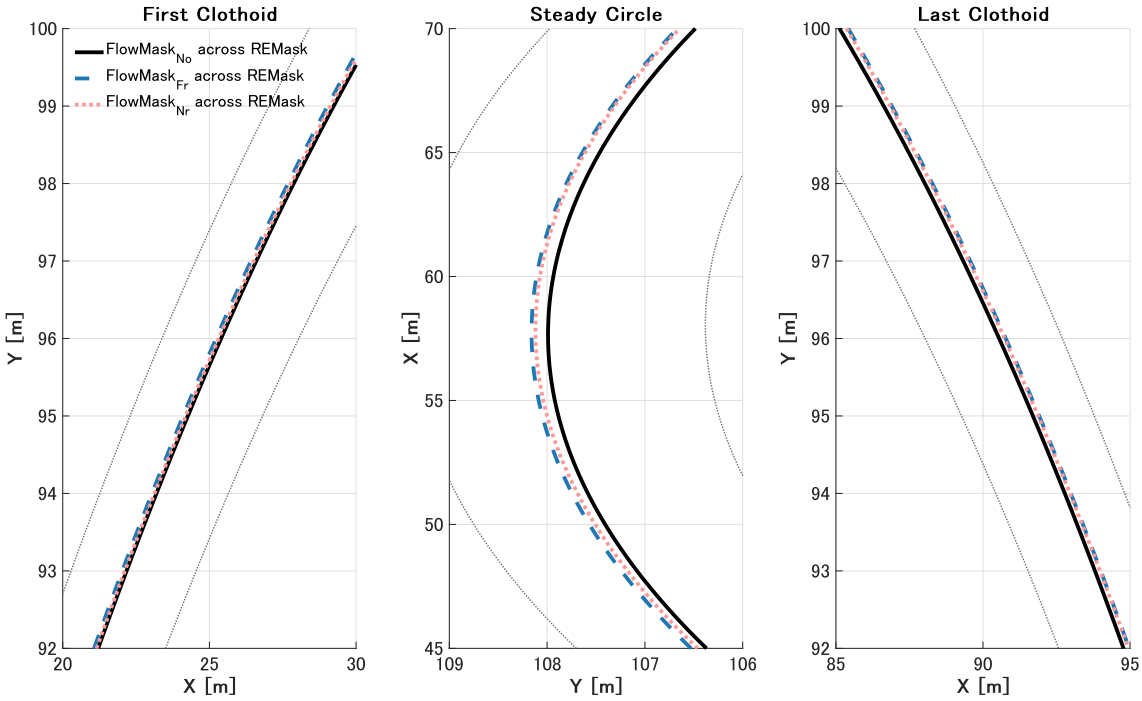

Figure 4.7: Average trajectory plots for the three phases of *CSC* trials (first clothoid, circle and last clothoid, see Figure 2B) across REMask.

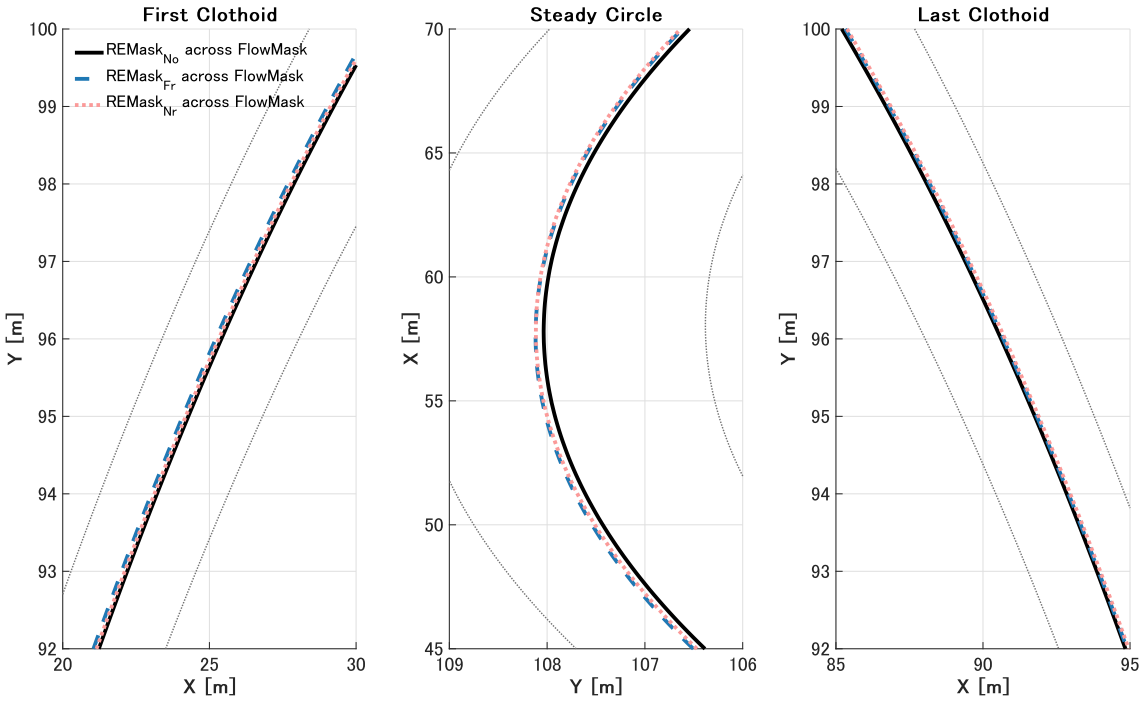

Figure 4.8: Average trajectory plots for the three phases of *CSC* trials (first clothoid, circle and last clothoid, see Figure 2B) across FlowMask.

from the road centre. As can be seen in Table 4.1, the ANOVA revealed a main effect of FlowMask, but no main effect of RoadMask, and no interaction. The main effect of

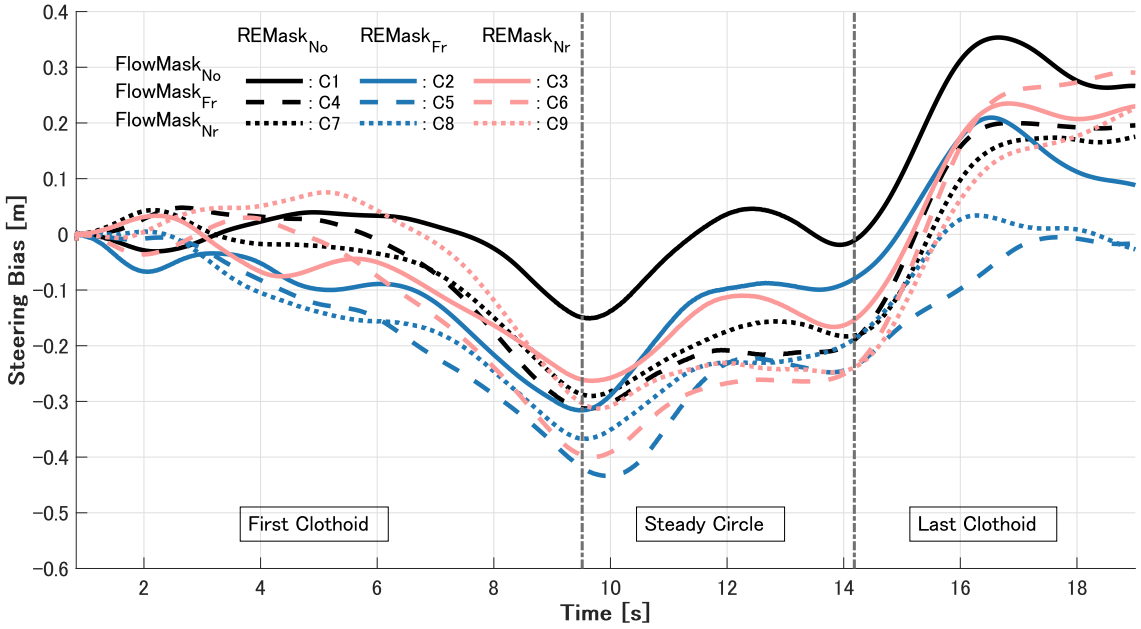

Figure 4.9: Results of Steering Bias plot. Average steering bias relative to the road centre for the three phases of *CSC* trials (first clothoid, circle and last clothoid, see Figure 4.3). Negative values indicate understeering (outside position relative to the centreline in Figure 4.2) and positive values indicate oversteering (inside positions relative to the centreline).

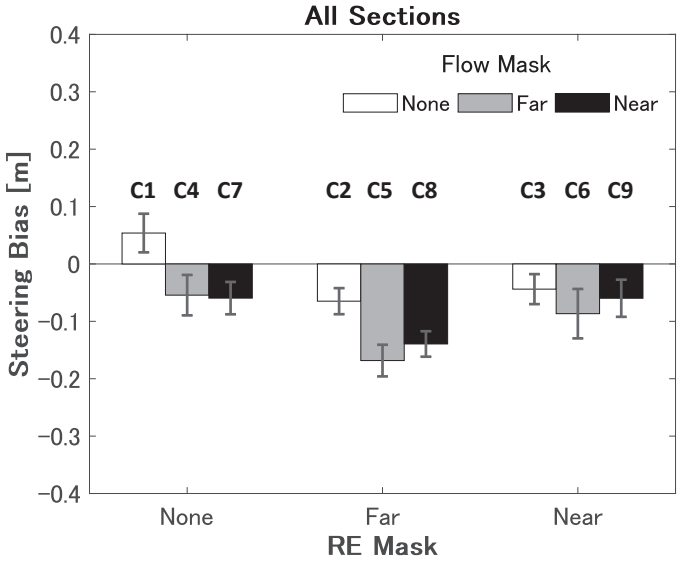

Figure 4.10: Results of Steering Bias (All Phases). Error bars represent standard error of the mean.

FlowMask was caused by $FlowMask_{Fr}$ increasing *RMSE* relative to the other two flow conditions ($FlowMask_{No\ vs\ Fr}$: $p = .019$; $FlowMask_{Fr\ vs\ Nr}$: $p = .026$).

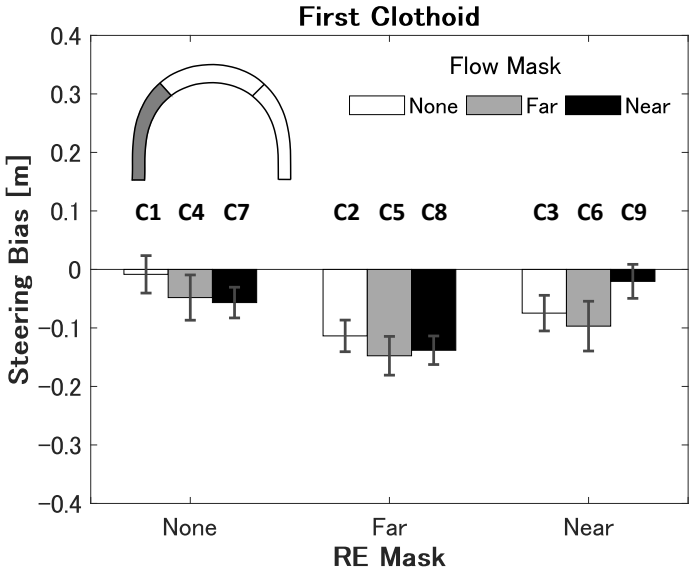

Figure 4.11: Results of Steering Bias (First Clothoid)

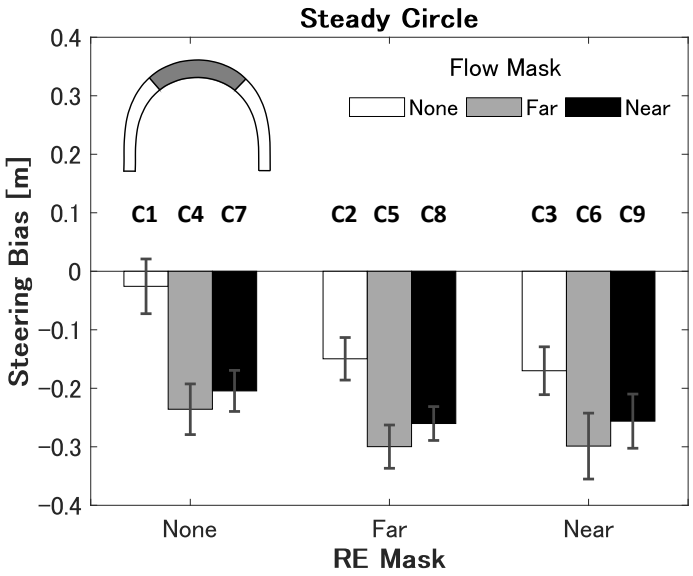

Figure 4.12: Results of Steering Bias (Steady Circle)

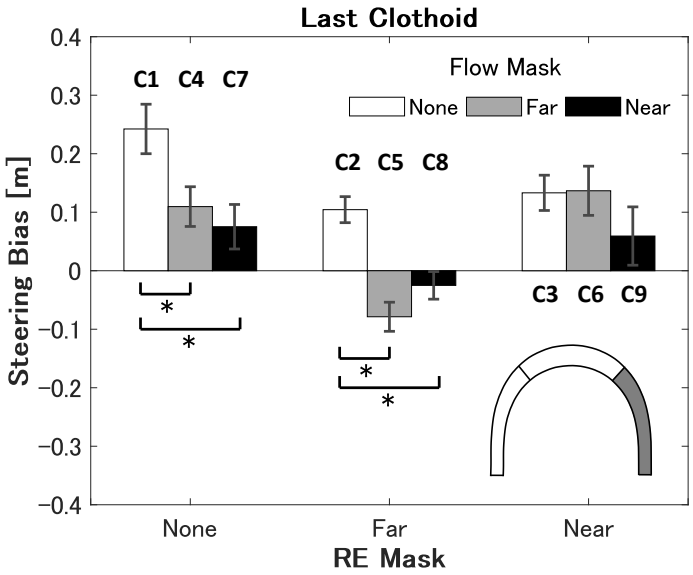

Figure 4.13: Results of Steering Bias (Last Clothoid). Stars represent key comparisons where interactions are present.

Table 4.1: ANOVA main effects and interactions for *SB* and *RMSE* for *CSC*.

Variable		*SB*				*RMSE*
		All Phases	First Clothoid	Steady Circle	Last Clothoid	
Flow	F	14.00	1.73	25.16	21.25	6.98
	df	1.45, 27.55	1.35, 25.61	2, 38	1.36, 25.80	2, 38
		($\epsilon = .73^{\dagger}$)	($\epsilon = .67^{\dagger}$)		($\epsilon = .68^{\dagger}$)	
	p	$< .001^{*}$	.20	$< .001^{*}$	$< .001^{*}$	$.003^{*}$
	η_p^2	.42	.083	.57	.53	.27
RE	F	10.43	9.54	4.56	16.60	2.18
	df	1.21, 22.89	1.30, 24.68	1.37, 26.00	1.30, 24.73	1.30, 24.72
		($\epsilon =^{\dagger}$)	($\epsilon = .65^{\dagger}$)	($\epsilon = .68^{\dagger}$)	($\epsilon = .65^{\dagger}$)	($\epsilon = .65^{\dagger}$)
	p	$.002^{*}$	$.003^{*}$	$.032^{*}$	$.001^{*}$	.15
	η_p^2	.35	.33	.19	.47	.10
Flow × RE	F	1.86	2.29	.98	4.99	2.31
	df	2.95, 56.10	2.89, 54.88	2.95, 56.04	3, 56.94	2.73, 51.95
		($\epsilon = .74^{\dagger}$)	($\epsilon = .72^{\dagger}$)	($\epsilon = .74^{\dagger}$)	($\epsilon = .74^{\dagger}$)	($\epsilon = .68^{\dagger}$)
	p	.15	.091	.41	$.004^{*}$	.10
	η_p^2	.089	.11	.049	.21	.11

* : $p < .05$; † : $\epsilon < .75$ (Greenhouse-Geisser corrections are applied)

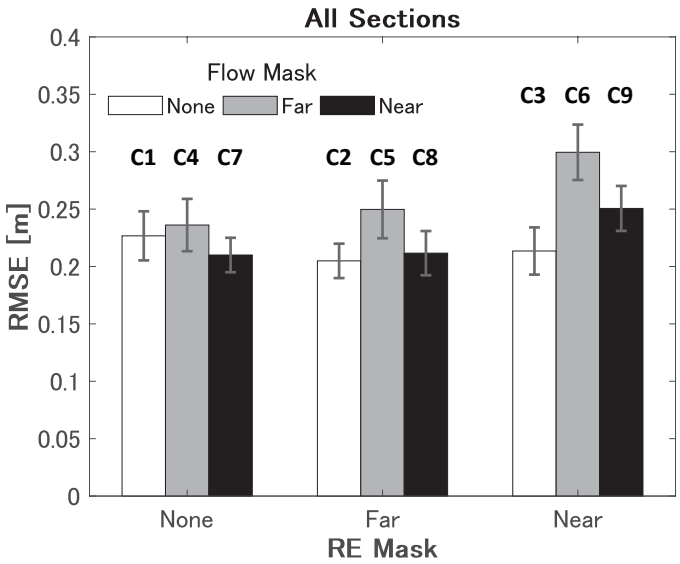

Figure 4.14: Results of average Root-Mean-Squared-Error relative to the road centre for *CSC*. Error bars represent standard error of the mean.

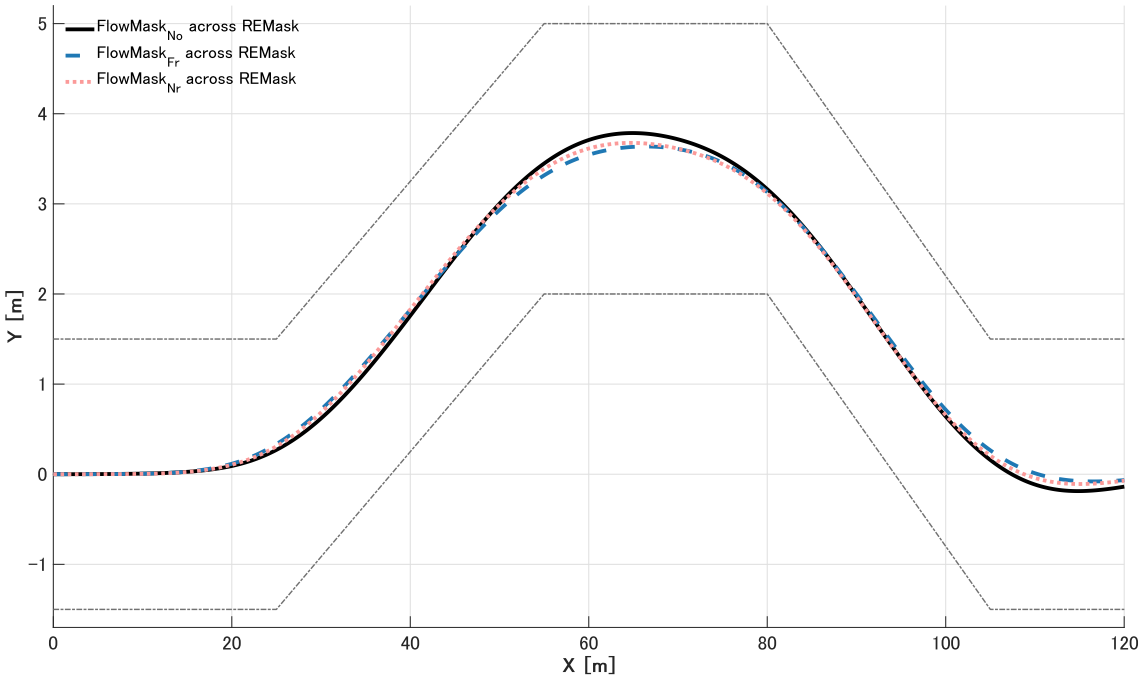

Figure 4.15: Average steering trajectories for the *DLC* task across REMask conditions. Note: vertical and horizontal axes (in metres) are not to scale to make trajectory differences easier to view.

4.3.2 DLC Steering Task

The *DLC* task consisted of a series of straight sections of road connected by large, sudden changes in road direction (Figure 4.15 and 4.16). During analysis the whole trajectory was divided into 5 phases aligned with each change in direction (see Figure 4.5): 1) First Straight (0.84 – 2.69 s), 2) First Lane Change (2.69 – 4.96 s), 3) Middle Straight (4.96 – 6.83 s), 4) Final Lane Change (6.83 – 8.72 s), 5) Final Straight (8.72 – 10.00 s). Whilst the straight sections themselves required little/no steering (if the trajectory was aligned with the road), the sudden changes in direction introduce a need to make large corrections. These characteristics should create conditions where greater emphasis is placed upon far road information in the moments preceding the direction change than during the *CSC* steering task.

Initiation Point

The Initiation Point indicates the time at which the first major steering response was produced on the *DLC* road. The results of the ANOVA (Table 4.2) shows that there were reliable differences in Initiation Point across Flow and Road Edge conditions. The av-

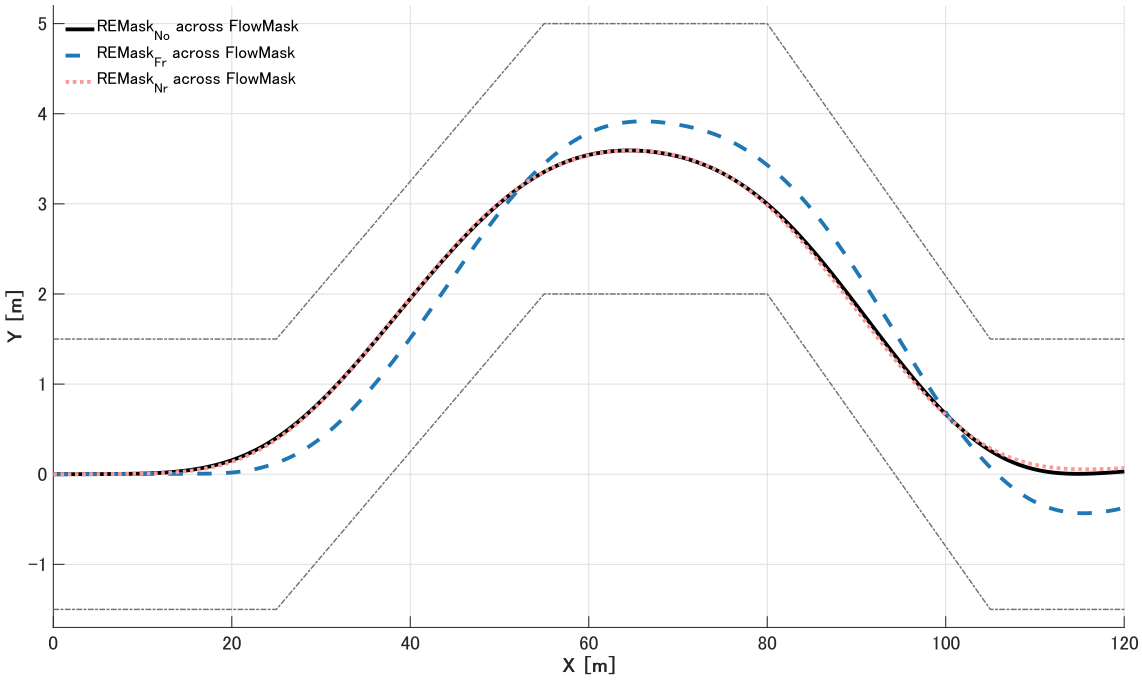

Figure 4.16: Average steering trajectories for the *DLC* task across FlowMask conditions.

erage trajectories across REMask and FlowMask condition are displayed in Figure 4.15 and 4.16, and the most obvious pattern is the lagged trajectories that occur when far road-edge information is removed ($REMask_{Fr}$, blue), compared to conditions where far road-edge information was available (e.g. Control, $REMask_{Nr}$). Figure 4.17 shows the heading angle of the vehicle across the trajectory which is used to identify the region that marks out the initiation point. Figure 4.18 shows the average timing of steering initiation for each condition. $REMask_{Fr}$ was lagged compared to the other REMask conditions ($REMask_{No\ vs\ Fr}, p < .001; REMask_{Fr\ vs\ Nr}, p < .001$). In contrast $REMask_{Nr}$ did not cause reliable differences in initiation point lag compared to $REMask_{No}$ ($REMask_{No\ vs\ Nr}, p = 1.0$). The flow mask also caused changes in the Initiation Point, though these effects were more subtle. Removal of far flow ($FlowMask_{Fr}$) actually caused earlier steering (less lag) compared to when flow was unmasked ($FlowMask_{No\ vs\ Fr}, p = .031$). There seemed to be no systematic differences between initiation point when the near region was masked ($FlowMask_{No\ vs\ Nr}, p = .33$).

Steering Bias

The lag in steering initiation due to $REMask_{Fr}$ (Figure 4.17, 4.18) manifests in biased steering during the initial straight (Figure 4.20). Drivers without road-edge preview stay

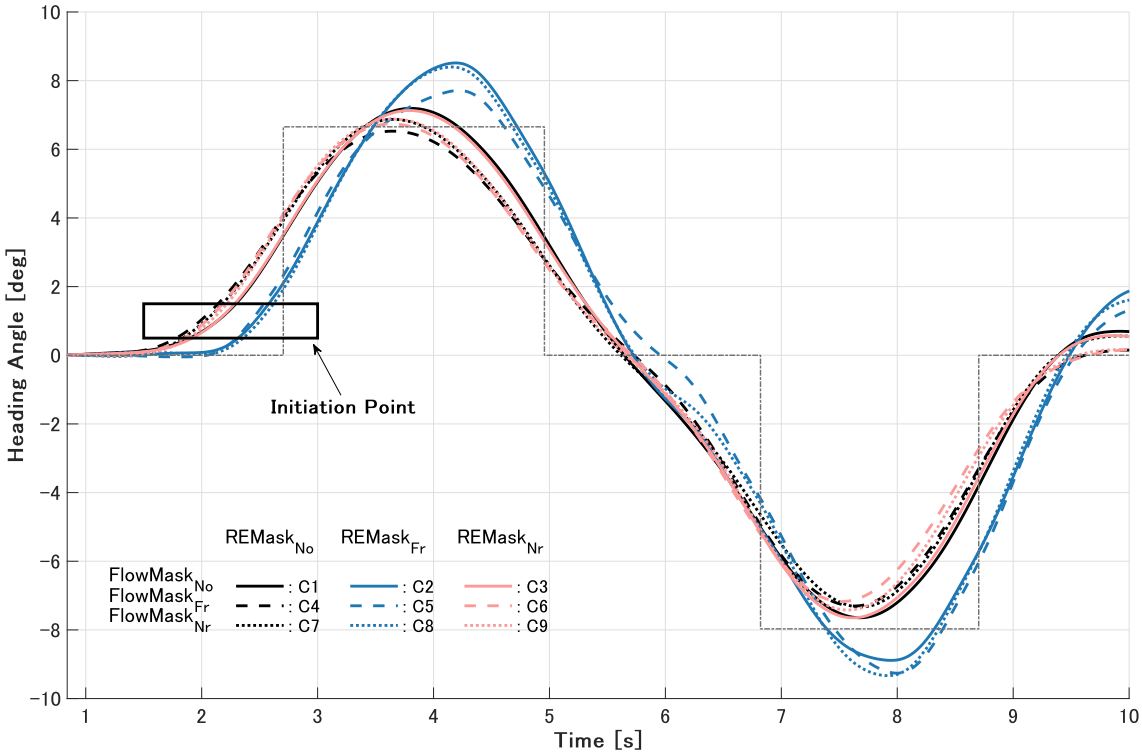

Figure 4.17: Results of average heading change plots, with the initiation point marked.

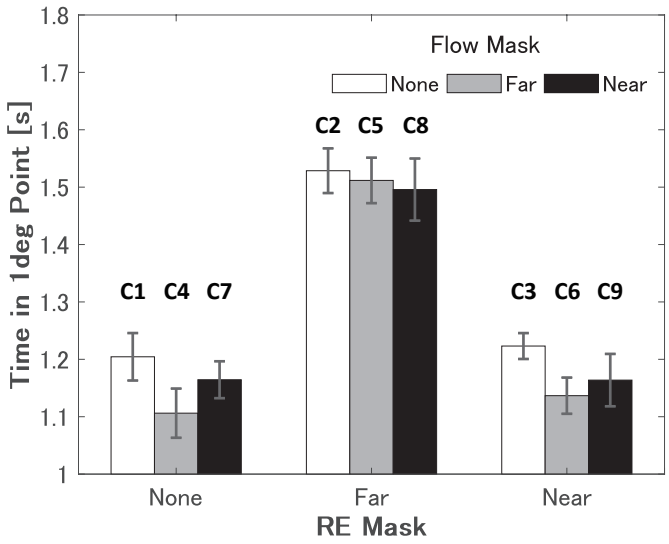

Figure 4.18: Results of average Initiation Point. Error Bars represent standard error of the mean.

close to the midline, whereas drivers with preview anticipate and begin to steer early in the direction of the bend (see Table 4.3). These differences cause relative understeering around the initial bend during the $REMask_{Fr}$ conditions (Figure 4.21), and lagged steering through the remainder of the course (Figures 4.22-4.24).

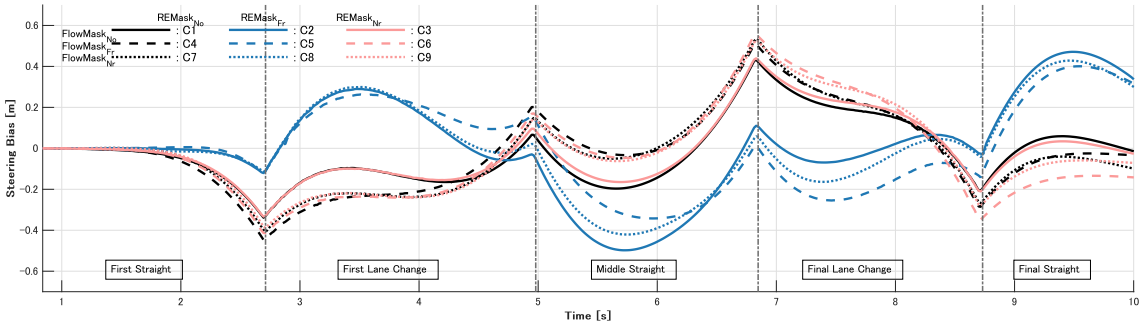

Figure 4.19: Results of Steering Bias averaged across all participants. Note that in this task negative values indicate a leftward position relative to the centreline (see Figure 4.15 and 4.16) and positive values indicate rightward positions relative to the centreline (not oversteering and understeering as in the *CSC* task).

The change in steering associated with the absence of preview information is entirely predictable. Perhaps more interesting is the gradual emergence (after the First Straight) of differences in steering depending on whether flow information was masked or not. The steering bias differences are clearest for Middle Straight and Final Straight phases (Figures 4.22, 4.24), where a road position is adopted consistent with greater corner cutting when either Near or Far flow masks are applied (see significant main effects for Middle Straight and Final Straight in Table 4.3).

For the most part, these effects (lagged steering due to lack of road preview; corner cutting when either flow section is masked) appear to be largely independent of each other. For the final lane change, however, an interaction emerges (Table 4.3; Figure 4.23), due to a large isolated shift in understeering for $FlowMask_{Fr}$, but only when the $REMask_{Fr}$ is applied (Figure 4.23). It is worth noting that the interaction is only present for the final lane change (not the first lane change) and also disappears during the final straight, so it is difficult to conclusively determine whether this specific combination of $FlowMask_{Fr}$ and $REMask_{Fr}$ conditions as being processed in a qualitatively different way to the other $REMask_{Fr}$ conditions.

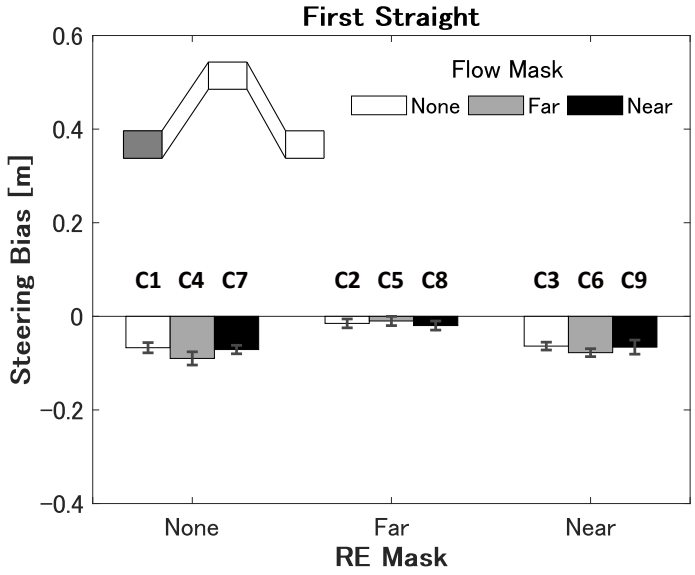

Figure 4.20: Results of average Steering Bias relative to the road centre for the five phases of the double lane change trials (First Straight). Where there is an interaction present the stars denote significant contrasts. Error bars represent standard error of the mean.

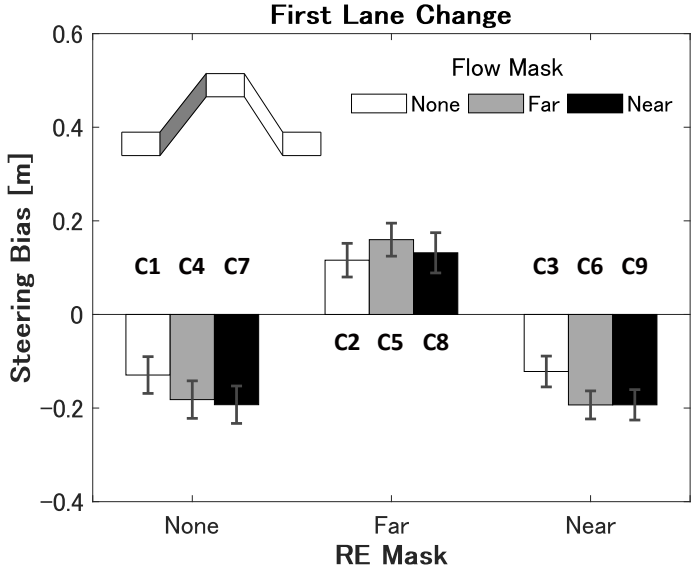

Figure 4.21: Results of average Steering Bias relative to the road centre for the five phases of the double lane change trials (First Lane Change)

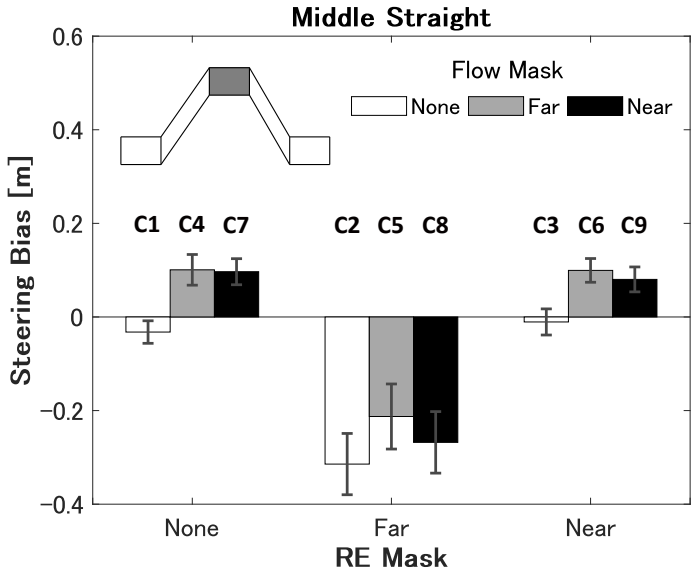

Figure 4.22: Results of average Steering Bias relative to the road centre for the five phases of the double lane change trials (Middle Straight)

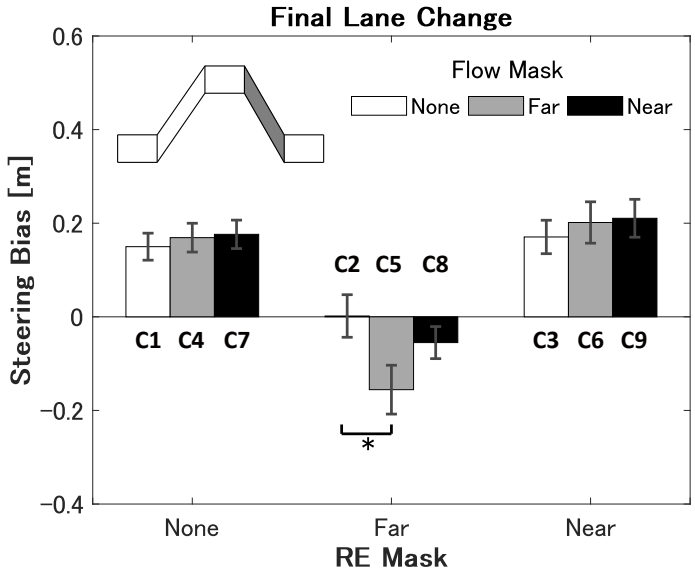

Figure 4.23: Results of average steering bias relative to the road centre for the five phases of the double lane change trials (Final Lane Change)

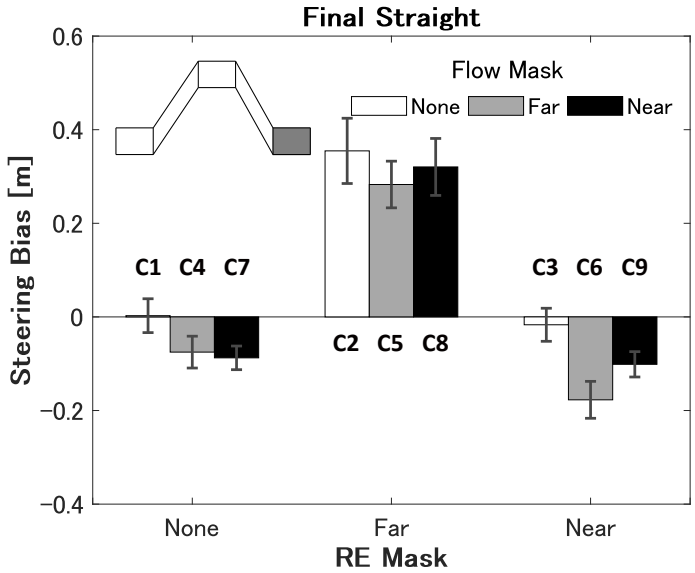

Figure 4.24: Results of average Steering Bias relative to the road centre for the five phases of the double lane change trials (Final Straight)

Table 4.2: ANOVA main effects and interaction for Initiation Point and *RMSE* for *DLC*.

Variable		Initiation Point	*RMSE*
Flow	F	3.73	1.48
	df	2, 38	2, 38
	p	.033*	.24
	η_p^2	.16	.072
RE	F	50.80	2.30
	df	1.34, 25.49 ($\epsilon = .67^{\dagger}$)	1.06, 20.12 ($\epsilon = .53^{\dagger}$)
	p	$< .001$*	.14
	η_p^2	.73	.11
Flow × RE	F	.69	4.13
	df	4, 76	2.74, 52.02 ($\epsilon = .69^{\dagger}$)
	p	.57	.013*
	η_p^2	.035	.18

* : $p < .05$; † : $\epsilon < .75$ (Greenhouse-Geisser corrections are applied)

Root-Mean-Squared Error

Since the *DLC* contains sections where bias was observed in opposite directions (i.e. there are an equal number of left and right turns), it might be expected that directional errors from one phase to the next effectively cancel out - especially the phases where the driver is coming up to a bend in the opposite direction to the one they have just exited. To examine deviation of lateral position the unsigned *RMSE* scores were calculated (Figure 4.25). While there were no main effects of REMask or FlowMask, there was an interaction between these factors (see Table 4.2). The interaction is driven by there being no reliable differences across levels of FlowMask during $REMask_{Fr}$, but during both $REMask_{No}$ and $REMask_{Nr}$ there was an effect of $FlowMask_{Nr}$ ($p = .041$) and $FlowMask_{Fr}$ ($p = .007$), causing greater steering errors than $FlowMask_{No}$.

Table 4.3: ANOVA main effects and interaction for *SB* for *DLC*.

Variable		*SB*				
		First St	First LC	Mid St	Final LC	Final St
Flow	F	1.11	4.38	14.45	2.04	11.42
	df	2, 38	2, 38	2, 38	2, 38	2, 38
	p	.34	.019*	< .001*	.14	< .001*
	η_p^2	.055	.19	.43	.097	.38
RE	F	22.97	44.54	25.78	31.91	48.90
	df	1.48, 28.20 (ϵ = .74†)	1.12, 21.22 (ϵ = .56†)	1.11, 21.05 (ϵ = .55†)	1.26, 23.85 (ϵ = .63†)	1.09, 20.6 (ϵ = .54†)
	p	< .001*	< .001*	< .001*	< .001*	< .001*
	η_p^2	.55	.70	.57	.63	.72
Flow × RE	F	.75	1.96	.736	5.27	1.91
	df	2.71, 51.48 (ϵ = .68†)	4, 76	4, 76	2.44, 46.30 (ϵ = .61†)	4, 76
	p	.52	.11	.57	.006*	.12
	η_p^2	.038	.093	.037	.22	.091

* : $p < .05$; † : $\epsilon < .75$ (Greenhouse-Geisser corrections are applied)

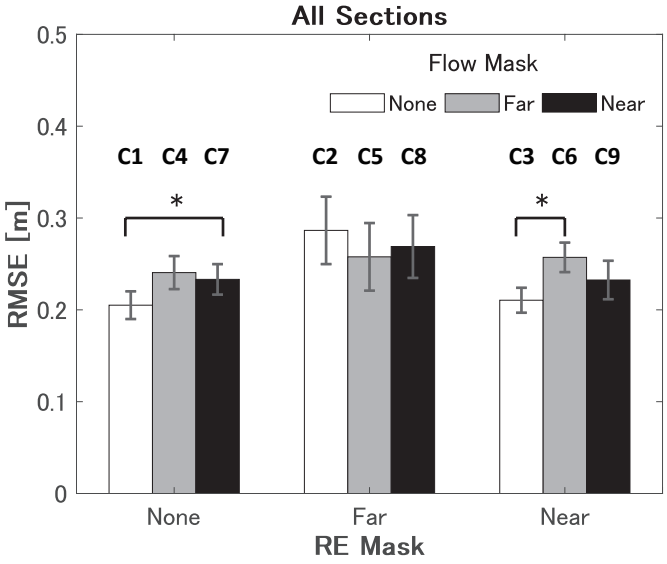

Figure 4.25: Results of average Root-Mean-Squared-Error relative to the road centre for *DLC*. Error bars represent standard error of the mean.

4.4 Discussion

The main purpose of the present study was to test whether optic flow influenced steering control when the availability of road edge information changed. If optic flow information did influence steering, then the secondary aim was to determine whether it interacted specifically with the signals provided by the road-edges for two-point steering control. To examine these issues, steering tasks were used that altered the utility of far-road information, whilst also specifically manipulating visual conditions in order to vary the presence of optic flow and road-edge information from near and far regions. Two main steering tasks were used (a clothoid bend (*CSC*) and a road with a double-lane change (*DLC*)), since these courses could be separated into subcomponents that allowed the examination of distinct steering phases where prospective signals would be more or less useful. Maintaining constant paths (straight line or constant curvature bends) should have been less affected by the absence of far road-edge information than phases where there was an upcoming curvature change or lane change. Indeed, for the *CSC* steering task this pattern was broadly observed: steering bias was affected most when a mask was applied to far road information during the the First and Last Clothoid phase, but there was little difference between near and far road masks for the constant curvature section. The *DLC* task was designed to place a greater emphasis on prospective control from the far road, and the results demonstrated that this was indeed the case: masking the far road caused large changes to steering across all phases of the *DLC* steering task, this was also reflected in poorer overall precision (*RMSE* scores) for the far road mask.

Having established road-edge mask conditions that caused systematic changes to steering, the next step was to determine whether the presence or absence of optic flow in near or far regions altered steering responses. Masking regions of optic flow did alter steering responses across conditions but this was true for both near and far flow masks and also for most phases of both *CSC* and *DLC* steering tasks. For the most-part the nature of the changes induced by the near or far flow mask appeared to be similar: masking either flow region caused understeering during *CSC* and increased corner cutting during *DLC*. At first glance this pattern may seem contradictory, however, the types of steering response required are qualitatively different for the two tasks. The *CSC* trials require gradual adjustment to steering to ensure that a mid-road position is maintained, and these sorts of corrections seem to be supported by global optic flow quality. In contrast, the *DLC* re-

quires a sudden large realignment of the locomotor axis from one straight road section to another straight road section. In many ways this is similar to conditions that require the observer to become aligned with an eccentric target [36, 37]. In this previous work degrading global optic flow was observed to cause more direct trajectories to be taken due to participants executing rapid re-alignment of trajectories rather than controlling steering to make gradual trajectory changes in steering [37] (Figure 4.25). It seems, therefore, that it is the quality of the global flow pattern that is the primary contributor to steering responses across the range of situations examined here (consistent with H1C [119]) rather than there being a specific region of flow supporting use of near or far road edges for two-point control. There has been some circumstantial evidence that flow from far regions may be more important for steering control than flow from near regions [97, 128]. In the present study this wasn't a pattern that was universally observed, but there were instances consistent with far flow sometimes having a greater role: we observed that masking far flow led to increased steering errors accrued across the whole time-course of *CSC* bends (though there were no reliable differences in steering bias), and also observed earlier turning during the first phase of the *DLC* task when far flow was absent.

As outlined in Hypothesis 2, differential effects of near and far optic flow depending on near and far road edges could be considered as evidence for optic flow having an input into two-point steering control. However, we would urge caution in interpreting our findings in this way. Firstly, the majority of the effects of optic flow on steering appear to be largely independent of the presence or absence of near/far road-edge components. The *DLC* steering task was designed to emphasise the need for preview information, so if the use of flow information was dependent on far road edge signals (as seems to be the case for flow speed [107]), then we would expect to see clear interactions with the presence or absence of far road information. Instead, for the majority of the course there was no interaction between road-edges and optic flow suggesting that there is limited use of optic flow for anticipatory control in these conditions. Secondly, whilst interactions were found for some steering phases/metrics (e.g. steering bias during the final lane change of *DLC* and total course *RMSE* for *DLC*), the pattern was not a consistent one. The far flow / far road interaction supports H2A, however the near flow / far road interaction is more consistent with H2B. It seems, therefore, that the relationship between the use of optic flow and road edges is not straightforward. The *CSC* task was designed to place greater emphasis on steering stabilisation, and in that task interactions between optic flow and

road-edges emerged across the time-course of the bend (during the final phase of steering). It seems then that when performing a complex visual-motor steering response there will be complex interactions between the use of optic flow and road edge information, but not in a fashion that can be captured simply using a two-point control model.

One aspect of steering control that was not examined in the present study was the impact of differential gaze strategies on the use of optic flow and road edge information. Previous work [48, 107] highlighted that gaze patterns change depending on the road edge components visible in the scene. The present study controlled this factor by enforcing gaze fixation on a far point, in a region where gaze usually falls when steering along a road with no masked information [37]. Placing gaze at this point may have unintentionally led to additional emphasis on the information available from around the point of fixation (the far region), and gaze fixation at this point may also have provided a further source of information to aid steering [129]. One issue worth mentioning is that gaze behaviours were not directly measured, rather we relied on participants complying with the fixation instructions. Our previous work demonstrates that participants are quite reliable at following these instructions [37] especially when they are looking where they want to steer, however, it is possible that intrusive saccades took the eye away from the point of fixation for brief periods during some trials. It seems unlikely that the reliable patterns of behaviour observed in this study can be explained by the odd failure to fixate since the only likely outcome would be more variable steering responses for those conditions depending on the extent to which intrusive saccades were employed. Future studies could examine similar combinations of near/far flow and road masks with no fixation requirements to determine the way in which gaze patterns adapt to removal of information sources, and the degree to which they can effectively compensate for the loss of information. Conditions C6 ($REMask_{Fr} + FlowMask_{Nr}$) and C8 ($REMask_{Nr} + FlowMask_{Fr}$) would be particularly interesting test cases for the gaze fixation system since in these conditions useful information needs to be retrieved from two separate parts of the scene at the same time, leading so potentially conflicting gaze demands.

The present work controlled locomotor speed, keeping this variable constant. It might be expected that flow information would have more influence over steering as the signal quality increases, and this may naturally occur when travelling at higher speeds. Whilst changes to flow speed have been studied independent of the road edges [107] further experiments are needed to systematically vary locomotor speed in the presence of near

and/or far components to test whether drivers rely more on flow at higher speeds.

Overall our findings suggests that global optic flow does reliably contribute to the nature of steering responses, but the signal does not seem to be a primary input to the estimation of the near or far components as described by the two-point control model.

Chapter 5

Conclusion

In this thesis, we constructed a human-like and high-performance automated driving system based on knowledge from the field of Psychology, and we applied the experimental results in the field of Engineering to understand driver steering behavior. The aim of these studies was to construct Human-in-the-Loop research systems and to facilitate both research fields based on the approach of each other.

In Chapter 2, we provided an overview of optical flow modeling and the control method based on optical flow. The result of optical flow modeling shows that optical flow is effective in perceiving the direction of self-motion since FoE (Focus of Expansion) is consistent with the future path generated by the vehicle motion. Then, we proposed an optical flow controller. The result of the proposed optical flow controller with respect to the target point distance shows the same behavior in terms of driving precision as the driver fixation-steering behavior between expert and novice drivers. Therefore, the proposed method is concluded to be a human-like controller. The contribution of this chapter was to implement the knowledge of previous psychological experiments into control theory.

In Chapter 3, we presented the preview/predictive driver model based on optical flow. The preview/predictive driver model was analyzed from the perspective of optical flow, and it reveals that the previous model includes optical flow information without the element of eye-movements. Then, we proposed a new preview/predictive model based on the human visual behavior. This model can include the aspect of optical flow. The results of the proposed model show that the proposed model can improve both the control performance and ride quality compared to the previous model. The contribution of this chapter was to develop the results of Chapter 2 into the famous driver model.

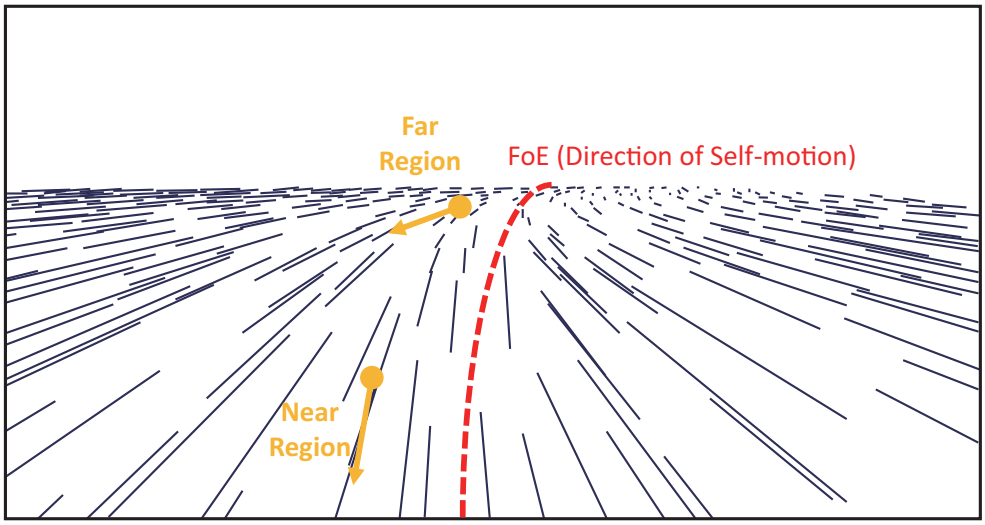

Figure 5.1: The difference between optic flow in the far and near region

Chapter 4 provided the psychological contribution for understanding driver steering behavior within the scope of the Two-point steering model. The results from Chapter 2, in which optic flow from the far region was found to be effective for achieving precise driver steering, was applied to the experimental design, which uses optic flow/road edges mask. The aim of the experiment was to figure out the relationship between the steering performance and the optic flow information with respect to driver gazing. The results show that the global optic flow influences Steering Bias (SB), which is a directional accuracy metric, regardless of the specific area of vision, and that optic flow from the far region is effective for Root-mean-squared error (RMSE), which is a precision metric. This result for RMSE is consistent with the results in Chapter 2 (Figure 2.17 and Figure 4.14). It seems to be because FoE is derived by the lateral component of optic flow. Optic flow in the far region is obviously larger than that in the near region, as shown in Figure 5.1. Therefore, it is easy for humans to perceive the direction of self-motion from the far region. The design of this chapter was influenced by the results of Engineering, whereas Chapters 2 and 3 were based on the application of the knowledge acquired from the Psychology aspect to Engineering.

Control theory, e.g. nonlinear control such as Adaptive control and Sliding mode control, and Machine Learning techniques, e.g. Deep Learning and Reinforcement Learning, have improved considerably to become sufficient under limited conditions. Thus, the ability of human beings has enlarged along with the growth of the above technologies. However, there is always an uncanny valley for any field of robotics. For instance, human

beings sympathize with humanoid robots as they are approaching human appearance. However, beyond a certain threshold, humans will feel the humanoid robot gruesome. This is said to be the same in the field of automatic driving vehicles. This is the most difficult part in the field of Engineering at present, and this has not been introduced to the current control theory and machine learning techniques. Therefore, we started to do research with Human-in-the-Loop research systems in the field of the autonomous vehicle systems. We believe that the series of studies in this thesis will contribute to expanding the research in not only the autonomous vehicle systems but also the whole of Science and Engineering. In the specific future research related to this thesis, it is necessary to clarify what is a system having an affinity with the driver. The proposed systems in this thesis were constructed by only driver's visual perception, but humans are definitely influenced by sensorimotor systems. The affinity with humans must be evaluated by both visual and sensorimotor perception systems. As a result, we can introduce the degree of affinity into system evaluation in terms of human feelings. Such systems which have high affinity with humans will contribute to our future society.

The author believes that in the 21st century, the transdisciplinary research fields with humans such as "Cybernetics", which is the scientific study of control and communication in animals and mechanics [130], and "Embodiment", which is a relationship between the human body and the environment [17], should be considered more, in order to enlarge the capability of robotics. In order to do that, we need to focus on not only robotics but also the understanding of human beings. The author wishes to contribute to these academic fields based on his own experience and knowledge throughout his life.

References

[1] Case - intuitive mobility. https://www.daimler.com/case/en/. accessed: June 26 2018.

[2] C. Johnston and J. Walker. Peak car ownership: The market opportunity for electric automated mobility services. https://www.rmi.org/wp-content/uploads/2017/03/Mobility_PeakCarOwnership_Report2017.pdf, 2017. accessed: June 26 2018.

[3] T. Keeney. Mobility-as-a-service: Why self-driving cars could change everything. http://research.ark-invest.com/hubfs/1_Download_Files_ARK-Invest/White_Papers/Self-Driving-Cars_ARK-Invest-WP.pdf, 2017. accessed: June 26 2018.

[4] J. Arbib and T. Seba. Rethinking transportation 2020-2030: The disruption of transportation and the collapse of the internal-combustion vehicle and oil industries. https://static1.squarespace.com/static/585c3439be65942f022bbf9b/t/591a2e4be6f2e1c13df930c5/1494888038959/RethinkX+Report_051517.pdf, 2017. accessed: June 26 2018.

[5] T. Litman. Autonomous vehicle implementation predictions: Implications for trannsportplanning. https://www.vtpi.org/avip.pdf, 2018. accessed: June 26 2018.

[6] Center for Global Policy Solutions. Stick shift: Autonomous vehicles, driving jobs, and the future of work. http://globalpolicysolutions.org/wp-content/uploads/2017/03/cgps-autonomous-cars.pdf, 2017. accessed: June 26 2018.

[7] D. Milakis, B. van Arem, and B. van Wee. Policy and society related implications of automated driving: A review of literature and directions for future research. *Jounal of Intelligent Transportation Systems*, 21(4):324–348, 2017.

[8] D. J. Fagnant and K. M. Kockelman. Preparing a nation for autonomous vehicles: opportunities, barriers and policy recommendations. *Transportation Research Part A: Policy and Practice*, 77:167–181, 2015.

[9] Government of Japan Cabinet Office. White paper on traffic safety in japan 2017. http://www8.cao.go.jp/koutu/taisaku/h29kou_haku/english/wp2017-pdf.html, 2017. accessed: June 26 2018.

[10] Statistics of Japan. Statistics about road traffic. https://www.e-stat.go.jp/en/stat-search/files?page=1&layout=datalist&toukei=00130002&tstat=000001027458&cycle=7&year=20170&month=0&result_back=1&result_page=1&second=1&second2=1&tclass1val=0, 2017. accessed: June 26 2018.

[11] McKinsey&Company. Automotive revolution - perspective towards 2030: How the convergence of disruptive technology-driven trends could transform the auto industry. https://goo.gl/QL8zjZ, 2016. accessed: June 26 2018.

[12] SAE International. Automated driving: Levels of driving automation are defined in new sae international standard j3016. http://media.cygnus.com/files/base/MASS/document/2017/04/automated_driving.pdf, 2014. accessed: June 26 2018.

[13] E. Ohn-Bar and M. M. Trivedi. Looking at humans in the age of self-driving and highly automated vehicles. *IEEE Transactions on Intelligent Vehicles*, 1(1):90–104, 2016.

[14] M. A. Sasse, S. Brostoff, and D. Weirich. Transforming the 'weakest link' - a human/computer interaction approach to usable and effective security. *BT Technology Journal*, 19(3):122–131, 2001.

[15] M. Bojarski, D. D. Testa, D. Dworakowski, B. Firner, B. Flepp, P. Goyal, L. D. Jackel, M. Monfort, U. Muller, J. Zhang, X. Zhang, J. Zhao, and K. Zieba. End to end learning for self-driving cars. *arXiv:1604.07316*, 2016.

[16] N. Merat A. H. Jamson, F. C. H. Lai, M. Daly, and O. M. J. Carsten. Transition to manual: Driver behaviour when resuming control from a highly automated vehicle. *Transportation Research Part F: Traffic Psychology and Behaviour*, 27:274–282, 2014.

[17] R. Pfeifer and C. Scheier. *Understanding Intelligence*. MIT Press, 2001.

[18] J. J. Gibson. *Perception of the visual world*. Boston:Houghton Mifflin, 1950.

[19] J. J. Gibson. Visually controlled locomotion and visual orientation in animals. *British Journal of Psychology*, 49(3):182–194, 1958.

[20] W. H. Warren and D. J. Hannon. Direction of self-motion is perceived from optical flow. *Nature*, 336:162–163, 1988.

[21] W. H. Warren and D. J. Hannon. Eye movements and optical flow. *Journal of the Optical Society of America*, A7:160–169, 1992.

[22] C. S. Royden, M. S. Banks, and J. A. Crowel. The perception of heading during eye movements. *Nature*, 360:583–585, 1992.

[23] C. S. Royden, J. A. Crowel and M. S. Banks. Estimating heading during eye movements. *Vision Research*, 34(23):3197–3214, 1994.

[24] W. H. Warren, B. A. Kay, W. D. Duchon, and S. Sahuc. Optic flow used to control human walking. *Nature Neuroscience*, 4:213–216, 2001.

[25] R. M. Wilkie and J. P. Wann. Eye-movements aid the control of locomotion. *Journal of Vision*, 3:677–684, 2003.

[26] R. M. Wilkie and J. P. Wann. Judgements of path, not heading, guide locomotion. *Journal of Experimental Psychology: Human Perception and Performance*, 32(1):88–96, 2006.

[27] T. Higuchi. Visuomotor control of human adaptive locomotion: understanding the anticipatory nature. *Frontiers in Psychology*, 4(277):1–9, 2013.

[28] W. H. Warren, D. R. Mestre, A. W. Blackwell, and M. W. Morris. Perception of circular heading from optical flow. *Journal of Experimental Psychology: Human Perception and Performance*, 17:28–43, 1991.

[29] C.S. Royden. Analysis of misperceived observer motion during simulated eye rotations. *Vision Research*, 34(23):3215–3222, 1994.

[30] N. G. Kim and M. T. Turvey. Visually perceiving heading on circular and elliptical paths. *Journal of Experimental Psychology: Human Perception and Peformance*, 24(6):1690–1704, 1998.

[31] J. Cheng and L. Li. Perceiving path from optic flow. *Journal of Vision*, 11(22):1–15, 2011.

[32] J. Saunders and K. Ma. Can observers judge future circular path relative to a target from retinal flow? *Journal of Vision*, 11(16):1–17, 2011.

[33] O. W. Layton and N. A. Browning. A unified model of heading and path perception in primate mstd. *PLoS Computational Biology*, 10(2):1–20, 2014.

[34] S. K. Rushton, J. M. Harris, M. R. Lloyd, and J. P. Wann. Guidance of locomotion on foot uses perceived target location rather than optic flow. *Current Biology*, 8(21):1191–1194, 1998.

[35] J. P. Wann and M. F. Land. Steering with or without the flow: is the retrieval of heading necessary? *Trends in Cognitive Sciences*, 4(8):319–324, 2000.

[36] R. M. Wilkie and J. P. Wann. Driving as night falls: the contribution of retinal flow and visual direction to the control of steering. *Current Biology*, 12(23):2014–2017, 2002.

[37] R. M. Wilkie and J. P. Wann. Controlling steering and judging heading: retinal flow, visual direction, and extraretinal information. *29*, 2:363–378, 2003.

[38] J. P. Wann and R. M. Wilkie. *Optic Flow and Beyond*, chapter How do we control high speed steering? Springer, 2004.

[39] M. F. Land and D. N. Lee. Where we look when we steer. *nature*, 369:742–744, 1994.

[40] F. Mars. Driving around bends with manipulated eye-steering coordination. *Journal of Vision*, 8(10):1–11, 2008.

[41] F. I. Kandil, A. Rotter, and M. Lappe. Driving is smoother and more stable when using the tangent point. *Journal of Vision*, 9(11):1–11, 2009.

[42] K. D. Robertshaw and R. M. Wilkie. Does gaze influence steering around a bend? *Journal of Vision*, 8(18):1–13, 2008.

[43] R. M. Wilkie, G. K. Kountouriotis, and N. Merat. Using vision to control locomotion: looking where you want to go. *Experimental Brain Research*, 204(4):539–547, 2010.

[44] O. Lappi, J, Pekkanen, and T. H. Itkonen. Pursuit eye-movements in curve driving differentiate between future path and tangent point models. *PLoS ONE*, 8(7):1–16, 2013.

[45] O. Lappi, E. Lehtonen, J. Pekkanen, and T. Itkonen. Beyond the tangent point: Gaze targets in naturalistic driving. *Journal of Vision*, 13(11):1–18, 2013.

[46] O. Lappi. Future path and tangent point models in the visual control of locomotion in curve driving. *Journal of Vision*, 14(21):1–22, 2014.

[47] T. Itkonen, J. Pekkanen, and O. Lappi. Driver gaze behavior is different in normal curve driving and when looking at the tangent point. *PLoS ONE*, 10(8):1–19, 2015.

[48] G. K. Kountouriotis, R. C. Floyd, P. H. Gardner, N. Merat, and R. M. Wilkie. The role of gaze and road edge information during high-speed locomotion. *Journal of Experimental Psychology: Human Perception and Performance*, 38(3):682–702, 2012.

[49] E. Lehtonen, O. Lappi, and H. Summala. Anticipatory eye movements when approaching a curve on a rural road depend on working memory load. *Transportation Research Part F: Traffic Psychology and Behaviour*, 15(3):369–377, 2012.

[50] E. Lehtonen, O. Lappi, H. Kotkanen, and H. Summala. Look-ahead fixations in curve driving. *Ergonomics*, 56(1):34–44, 2013.

[51] E. Lehtonen, O. Lappi, I. Koirikivi, and H. Summala. Effects of driving experience on anticipatory look-ahead fixations in real curve driving. *Accident Analysis & Prevention*, 70:196–208, 2014.

[52] M. F. Land. *Motion Vision*, chapter Does steering a car involve perception of the velocity flow field?, pages 227–235. Springer, 2001.

[53] H. Inou, T. Fukao, S. Totsuka, and Y. Okafuji. Development of automatic steering control system based on optical flow model. *In Proceedings of 12th International Symposium on Advanced Vehicle Control*, 2014.

[54] H. Inou, T. Fukao, S. Totsuka, and Y. Okafuji. Development of steering control system based on optical flow model. *Transactions of Society of Automotive Engineers of Japan*, 46(2):443–448, 2015. (in Japanese).

[55] C. J. Nash and D. J. Cole. Development of a novel model of driver-vehicle steering control incorporating sensory dynamics. *The Dynamics of Vehicles on Roads and Tracks: Proceedings of the 24th International Symposium on Dynamics of Vehicles on Roads and Tracks*, pages 57–66, 2016.

[56] C. J. Nash, D. J. Cole, and R. S. Bigler. A review of human sensory dynamics for application to models of driver steering and speed control. *Biological Cybernetics*, 110(2-3):91–116, 2016.

[57] D. N. Lee. A theory of visual control of braking based on information about time-to-collision. *Perception*, 5(4):437–459, 1976.

[58] M. A. Goodrich and E. R. Boer. Characterization of dynamic human braking behavior with implications for acc design. *in Proceedings of IEEE International Conference on Intelligent Transportation Systems*, pages 964–969, 1999.

[59] T. Kondoh, T. Yamamura, S. Kitazaki, N. Kuge, and E. R. Boer. Identification of visual cues and quantification of drivers perception of proximity risk to the lead vehicle in car-following situations. *in Proceedings of Driving Simulation Conference Asia/Pacific*, 2006.

[60] T. Wada, S. Doi, N. Tsuru, K. Isaji, and H. Kaneko. Characterization of expert drivers' last-second braking and its application to a collision avoidance system. *IEEE Transaction on Intelligent Transportation Systems*, 11(2):413–422, 2010.

[61] K. Yoshimoto. Simulation of man-automobile system by the driver's steering model with predictability. *Bulletin of the Japan Society of Mechanical Engineers*, 12(51):495–500, 1969.

[62] D. D. Salvucci. Modeling driver behavior in a cognitive architecture. *Human Factors*, 48(2):362–380, 2006.

[63] B.R. Fajen and W.H. Warren. Behavioral dynamics of steering, obstacle avoidance, and route selection. *Journal of Experimental Psychology : Human Perception and Performance*, 29(2):343–362, 2003.

[64] E. Malis. Survey of vision-based control. *In ENSIETA European Naval Ship Design Short Course*, 2002.

[65] F. Chaumette and S. Hutchinson. Visual servo control i: Basic approaches. *Robotics and Automation Magazine*, 13(4):82–90, 2006.

[66] W. E. Green, P. Y. Oh, and G. Barrows. Flying insect inspired vision for autonomous aerial robot maneuvers in near-earth environments. *IEEE International Conference on Robotics and Automation*, 3:2347–2352, 2004.

[67] P. Questa, E.Grossmann, and G. Sandini. Camera self orientation and docking maneuver using normal flow. *SPIE's 1995 Symposium on OE/Aerospace Sensing and Dual Use Photonics*, pages 274–283, 1995.

[68] R. N. Jazar. *Vehicle dynamics: theory and application*. Springer, 2009.

[69] J.-J. E. Slotine and W. Li. *Applied nonlinear control*. Prentice Hall, 1990.

[70] G. Farneback. Two-frame motion estimation based on polynomial expansion. *In Scandinavian Conference on Image Analysis*, 2003.

[71] J. D. Lee. Technology and teen drivers. *Journal of Safety Research*, 38:203–213, 2007.

[72] J. Duncan, P. Williams, and I. Brown. Components of drivging skill: experience does not mean expertise. *Ergonomics*, 34:919–937, 1991.

[73] D. E. Crundall and G. Underwood. Effects of experience and processing demands on visual information acquisition in drivers. *Ergonomics*, 41:448–458, 1998.

[74] H. Summala, T. Nieminen, and M. Punto. Maintaining lane position with peripheral vision during in-vehicle tasks. *Human Factors*, 38:442–451, 1996.

[75] P. M. van Leeuwen, R. Happee, and J. C. F. de Winter. Changes of driving performance and gaze behavior of novice drivers during a 30-min simulator-based training. *Proceedings of 6th International Conference on Applied Human Factors and Ergonomics and Affiliated Conferences*, pages 3325–3332, 2015.

[76] G. Underwood, P. Chapman, N. Brocklehurst, J. Underwood, and D. Crundall. Visual attention while driving: sequences of eye fixations made by experienced and novice drivers. *Ergonomics*, 46:629–646, 2003.

[77] G. J. Blaauw. *Car driving as a supervisory control task*. PhD thesis, TNO-Institute for Perception, 1984.

[78] R. R. Mourant and T. H. Rockwell. Visual information seeking of novice drivers. *In Proceedings of 1970 International Automobile Safety Conference Compendium*, pages 704–711, 1970.

[79] A. S. Cohen. Car drivers' pattern of eye fixations on the road and in the laboratory. *Perceptual and Motor Skills*, 52:512–522, 1981.

[80] R. R. Mourant and T. H. Rockwell. Strategies of visual search by novice and experienced drivers. *Human Factors*, 14:325–335, 1972.

[81] C. C. Macadam. Understanding and modeling the human driver. *Vehicle System Dynamics*, 43(1-3):101–134, 2003.

[82] M. Kondo. Directional stability (when steering is added). *Journal of the Society of Automotive Engineers of Japan*, 7(1-3):101–134, 1953.

[83] C. C. Macadam. An optimal preview control for linear systems. *Journal of Dynamic Systems, Measurement and Control*, 102(3):188–190, 1980.

[84] Carsim educational user manual. `http://www.eggert.highpeakpress.com/ME485/Docs/CarSimEd.pdf`. accessed: June 26 16 2018.

[85] R. S. Sharp, D. Casanova, and P. Symonds. A mathematical model for driver steering control, with design, tuning and performance results. *Vehicle System Dynamics*, 33:289–326, 2000.

[86] A. Y. Ungoren and H. Peng. An adaptive lateral preview driver model. *Vehicle System Dynamics: International Journal of Vehicle Mechanics and Mobility*, 43(4):245–259, 2005.

[87] G. Prokop. Modeling human vehicle driving by model predictive online optimization. *Vehicle System Dynamics*, 35(1):19–53, 2001.

[88] M. F. Land and D. N. Lee. Where we look when we steer. *Nature*, 369:742–744, 1994.

[89] D. D. Salvucci and R. Gray. A two-point visual control model of steering. *Perception*, 33(10):1233–1248, 2004.

[90] J. Edelmann, M. Plochl, W. Reinalter, and W. Tieber. A passenger car driver model for higher lateral accelerations. *Vehicle System Dynamics*, 45(12):1117–1129, 2007.

[91] S. D. Keen and D. J. Cole. Bias-free identification of a linear model-predictive steering controller from measured driver steering behavior. *IEEE transactions on systems, man, and cybernetics, Part B*, 42(2):434–443, 2012.

[92] T. Qu, H. Chen, Y. Ji, H. Guo, and D. Cao. Modeling driver steering control based on stochastic model predictive control. *Proceedings of IEEE International Conference on Systems, Man, and Cybernetics*, 2013.

[93] A. J. Pick and D. J. Cole. A mathematical model of driver steering control including neuromuscular dynamics. *Journal of Dynamic Systems, Measurement, and Control*, 130(3):031004 1–9, 2008.

[94] N. Mehrabi, R. S. Razavian, and J. McPhee. A physics-based musculoskeletal driver model to study steering tasks. *Journal of Computational Nonlinear Dynamics*, 10(2):021012 1–8, 2015.

[95] S. Schnelle, J. Wang, H. Su, and R. Jagacinski. A driver steering model with personalized desired path generation. *IEEE Transactions on Systems, Man, and Cybernetics: Systems*, 47(1):111–120, 2017.

[96] S. Schnelle and J. Wang. A personalizable driver steering model capable of predicting driver behaviors in vehicle collision avoidance maneuvers. *IEEE Transactions on Human-Machine Systems*, 47(5):625–635, 2017.

[97] Y. Okafuji, T. Fukao, and H. Inou. Development of automatic steering system by modeling human behavior based on optical flow. *Journal of Robotics and Mechatronics*, 27(2):136–145, 2015.

[98] Y. Okafuji, T. Fukao, Y. Yokokohji, and H. Inou. Optical flow-based control for automatic steering systems. *in Proceedings of IEEE/SICE International Symposium on System Integration*, 2015.

[99] C. Liu, D. C. Gazis, and T. W. Kennedy. Human judgment and analytical derivation of ride quality. *Transportation Science*, 33(3):290–297, 1999.

[100] J. K. Hedrick, M. Tomizuka, and P. Varaiya. Control issues in automated highway systems. *IEEE Control Systems*, 14(6):21–32, 1994.

[101] E. Donges. A two-level model of driver steering behavior. *Human Factors*, 20:691–707, 1978.

[102] E. R. Boer. What preview elements do drivers need? *IFAC-Papers OnLine*, 49(19):102–107, 2016.

[103] M. Land and J. Horwood. Which parts of the road guide steering? *Nature*, 377:339–340, 1995.

[104] A. Chatziastros, G. M. Wallis, and H. H. Bülthoff. The effect of field of view and surface texture on driver steering performance. In A. G. Gale, editor, *Vision in Vehicles VII*, pages 253–260. Elsevier, 1999.

[105] S. Cloete and G. Wallis. Visuomotor control of steering: The artefact of the matter. *Experimental Brain Research*, 208:475–489, 2011.

[106] I. Frissen and F. Mars. The effect of visual degradation on anticipatory and compensatory steering control. *The Quarterly Journal of Experimental Psychology*, 67:499–507, 2014.

[107] C. D. Mole, G. Kountouriotis, J. Billington, and R. M. Wilkie. Optic flow speed modulates guidance level control: New insights into two-level steering. *Journal of Experimental Psychology: Human Perception and Performance*, 42(11):1818–1838, 2016.

[108] F. Mars and P. Chevrel. Modelling human control of steering for the design of advanced driver assistance systems. *Annual Reviews in Control*, 44:292–302, 2017.

[109] G. Markkula, O. Benderius, and M. Wahde. Comparing and validating models of driver steering behaviour in collision avoidance and vehicle stabilisation. *Vehicle System Dynamics*, 52:1658–1680, 2014.

[110] C. You and P. Tsiotras. Optimal two-point visual driver model and controller development for driver-assist systems for semi-autonomous vehicles. *In proceedings of 2016 American Control Conference*, pages 5976–5981, 2016.

[111] C. Sentouh, P. Chevrel, F. Mars, and F. Claveau. A sensoriomotor driver model for steering control. *In Proceedings of IEEE International Conference on Systems, Man and Cybernetic*, pages 2462–2467, 2009.

[112] L. Saleh, P. Chevrel, F. Mars, J. F. Lafay, and F. Claveau. Human-like cybernetic driver model for lane keeping. *In Proceedings of the 18th World Congress of the International Federation of Automatic Control*, pages 4368–4373, 2011.

[113] H. Neumann and B. Deml. The two-point visual control model of steering-new empirical evidence. In V. G. Duffy, editor, *Digital Human Modeling*, pages 493–502. Springer, 2011.

[114] A. C. Beall and J. M. Loomis. Visual control of steering without course information. *Perception*, 25:481–494, 1996.

[115] L. Li and J. Chen. Relative contributions of optic flow, bearing, and splay angle information to lane keeping. *Journal of Vision*, 10(16):1–14, 2010.

[116] R. M. Wilkie, J. P. Wann, and R. S. Allison. Active gaze, visual look-ahead, and locomotor control. *Journal of Experimental Psychology: Human Perception and Performance*, 34:1150–1164, 2008.

[117] R. M. Wilkie, D. R. Poulter, and J. P. Wann. Where you look when you learn to steer. *Journal of Vision*, 4(8), 2004.

[118] R. M. Wood, M. A. Harvey, C. E. Young, A. Beedie, and T. Wilson. Weighting to go with the flow? *Current Biology*, 10(15):R545–546, 2000.

[119] G. K. Kountouriotis, C. D. Mole, N. Merat, and R. M. Wilkie. The need for speed: Global optic flow speed influences steering. *Royal Society Open Science*, 3:160096, 2016.

[120] G. K. Kountouriotis, K. A. Shire, C. D. Mole, P. H. Gardner, N. Merat, and R. M. Wilkie. Optic flow asymmetries bias high-speed steering along roads. *Jounal of Vision*, 13(23), 2013.

[121] J. P. Wann and D. K. Swapp. Why you should look where you are going. *Nature Neuroscience*, 3:647–648, 2000.

[122] L. Li and D. C. Niehorster. Influence of optic flow on the control of heading and target egocentric direction during steering toward a goal. *Journal of Neurophysiology*, 112(4):766–777, 2014.

[123] M. McManus, S. D'Amour, and L. R. Harris. Using optic flow in the far peripheral field. *Journal of Vision*, 17(3):1–11, 2017.

[124] Y. Okafuji, T. Fukao, Y. Yokokohji, and H. Inou. Design of a preview driver model based on optical flow. *IEEE Transaction on Intelligent Vehicles,*, 1(3):266–276, 2016.

[125] International Organization for Standardization. Passenger cars - test track for a severe lane-change manoeuvre. part 1: Double lane-change, iso 2888-1, 1999.

[126] E. R. Girden. *ANOVA Repeated Measures*. SAGE Publications, Inc., 1991.

[127] R. K. Raw, G. K. Kountouriotis, M. Mon-Williams, and R. M. Wilkie. Movement control in older adults: Does old age mean middle of the road? *Journal of Experimental Psychology: Human Perception and Performance*, 38:735–745, 212.

[128] C. N. Authié and D. R. Mestre. Path curvature discrimination: Dependence on gaze direction and optical flow speed. *PLoS ONE*, 7(e31479), 2012.

[129] R. M. Wilkie and J. P. Wann. The role of visual and nonvisual information in the control of locomotion. *Journal of Experimental Psychology: Human Perception and Performance*, 31:901–911, 2005.

[130] N. Wiener. *Cybernetics: or Control and Communication in the Animal and the Machine*. MIT Press, 1965.

Publications

Publications related to this thesis are following:

Chapter 2

Journal

1. Yuki Okafuji, Takanori Fukao, Hiroshi Inou, “Development of automatic steering system by modeling human behavior based on optical flow”, *Journal of Robotics and Mechatronics*, Vol. 27, No. 2, pp.136-145, 2015

International Conference

1. Yuki Okafuji, Takanori Fukao, Yasuyoshi Yokokohji, Hiroshi Inou, “Optical flow-based control for automatic steering systems”, *2015 IEEE/SICE International Symposium on System Integration (SII2015)*, 2015

Domestic Conference

1. Yuki Okafuji, Takanori Fukao, Yasuyoshi Yokokohji, Hiroshi Inou, “Optical flow-based control considering camera motion for automatic steering sysmtes”, *The 58th Japan Automatic Control Conference*, 2015 (in Japanese)

2. Yuki Okafuji, Takanori Fukao, Hiroshi Inou, “Automatic steering system based on optical flow”, *The Robotics and Mechatronics Conference 2014 (ROBOMECH2014)*, 2014 (in Japanese)

Chapter 3

Journal

1. Yuki Okafuji, Takanori Fukao, Yasuyoshi Yokokohji, Hiroshi Inou, "Design of a preview driver model based on optical flow", *IEEE Transaction on Intelligent Vehicles*, Vol. 1, No. 3, pp.266-276,2016

Domestic Conference

1. Yuki Okafuji, Takanori Fukao, Yasuyoshi Yokokohji, Hiroshi Inou, "Understanding and application of predictive model based on optical flow", *The 59th Annual Conference of the Institute of Systems, Control, and Information Engineers (SCI'15)*, 2015 (in Japanese)

Chapter 4

Journal

1. Yuki Okafuji, Callum D. Mole, Natasha Merat, Takanori Fukao, Yasuyoshi Yokokohji, Hiroshi Inou, and Richard M. Wilkie, "Steering bends and changing lanes: the impact of optic flow and road edges on two point steering control", *Journal of Vision* (submitted)

Other Publications

Journal

1. Hiroshi Inou, Takanori Fukao, Seiji Totsuka, Yuki Okafuji, "Development of steering control system based on optical flow model", *Transaction of Society of Automotive Engineering of Japan*, Vol. 46, No. 2, pp.443-448, 2015 (in Japanese)

International Conference

1. Yuki Okafuji, Callum D. Mole, Richard M. Wilkie, Natasha Merat, "Examining how driver steering behaviour is affected by optic flow after resuming control from a highly automated vehicle", *The Human Factors and Ergonomics Society Europe Annual Meeting (HFES Europe)*, 2017

2. Hiroshi Inou, Takanori Fukao, Seiji Totsuka, Yuki Okafuji, "Development of Automatic Steering System Based on Optical Flow Model", *12th International Symposium on Advanced Vehicle Control (AVEC'14)*, 2014

Technical Report

1. Yuki Okafuji, "Analysis of driver steering behavior affected by optic flow in TRANSITION", *Memoirs of the Graduate Schools of Engineering and System Informatics*, Vol. 9, 2017 (in Japanese)

2. Hiroshi Inou, Takanori Fukao, Seiji Totsuka, Yuki Okafuji, "Development of steering control system based on optical flow model", *DENSO Technical Review*, Vol. 20, pp.123-130, 2015 (in Japanese)

Domestic Conference

1. Yuki Okafuji, Takanori Fukao, Yasuyoshi Yokokohji, Hiroshi Inou, "A study on correlation of lateral control of a vehicle", *The Robotics and Mechatronics Conference 2017 (ROBOMECH2017)*, 2017 (in Japanese)

2. Yuki Okafuji, Takanori Fukao, Yasuyoshi Yokokohji, Hiroshi Inou, "Simulator construction considering real environmental measurement for automatic steering based on optical flow", *The 59th Annual Conference of the Institute of Systems, Control, and Information Engineers (SCI'16)*, 2016 (in Japanese)

3. Hiroshi Inou, Takanori Fukao, Seiji Totsuka, Yuki Okafuji, "Development of steering control system based on optical flow model", *2014 JSAE Annual Congress (Spring)*, 2014 (in Japanese)

Doctor Thesis, Kobe University

"Studies on Design of Automatic Driving Systems and Analysis of Driving Behavior based on Driver's Visual Perception", 145 pages
Submitted on July, 11, 2018

The date of publication is printed in cover of repository version published in Kobe University Repository Kernel.